The Role of Ketone Bodies in Autophagic Flux, Cellular Energetics and Injury-induced Neurotoxicity

by

Jana Wurz

Dissertation presented for the degree of

Master's (Physiological Sciences)

in the Faculty of Science at

Stellenbosch University

March 2016

Supervisor: Dr. Benjamin Loos

DECLARATION

March 2016

I, the undersigned, declare that the entirety of the work contained in this dissertation is my own, original work, that I am the sole author thereof (save to the extent explicitly stated otherwise), that reproduction and publication thereof by Stellenbosch University will not infringe on any third party rights and that I have not previously in its entirety or in part submitted it for obtaining any qualification.

Date: …………………………………………………

Signature: …………………………………………………

SUMMARY

Introduction. Alzheimer's disease is the most common neurodegenerative disease and leading cause of dementia globally, with an increasing prevalence especially in developing countries such as South Africa. Currently, no single disease modifying treatment exists.. Alzheimer's disease has a complex pathophysiology with the main causative factor involving defective proteolytic pathways, including the process of macroautophagy, and toxic amyloid beta aggregation. In addition, metabolic perturbations as well as disrupted mitochondrial dynamics are implicated. These disruptions culminate in neuronal cell death. Recently, ketone bodies have shown beneficial effects in the context of neurodegenerative diseases including Alzheimer's disease, indicating improvements in both molecular disruptions as well as cognition. However, although literature implicates a role for autophagy in alleviating protein accumulation, the mechanism of action remains largely unclear.

Aims. The aim of this project was therefore assess the effects of the ketone body beta-hydroxybutyrate in neuronal cells under basal conditions and in an injury model. We aimed to assess four parameters intimately linked to cellular survival in these two models: cellular viability, autophagic flux, mitochondrial network morphology and intracellular ATP supply. We hypothesized that ketone bodies will protect neurons from paraquat-induced neurotoxicity by increasing ATP levels through increasing autophagic flux.

Methods. GT1-7 cells were cultured using DMEM supplemented with 10% FBS under standard conditions (5% CO_2, 37 °C). To assess the role of ketone bodies under basal conditions, Western blot analysis of amyloid precursor protein (APP), amyloid beta (Aβ), beta site APP cleaving enzyme (BACE), p62 and LC3-II proteins was performed. Fluorescence microscopy was performed utilizing fluorochromes targeting APP, Aβ and BACE. Quantitative assessment of neuronal ATP was completed using a luciferase-based assay. Qualitative assessment of neuronal ATP distribution was performed by transfecting cells with a FRET-based ATP indicator, ATeam, and by capturing images with fluorescence microscopy. For all the experiments in the first model, treatment with the autophagosomal/lysosomal fusion inhibitor, bafilomycin A_1, was included to assess autophagic flux. To assess the role of ketone bodies in response to injury, cells were exposed to the herbicide paraquat and Western blot analysis of LC3 and cleaved PARP, an

apoptotic protein, was performed. A WST-1 reductive capacity assay was completed and mitochondrial morphology assessed by means of the mitochondrial polarization-dependent fluorochrome, tetramethylrhodamine ethyl ester (TMRE), capturing and analysing images with ImageJ software. In addition transmission electron microscopy was performed to indicate neuronal ultrastructure, ATP quantification and qualitative assessment as well as flow cytometry to indicate reactive oxygen species (ROS) by using both dichlorofluorescein (DCF) to indicate general ROS and TMRE to assess mitochondrial polarization.

Results. Under basal conditions, it was observed that the ATP distribution within cells changed to large areas of detected signal when treating cells with ketone bodies and bafilomycin. There were no significant differences in detected ATP levels between treatment groups. Western blot results revealed that bafilomycin treatment resulted in a strong trend towards increased protein levels of BACE and APP, and a significant decrease in Aβ levels. Decreased p62 protein expression was observed upon ketone body treatment as well as a strong trend for decreased LC3-II protein levels upon bafilomycin treatment. Fluorescence microscopy revealed that bafilomycin treatment caused accumulation of APP, BACE and Aβ, and increased nuclear signal of BACE and APP. For the injury-induced model the WST-1 assay results reveal that paraquat caused a significant decrease in reductive capacity, which ketone body supplementation rescued by significantly increasing reductive capacity. Western blot analysis revealed a strong trend for decreased LC3-II protein expression upon bafilomycin treatment. No differences between groups were observed for cleaved PARP.

Mitochondrial morphological assessment indicated a highly fused network in the control and ketone body group, and a highly fragmented state upon paraquat treatment, which was improved to a more fused state upon ketone body co-treatment. No significant differences were observed in the flow cytometry data, however a similar trend for increased fluorescence intensity upon ketone body and paraquat co-treatment was present in cells stained with DCF and TMRE. ATP concentration and distribution was severely affected by paraquat treatment, which decreased detected ATP levels and signal. Ketone body treatment caused a change in ATP distribution apparent as large 'hotspots', however, did not significantly increase ATP concentration in the co-treatment group. Transmission electron microscopy indicated intact, elongated mitochondria in the control and ketone

body groups, as well as well-defined vacuolar structures. They were increased upon ketone body supplementation. Paraquat exposure caused mitochondrial disruption as indicated by swollen mitochondria with decreased integrity as well as less well defined vacuolar structures. Fewer vacuolar structures were observed in the co-treatment group.

Discussion and conclusion. Our results suggest that ketone body exposure increases autophagic flux and decreases the presence of amyloid-associated proteins. In addition, ketone bodies confer protection from neurotoxicity and improve mitochondrial network connectivity. Our results further indicate a role for ketone bodies in localized ATP supply. Taken together, ketone body exposure may hold great potential as an adjuvant therapy in the context of neurodegeneration.

OPSOMMING

Inleiding. Alzheimersiekte is die mees algemene neurodegeneratiewe siekte en wêreldwyd toemend die vernaamste oorsaak van demensie. Ontwikkelende lande soos Suid-Afrika sal veral beïnvloed word. Huidiglik bestaan daar geen enkele behandeling nie. Die patologiese aspekte van die fisiologie van Alzheimersiekte is kompleks, maar die vernaamse oorsaaklike faktor behels foutiewe proteolitiese weë, insluitend makroautofagie, en toksiese amyloid beta opeenhoping. Daarbenewens word metaboliese versteurings sowel as 'n ontwrigte mitochondriese dinamiek geïmpliseer. Hierdie versteurings veroorsaak uiteindelik die dood van neurone. Dit is onlangs bewys dat ketoonliggame voordelige gevolge het in die konteks van neurodegeneratiewe siektes, insluitend Alzheimersiekte waar verbeterings in beide molekulêre versteurings sowel as kognisie waargeneem is. Nieteenstaande die rol van autofagie om proteïn opeenhoping te verlig rapporteer in die literatuur, is die meganisme van aksie steeds onduidelik.

Doel. Die doel van hierdie projek was dus om die uitwerking van die ketoonliggaam beta-hidroksie butiraat te bepaal onder basis toestande en in 'n beseringsmodel. Ons doel was om vier bepalers wat nou gekoppel is met sellulêre oorlewing in die twee modelle te assesseer: seloorlewing, autofagiese stroming, mitochondriese netwerk morfologie en intrasellulêre ATP verskaffing. Ons hipotese was dat ketoonliggame neurone sal beskerm van paraquat-induseerde neurotoksisiteit, deur ATP vlakke te vermeerder deur die toename van autofagiese stroming.

Metodes. GT1-7 selle was deur middel van selkultuur geweek met behulp van DMEM verryk met 10% FBS onder standaard toestande (5% CO_2, 37 °C). Western blot analise van APP, Aβ, BACE, p62 en LC3-II proteïnvlakke was onderneem om die effek van ketoonliggame onder basis toestande te bepaal. Fluoressensie-gebaseerde mikroskopie was onderneem deur fluorochrome te gebruik gerig aan APP, Aβ en BACE. Kwantitatiewe evaluering van neuronale ATP was voltooi met behulp van 'n lusiferaas-baseerde toets. Kwalitaties evaluering van neuronale ATP verspreiding was uitgevoer deur selle met 'n FRET-gebaseerde ATP wyser, ATeam, te transfekteer en af te beeld met fluoresserende mikroskopie. Bafilomycin, 'n inhibeerder van autofagosomale/lisosomale samesmelting, was gebruik om selle te behandel in alle eksperimente van die eerste model om die autofagiese

stroming te assesseer. Selle is blootgestel aan paraquat, 'n onkruiddoder, om die effek van ketoonliggame te bepaal in reaksie tot skade, en dan is Western blot analise van LC3 en gekliefde PARP, 'n apoptotiese proteïen, onderneem. 'n WST-1 toets, wat reduktiewe kapasitieit aandui, is voltooi en mitochondriese morfologie is geassesseer deur die mitochondriese polarisasie-afhanklike fluorokroom, tetrametielrodamien etielester (TMRE) te gebruik, beelde te neem en te analiseer met behulp van ImageJ sagteware. Verder was transmissie elektron mikroskopie onderneem om neuronale ultrastruktuur aan te dui, sowel as ATP kwantifikase en kwalitatiewe assessering en vloeisitometrie om reaktiewe suurstof spesies (ROS) aan te dui deur gebruik van beide dichlorofluoresien (DCF) vir algemene ROS en TMRE as aanduiding van mitochondriese polarisasie.

Resultate. Onder basis toestande is daar 'n verskil in ATP verspreiding waargeneem, met ketoonliggaam en bafilomycin behandeling wat die ATP verspreiding tot groot areas binne selle verander het. Geen beduidende verskille in the ATP vlakke van die behandelings groepe was teenwoordig nie. Die Western blot metode het aangetoon dat bafilomycin behandeling 'n sterk neiging tot toegenome proteïen vlakke van BACE en APP tot gevolg het, asook 'n beduidende afname in Aβ vlakke. Ketoonliggaam behandeling het 'n sterk tendens tot die afname in p62 proteïn uitdrukking tot gevolg gehad, en bafilomycin behandeling het verder 'n sterk tendens tot die afname van LC3-II proteïnvlakke veroorsaak. Fluoressensie mikroskopie het uitgewys dat bafilomycin behandeling die opeenhoping van APP, BACE and Aβ veroorsaak en die selkern sein van BACE en APP verhoog. Die WST-1 toets resultate het aangedui data paraquat 'n beduidende afname in reduktiewe vermoë tot gevolg het, wat ketoonliggaam aanvullings beredder het deur die reduktiewe kapasiteit weer beduidend te herstel. Western blot analise het 'n sterk tendens vir die afname in LC3-II proteïen uitdrukking in reaksie op bafilomycin behandeling aangetoon. Daar is geen verskille tussen groepe vir gekliefde PARP waargeneem nie.

Mitochondriale morfologiese assessering het 'n hoogs geïntegreerde netwerk vir die kontrole en ketoonliggaam groep uitgewys, en ook dat 'n hoogs gefragmenteerde toestand voorkom in reaksie tot paraquat behandeling, wat tot 'n meer geïntegreerde toestand verbeter het met ketoonliggaam mede-behandeling. Geen beduidende verskille is waargneem in die vloeisitometrie data nie, alhoewel dieselfde tendens vir hoë fluoressensie intensiteit in reaksie op gesamentlike ketoonliggaam en paraquat behandeling in selle wat

gekleur is met DCF en TMRE aangewys is. Paraquat behandeling het ATP konsentrasie en verspreiding beduidend beïnvloed, asook die ATP vlakke en sein verminder.   Ketoonliggaam behandeling het 'n verandering in ATP verspreiding tot gevolg gehad wat voorkom het as groot 'hotspots'.   Transmissie elektron mikroskopie het aangedui dat verlengde mitochondria, en goed gedefinieerde vakuoolstrukture in die kontrole en ketoonliggaam groepe voorgekom het. Hierdie strukture het vermeerder nadat ketoonliggame toegedien is. Paraquat blootstelling het mitochondriale disrupsie tot gevolg gehad, soos aangedui is deur geswelde mitochondria met afgenome integriteit en swakker gedefinieerde vakuool strukture. Minder vakuool strukture is waargeneem in die gesamentlike behandeling groep.

Bespreking en gevolgtrekking. Die resultate verskaf 'n aanduiding dat ketoonliggame 'n toename in autofagiese stroming veroorsaak en 'n afname in die voorkoms van spesifieke amyloid-geassosieerde proteïene. Verder verleen ketoonliggame ook beskerming teen neurotoksisiteit en verbeter mitochondriale netwerk verbindingsstatus. Ons dui verder daarop dat ketoonliggame 'n rol speel in plaaslike ATP beskikbaarheid. Om saam te vat; ketoonliggame het beduidende potensiaal as 'n toegevoegde terapie in die konteks van neurodegenerasie.

ACKNOWLEDGEMENTS

LIST OF CONFERENCES

- The International Cell Death Society meeting (May 2014). Protea hotel, Stellenbosch. Attended.

- Microscopy Society of South Africa (December 2014). Protea hotel, Stellenbosch. Poster presentation: 'ATP visualization in an *in vitro* model for Alzheimer's disease'.

- Physiological Society of South Africa (September 2015). Khaya iBhubesi, Parys. Oral presentation in the Wyndham student competition: 'The effect of ketone bodies in the context of Alzheimer's disease and autophagy'.

INDEX

Chapter 3: RESULTS

Chapter 4: DISCUSSION AND CONCLUSION

LIST OF FIGURES

LIST OF TABLES

LIST OF ABBREVIATIONS

3xTg-AD	Triple-transgenic mouse model of Alzheimer's disease
4-HNE	4-hydroxynonenal
6-OHDA	6-hydroxydopamine
$A\beta_{42}$	Amyloid beta 1-42 peptide
AcCoA	Acetyl-coenzyme A
AD	Alzheimer's disease
ADAS-cog	Alzheimer's disease assessment scale
ADP	Adenosine diphosphate
AGC	Aspartate/glutamate carrier
AICD	APP protein intracellular domain
AIF	Apoptosis inducing factor
ALS	Amyotrophic lateral sclerosis
AMPA	A-amino-3-hydroxy-5-methyl-4-isoxazolepropionic acid
AMPK	Adenosine monophospateactivated kinase
Apaf-1	Apoptotic protease activating factor 1
ApoE	Apolipoprotein E
APP	Amyloid precursor protein
APP-CTF	APP C-terminal fragment
ATeam	Adenosine 5-triphosphate indicator based on epsilon subunit for analytical measurements
Atg	Autophagy-related
ATP	Adenosine triphosphate
AV	Autophagic vacuole(s)
Avt	Amino acid vacuolar transporters
BACE	Beta-site APP-cleaving enzyme
Bcl-2	B-cell lymphoma-2
Beclin-Vps	Bcl-2 interacting protein 1-vacuolar protein sorting

β-OHB	Beta-hydroxybutyrate
BOLD	Blood-oxygen-level-dependent
BSA	Bovine serum albumin
CAD	Caspase-activated DNase
cAMP	Cyclic adenosine monophosphate
CCCP	Carbonyl cyanide m-chlorophenylhydrazone
CDR	Clinical dementia rating
CFP	Cyan fluorescent protein
CO_2	Carbon dioxide
CSF	Cerebrospinal fluid
CypD	Cyclophilin D
DA	Dopamine
DAG	Diacylglycerol
DCF	2',7'-dichlorofluorescein
dH_2O	Distilled water
DISC	Death-inducing signaling complex
DMEM	Dulbecco's modified Eagle's medium
DMSO	Dimethyl sulfoxide
DNA	Deoxyribonucleic acid
Drp1	Dynamin related protein
DSM	Diagnostic and statistical manual for mental disorders
ECL	Enhanced chemiluminescence
EDTA	Ethylene diamine tetra-acetic acid
EP300	E1A binding protein p300
ER	Endoplasmic reticulum
ETC	Electron transport chain
F_oF_1-ATPase	ATP synthase consisting of F0 and F1 subunits
FBS	Fetal bovine serum

FDA	Food and drug administration
FDG	2-[F-18]fluoro-2-deoxy-D-glucose
Fis1	Fission protein
fMRI	Functional magnetic resonance imaging
FRET	Förster resonance energy transfer
GAPDH	Glyceraldehyde 3-phosphate dehydrogenase
GFP	Green fluorescent protein
GSK3	Glycogen synthase kinase 3
GTPase	Guanosinetriphosphatase
HD	Huntington's disease
HRP	Horse radish peroxidase
IDE	Insulin degrading enzyme
IGF-1	Insulin-like growth factor-1
IgG	Immunoglobulin G
IP3	Inositol triphosphate
IRS-1	Insulin receptor substrate-1
JNK1	c-Jun N-terminal kinase 1
KB	Ketone bodies
KD	Ketogenic diet
LDH	Lactate dehydrogenase
LSDs	Lysosomal storage diseases
LUT	Lookup table
MAP1-LC3	Microtubule-associated protein 1 light chain 3
MCI	Mild cognitive impairment
MCTs	Monocarboxylate transporters
Mfn	Mitofusin protein
MMSE	Mini-mental-state examination
mRNA	Messenger ribonucleic acid

mPTP	Mitochondrial permeability transition pore
mTOR	Mammalian target of rapamycin
MTT	3-(4,5-dimethylthiazol-2-Yl)-2,5-diphenyltetrazolium bromide
Na^+/ K^+-ATPase	Sodium-potassium adenosine triphosphatase
Na_3VO_4	Sodium orthovanadate
NADH	Nicotinamide adenine dinucleotide (reduced form)
NADPH	Nicotinamide adenine dinucleotide phosphate (reduced form)
NaF	Sodium fluoride
NaOH	Sodium hydroxide
NCD	Neurocognitive disorder
NFT	Neurofibrillary tangle
NINCDS/ADRDA	National institute of neurological and communicative diseases and stroke/Alzheimer's disease and related disorders association
NMDA	N-methyl-D-aspartate
NOS	Nitric oxide synthase
Opa1	Optic atrophy 1
OxPhos	Oxidative phosphorylation
p70S6K	Phosphorylated p70S6 kinase
PBS	Phosphate-buffered saline
PD	Parkinson's disease
PDH	Pyruvate dehydrogenase
PDK1	3-phosphoinositide-dependent protein kinase-1
PE	Phosphatidylethanolamine
PET	Positron emission tomography
PFK	Phosphofructokinase-1
PFKFB3	6-phosphofructose-2-kinase/fructose-2,6-bisphosphatase-3
PGC-1α	Peroxisome proliferator-activated receptor-c coactivator 1α
PI	Propidium iodide
PIB	Pittsburgh compound B

PI3K	Phosphatidylinositol 3-kinase
PI-3-P	Phosphatidylinositol-3-phosphate
PIP3	Phosphatidylinositol (3,4,5)-trisphosphate
PKA	Protein kinase A
PMSF	Phenylmethylsulfonyl fluoride
PMT	Photomultiplier tube
PONR	Point-of-no-return
PPP	Pentose phosphate pathway
PSEN	Presenilin
PTEN	Phosphatase and tensin homologue deleted from chromosome 10
PVDF	Polyvinydilene difluoride
RIPA	Radioimmunoprecipitation assay buffer
RIPK1/RIP1	Receptor-interacting protein kinase 1
RNA	Ribonuclein acid
ROS	Reactive oxygen species
sAPPα	Soluble peptide APPα
SDS-PAGE	Sodium-dodecyl-sulfate-polyacrylamide gel electrophoresis
SQSTM1	Sequestome 1 (p62)
T2DM	Type 2 diabetes mellitus
TBS-T	Tris-buffered saline-Tween
TCA	Tricarboxylic acid
TEM	Transmission electron microscopy
TMRE	Tetramethylrhodamine ethyl ester
TNF	Tumour necrosis factor
TNFR	TNF receptor 1
Tris-HCl	Trisaminomethane hydrochloride
TSC	Tuberous sclerosis complex
ULK-1	Unc-51 like autophagy activating kinase 1

v-ATPase   Vacuolar H$^+$-ATPase

WST-1   Water soluble tetrazolium salt 1

YFP   Yellow fluorescent protein

Units of measurement

%	percentage
°C	degrees Celcius
µM	micromolar
µmol	micromole
µg	microgram
µl	microlitre
µm	micrometre
cm	centimetre
h	hour
hrs	hours
l	litre
min	minute(s)
ml	millilitre
mm	millimetre
mM	millimolar
ng	nanogram
nM	nanomolar
nm	nanometre
pM	picomolar
rpm	rotations per minute
sec	second(s)
V	volt

MOTIVATION FOR STUDY

Alzheimer's disease is the most prevalent neurodegenerative disease and the greatest contributor towards dementia. Its prevalence is increasing, and it is predicted that the global number of patients will rise to 106.8 million by 2050 (Brookmeyer *et al.,* 2007). Furthermore, low and medium income countries will be especially adversely affected, thus South Africa is substantially implicated in the disease burden (Wortmann, 2012). Researchers face the challenge of a multifaceted disease pathology. The identification of the major molecular disruptions involved, as well as identifying early events in the pathogenesis are crucial in order to prevent neurodegeneration. Currently no single disease modifying treatment exists. Mitochondria are present in high numbers in neurons and are essential for ATP synthesis. However, during Alzheimer's disease their functioning is impaired (Pagani and Eckert, 2011) and it is becoming increasingly clear that the dysfunction in ATP production is central in the disease pathogenesis. Macroautophagy,also referred to as autophagy is a major protein degradation system that plays an important role in cellular survival, likely through supplying metabolic substrates. Dysregulated autophagy has been identified in Alzheimer's disease (Nixon and Yang, 2011). Ketone bodies, a major alternative to glucose for fuelling the brain, have shown promising results in reducing the pathophysiological changes associated with Alzheimer's disease both molecularly and functionally (Van der Auwera *et al.,* 2005; Henderson *et al.,* 2009). However, the underlying molecular mechanisms that connect ketone bodies, amyloid aggregation, autophagy and ATP availability remain unclear. Therefore, in order to fully understand the efficacy of ketone bodies as a potential therapeutic strategy for Alzheimer's disease, it is necessary to understand their effects on the mechanisms that govern neuronal survival.

Chapter 1: LITERATURE REVIEW

1.1 Introduction

Alzheimer's disease (AD) is the most prevalent neurodegenerative disease, and the greatest contributor towards dementia. The global prevalence is increasing and it is estimated that the global number of AD patients will rise to 107 million by 2050 (Brookmeyer *et al.*, 2007). It is predicted that low and medium income countries will especially be adversely affected, placing South Africa at a greater risk for the number of people suffering from AD (Wortmann, 2012). High rates of dementia have a great economic impact as well; the total global societal cost of dementia in 2009 alone was estimated at $422 billion (Wimo *et al.*, 2010). There is currently no cure for AD, and the growing burden of disease makes finding an effective treatment for it a high priority. No single cause for the disease has been established thus far, however aging is likely the most important risk factor for developing AD (Saido, 2013). Moreover, pathological changes take place in the brains of aging patients years before overt AD manifests, thus illustrating the long disease progression (Chong and Sahadevan, 2005).
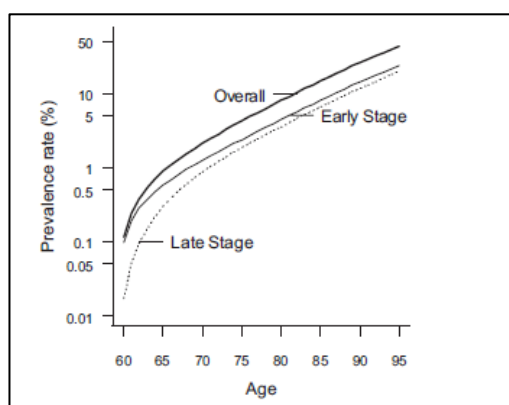
Figure 1.1: The prevalence rates of Alzheimer's disease according to disease state. (Brookmeyer *et al.,* 2007).

South Africa is a newly developing nation, with high levels of unemployment and poverty, and income inequality remains a major national challenge (Leibbrandt *et al.*, 2012). A polarized burden on health persists as well; non-communicable diseases are on the increase, while infectious diseases and maternal and child mortality still persists (Chopra *et al.*, 2009). In South Africa, an increase in age, together with illiteracy or lack of education, depressive illness, low fibre diet and vascular disease have been identified as factors increasing the risk for developing dementia, AD or vascular dementia (Kalaria *et al.*, 2008).

2

This presents a unique set of risk factors that increases the likelihood for developing dementia in this country (Kalaria *et al.*, 2008). Thus it is necessary to explore the link between the risk factors of aging, diet, metabolism and AD, and accordingly these will be discussed in this review.

In order to understand the underlying molecular mechanisms that drive the process of disease progression in AD, we have to turn our attention to physiological neuronal metabolism, their metabolic demands and protein degradative pathways first and then summarise the pathological changes characteristic of AD.

1.2 Overview of cerebral functioning

a. Neuronal metabolism

AD is an illness affecting primarily neuronal cells which have specific metabolic requirements. A brief overview of neuronal metabolism is necessary to understand neuronal cell death which occurs during AD.

The brain consists of primarily two cell types – neurons and astrocytes (glial cells or glia). These two cell types are highly interconnected and form functional networks through their spatial organization. Their metabolic profiles also reflects this co-dependency, by their utilization of different but complementary pathways (Bélanger *et al.*, 2011).

The brain contains sparse energy reserves, yet neurons have a high energy demand. Thus, a constant supply of energy substrates from the circulation is necessary. Glucose is considered the essential substrate but other metabolites derived from glucose such as pyruvate, lactate, and glutamate as well as alternative fuel sources such as ketone bodies (KB) can also be catabolized. Phosphorylated glucose, or glucose-6-phospate (glucose-6P), can enter one of three metabolic pathways to produce adenosine triphosphate (ATP). The first is glycolysis, which generates pyruvate, two ATP molecules and the reducing equivalent NADH (Bélanger *et al.*, 2011). Pyruvate can be further metabolised in the tricarboxylic acid (TCA) cycle and oxidative phosphorylation (OxPhos) in the mitochondria. Oxygen is required as an electron acceptor to generate the final products of 30-34 molecules of ATP and CO_2 in this route. An alternative use of pyruvate is its reduction to lactate by lactate dehydrogenase (LDH) in the

cytosol (Bélanger *et al.*, 2011). The second pathway to utilize glucose-6P is the pentose phosphate pathway (PPP) where the reducing equivalent NADPH is produced. A third avenue, possible in astrocytes, is glycogenesis where glucose-6P units are stored as glycogen. Indeed, astrocytes are the main site of glycogen storage in the adult brain (Bélanger *et al.*, 2011).

Astrocytes can be distinguished from neurons by their functional qualities. The definition of mature astrocytes includes the features of nonexcitability i.e. astrocytes cannot generate action potentials, measure of glycogen granules present, and close proximity and interactions with blood vessels through astrocytic processes (Kimelberg, 2010). These features provide a clue to the overarching function of astrocytes – to support neuronal activity. Astrocytes are much more than the static support network of cells previously thought, however. Evidence suggests that they are also 'excitable' in the sense that they are capable of releasing a host of molecules, so-called 'gliotransmitters', in response to internal or external stimuli (Volterra and Maldolesi, 2005). An example is the release of glutamate from astrocytes and subsequent neuronal activation in response to increased intracellular calcium.   Other functions of astrocytes include neuronal synchronization, by their involvement in stimulating postsynaptic neuronal excitability, and the regulation of cerebral blood flow by calcium-dependent gliotransmission, which facilitates changes in arteriolar tone (Volterra and Maldolesi, 2005). Astrocytes also form a close association with synapses and actively control synaptic transmission through their role in synapse formation, function and elimination (Chung *et al.*, 2015). In addition to these functions, it has been demonstrated that astrocytes occupy discrete regions without overlap, i.e. neighbouring astrocytes do not share the same underlying neuropil (Bushong *et al.*, 2002). In addition, Halassa *et al.* (2007) reported that a single astrocyte contacts 300-600 dendrites to form 'synaptic islands'. These findings illustrate the high dependence of neurons on glia.

Astrocytes play a key role in coupling synaptic activity to glucose metabolism. They are stellate cells with multiple processes that form a close interaction with capillaries and synaptic contacts, which are rich in neurotransmitter receptors, including glutamate receptors (Magistretti and Pellerin, 1999). These features make astrocytes ideally suited to their coupling role. Glutamate is the cerebral cortex's primary excitatory neurotransmitter.

4

The activation of afferent pathways triggers glutamate release from activated synaptic terminals, which affects the excitability of target neurons by binding to its receptors. Glutamate is swiftly taken up again by astrocytic processes which terminates its actions on postsynaptic neurons, a reaction dependent on the electrochemical gradient of sodium (Magistretti and Pellerin, 1999). Following re-uptake into astrocytes, glutamate is converted into glutamine which is released and taken up by neurons to replenish their glutamate reserves (Figure 1.2). Glutamate uptake by astrocytes also has a metabolic effect – it stimulates glucose utilization and lactate production via aerobic processes in affected cells. This process operates independently of glutamate receptors, but the activation of the Na^+/K^+-ATPase pump is a central event. Intracellular sodium levels rise concomitantly with glutamate uptake which activates the Na^+/K^+-ATPase and in this way stimulates glucose uptake and glycolysis (Magistretti and Pellerin, 1999).
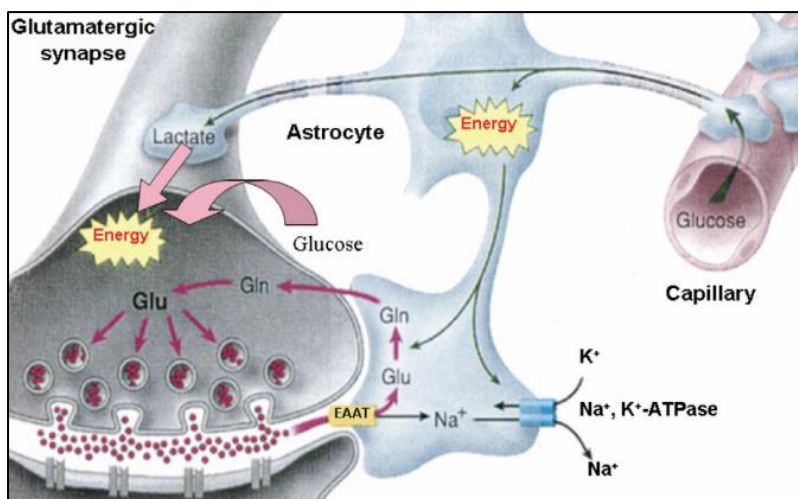
Figure 1.2: Neuron-glia metabolic coupling and glutamate shuttling (from Magistretti, 2006).

Astrocytes rely predominantly on the biochemical pathway of glycolysis as opposed toOxPhos, and freely take up glucose to convert it to lactate for ATP synthesis (Bélanger *et al.*, 2011). The preference for lactate as fuel substrate, as opposed to pyruvate, is a result of gene expression patterns in astrocytes. Specific enzymes are synthesized in accordance with these patterns, for example 6-phosphofructose-2-kinase/fructose-2,6-bisphosphatase-3 (PFKFB3), which activates the glycolytic enzyme phosphofructokinase-1 (PFK), is highly expressed. Low expression levels of the aspartate/glutamate carrier (AGC) are present and the conversion of pyruvate to lactate is favoured by inactivation and/or low expression of

pyruvate dehydrogenase (PDH) resulting in less pyruvate entering the TCA cycle (Bélanger *et al.*, 2011). This is important since the enzyme profile in this context dictates local availability of ATP (De Bock *et al.,* 2013).

Neurons are characterized by high energy demands, due to the high levels of macromolecule synthesis; a process which consumes the most ATP within cells (Buttgereit and Brand, 1995). They are mainly dependent on the OxPhos of substrates; a logical situation when one considers that OxPhos produces about 15 times more ATP than glycolysis (Bélanger *et al.*, 2011). The specific molecular features of neurons are responsible for their distinct metabolic profile. The glycolytic enzyme PFKFB3 is virtually non-existent in neurons due to its constant degradation, in contrast to the situation in astrocytes (Bélanger *et al.*, 2011). As a result there is a far lower rate of glycolysis. Experimental upregulation of glycolysis is not metabolically favourable and in fact detrimental to neurons, as it leads to apoptosis and oxidative stress (Herrero-Mendez *et al.*, 2009). This is thought to occur as a result of decreased flux through the PPP and thus diminished production of NADPH – an important antioxidant. An alternative fuel source utilized by neurons is lactate. It has been demonstrated that lactate is a preferred substrate above glucose (Smith *et al.*, 2003). Ketone bodies also have the ability to support basal energy needs, given that they are present at a sufficient concentration to saturate metabolism. It has recently been shown that they provide approximately as much as half of neurons' oxidative needs during activity (Chowdhury *et al.*, 2014). This matter deserves further attention in order to elucidate the extent of reliance on ketone bodies as an energetic substrate.

An increase in ketone metabolism represents a return to an early developmental pathway of substrate utilization, not usually relied upon for energy production in adulthood (Prins, 2008). Utilization of ketone bodies is an adaptive response to provide energy. It has very different properties to glucose metabolism that are relatively new and promising for example it has been shown to confer neuroprotection, which will form a focus point of this thesis. These properties mostly have the net effect of increased energy efficiency and antioxidant capacity (Prins, 2008). Its metabolism leads to specific beneficial outcomes which include: (i) areduction of the nicotinimide adenine dinucleotide (NAD) couple, (ii) a decrease in reduced Co-enzyme Q (translating to less superoxide formation), and (iii) a

reduction in the number of biochemical reactions required to enter the TCA cycle (Prins, 2008).

Different methods that assess brain metabolism have revealed tight coupling between energy demand and supply in the brain. Magnetic resonance imaging (MRI) is a tool widely used in diagnostic medicine to generate not only structural images of the organs but also data on the vascularization, perfusion and physico-chemical state of tissues (Logothetis, 2008). Functional MRI (fMRI) further enhances the scope of MRI as it enables the measurement of hemodynamic changes after enhanced neural activity. It is frequently used to demonstrate which areas of the brain are activated in response to execution of a specific task. The blood-oxygen-level-dependent (BOLD) contrast mechanism is routinely used to generate images of the human brain (Logothetis, 2008). Positron emission tomography (PET) is a technique where positron emitting radioisotopes are used to tag biologically active molecules. A positron-labelled probe is administered intravenously and a PET-scan is performed to determine the tissue concentration of the probe and labelled products over a certain period. An example of such a probe is 2-[F-18]fluoro-2-deoxy-D-glucose (FDG). FDG is an F-18-labelled glucose analog which is used to investigate the facilitated transport and phosphorylation of glucose. It is commonly used to study altered metabolic states which occur in disease states of the brain (Phelps, 2000). Pittsburgh compound B (PIB) is used to tag deposits of amyloid beta (Aβ) peptide, an important protein in AD pathology, present in neuronal tissue (Forsberg *et al.*, 2008).

b. The role of mitochondria in metabolism

Mitochondria are crucial for ATP generation, as well as for monitoring cellular functions such as the activation of cell death pathways and calcium regulation. They generate energy via the biochemical processes of the TCA cycle and OxPhos. Mitochondria are present in especially high numbers in the perikarya and the synapses (Pagani and Eckert, 2011), areas of high energy demand in functioning neurons.

Mitochondria exist as an interconnected network which is subject to dynamics of two opposing events: mitochondrial fission and fusion. Mitochondria are continuously moving along intracellular tubulin network structures and can present as fused with other

mitochondria (fusion) or as fragmented from the network to produce distinct rod or sphere shaped mitochondria (fission). In healthy neurons fission and fusion is in a state of equilibrium and facilitates intracellular movement of mitochondria. Mitochondrial networks comprised of fused mitochondria are beneficial to metabolically active cells, as this conformation favours ATP distribution. Fission in contrast is observed more often in quiescent cells (Westermann, 2010). Furthermore, fission is linked to cell death, as a result of defective mitochondria produced by fragmentation, while fusion is important for maintaining mitochondrial function and a healthy mitochondrial pool (Chan, 2006).

These dynamic events are controlled by different proteins belonging to the dynamin family. Dynamin related protein (Drp1) and fission protein (Fis1) are primarily responsible for fission (Reddy, 2009). Fis1 is localized on the outer mitochondrial membrane while Drp1 is mostly cytosplasmic, but a small fraction associates with the outer mitochondrial membrane which promotes mitochondrial fragmentation. Free radicals activate Fis1 to induce fission. Three major proteins are primarily responsible for controlling fusion. These are the mitofusin proteins Mfn1 and Mfn2, present on the outer mitochondrial membrane, and Opa1, localized on the inner mitochondrial membrane. Mfn1 allows fusion by mediating an oligomerization reaction between Mfn molecules of adjacent mitochondria (Reddy, 2009).

During apoptosis, fragmentation of the mitochondrial network occurs. Cells with Fis1 deficiency display increased fusion as well as resistance to apoptotic cell death. Opa1 depletion has shown the opposite effect – mitochondria in these cells are extensively fragmented and cells have an increased vulnerability to cell death (Lee *et al.*, 2004). The network state of mitochondria is sensitive to metabolic perturbations and can adapt to metabolic pertubations such as. a high fat diet or starvation by favouring fission or fusion (Hoppins, 2014). However, it has to be noted that the elucidated response is cell-type specific (Dietrich *et al.,* 2013). Furthermore it has been demonstrated that AMP-activated kinase (AMPK), a cardinal metabolic sensor, is activated when even mild disturbances in cellular ATP occur and in this way it acts as a primary sensor of mitochondrial function (Green *et al.,* 2014).

Mitochondria are responsible for cellular energy production and as such, are vital to maintaining cellular function. The next section will discuss ATP, the chief energy molecule

produced by mitochondria and utilized by cells in a hierarchy of ATP consuming processes (Buttgereit and Brand, 1995).

c. <u>ATP and neuronal metabolism</u>

The brain has high energy demands and although it competes with several other organs in terms of energy metabolism, its metabolic rate is nine times higher than the average mass-specific metabolic rate of the human body as a whole (Aiello and Wheeler, 1995). It metabolizes 50% of total body glucose, but constitutes only 2% of the body mass (Fehm *et al.*, 2006). ATP is the energetic 'currency' to which metabolic substrates such as glucose are broken down to, and is important for providing energy in order for cells to function. Dzeja and Terzic (2003) provide evidence that demonstrates the precisely controlled coupling between ATP demand and supply by an enzymatic network. This coupling is tightly regulated so that fluctuations in intracellular adenine nucleotide concentrations are rarely observed, even with increased metabolic flux (Dzeja and Terzic, 2003).

Synapses are heavily dependent on local ATP synthesis on functioning mitochondria, because of the great distance between neuronal cell soma and synaptic terminals. Electrical signalling processes and synaptic transmission consume the most ATP in the brain, based on a breakdown of activities that this entails, including ion pumping and vesicle recycling (Harris *et al.,* 2012). This is supported by Buttgereit and Brand (1995) who demonstrated that sodium and calcium cycling was the second greatest ATP-consuming process in cells. ATP is provided by the numerous mitochondria which occur here, precisely to generate ATP that can meet neuronal energy demands. The relationship between ATP demand and its localization is demonstrated by the fact that synaptic activity contributes significantly to ATP consumption and that it, in turn, fuels ATP production (Harris *et al.*, 2012). Despite evidence of ATP localizing at the synapses of neurons, there are few studies focusing on the localization of intracellular ATP, however some studies illustrate the strength of emerging techniques that focus on ATP localization in cells.
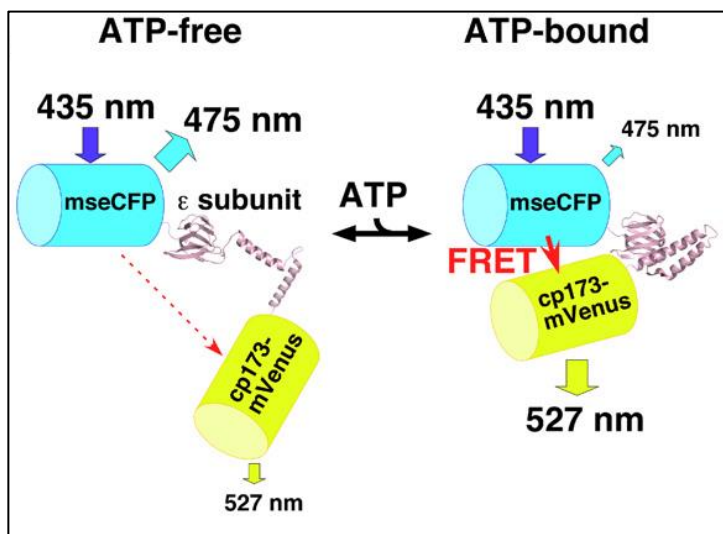
Figure 1.3: Schematic drawing of FRET-based ATP probe ATeam, AT1.03 which allows ATP localization studies (Imamura *et al.*, 2009).

There has been an increasing trend of monitoring ATP in single living cells using imaging and videoing techniques. These techniques become more accessible to researchers with the development and availability of advanced techniques such as super-resolution microscopy. Imamura *et al.* (2009) laid the groundwork for a live cell imaging method with an ATeam construct which labels intracellular ATP, targeted to particular regions. A Förster resonance energy transfer (FRET)-based ATP indicator was developed that consists of cyan and yellow fluorescent proteins (CFP and YFP) situated on either side of the ε subunit of bacterial F_oF_1-ATPase. Conformational changes are induced upon ATP binding and result in increased FRET efficiency (Figure 1.3). This type of assay provides an advantage compared to the ubiquitous luminescence assay as chemiluminescence is affected by other substrates, intracellular oxygen and pH, and its imaging is labour-intensive (Imamura *et al.*, 2009).

ATP visualization in live cells allows assessment, in real time, of its association with other cell components. In addition, it has the advantage of providing high spatial and temporal resolution. Another study utilizes a novel method to visualize ATP and demonstrates the experimental power of monitoring ATP in cells. The authors used a genetically encoded reporter of synaptic ATP to demonstrate the link between energy demand and availability. In that manner it was revealed that electrical activity places significant demands on ATP

10

production particularly in presynaptic terminals, and also drives ATP synthesis (Rangaraju *et al.*, 2014). De Bock *et al.* (2013) visualized ATP 'hotspots' by using the biosensor GO-ATeam. Large amounts of ATP are required for the contraction and protrusion of cellular extensions (lamellipodia and filopodia) of the cell tips, as they rely on remodelling of the actin cytoskeleton. Endothelial cell motile structures are situated far from mitochondria and thus rely on glycolysis for local ATP production. The authors describe high ATP concentrations in lamellipodia, and furthermore reveal that silencing PFKFB3, the glycolytic enzyme previously explained,, abolished this localization. Thus ATP is not uniformly distributed in the cell and metabolic demands determine where ATP is localized. This has thus far been confirmed in endothelial cells, and it can be speculated that this is also the case in neurons based on the high ATP levels present at synapses. Results such as these strongly suggest that it is possible, and highly informative, to deduce cellular ATP demands from the intracellular localization of ATP. Moreover, the subcellular localization of ATP is not routinely assessed, and research into neuronal ATP localization patterns is lacking. In addition, the localization of ATP in the presence of ketone bodies or during autophagy dysfunction remains largely unclear.

As we shall see, the protein degradation pathway of macroautophagy plays a particularly central role in neuronal metabolism and pathology, as it provides another means of contributing ATP under stress conditions.

d. Autophagy and lysosomes in the context of cellular metabolism

In 1955 De Duve and colleagues discovered a pattern in rat liver enzyme distribution which lead to the identification of lysosomes and the birth of autophagy research. The seminal work of the Yoshimori lab (Kabeya *et al.*, 2000) identified LC3-I and LC3-II, the first mammalian proteins associated with autophagosomes to be identified. Since then, a vast body of research has expanded our knowledge of the molecular factors involved in the process of autophagy. Autophagy is vitally important for survival, as demonstrated by the finding that mice in which autophagy is downregulated by deleting Atg3 die within a day of birth (Sou *et al.*, 2008). In addition, autophagy inhibition leads to neurodegeneration, as demonstrated by mouse models with Atg5 and Atg7 knockouts (Hara *et al.* 2006; Komatsu *et al.* 2005).

Autophagic machinery

Macroautophagy (from here onwards referred to as 'autophagy'), microautophagy and chaperone mediated autophagy represent one of two main protein catabolic pathways together with the ubiquitin-proteasome system (Nedelsky *et al.*, 2008). Autophagy is a dynamic process during which double-membraned sequestering vesicles, termed autophagosomes, encapsulate part of the cytosol and damaged organelles, fuse with lysosomes which contain acidic hydrolases, thereby degrading macromolecules into their constituents e.g. amino acids. The process of autophagy is characterized by discrete steps (Klionsky, 2005): (1) induction, (2) cargo selection, (3) nucleation of vesicle formation, (4) vesicle expansion and completion, (5) retrieval, (6) targeting, docking and fusion of the vesicle with the lysosome/vacuole and (7) breakdown of the intraluminal vesicle. It is possible for multiple lysosomes to fuse with a single autophagosome. Once autophagosomes have released their digested cargo back into the cytosol, lysosomes are reformed to enter the autophagic cycle again. Increased mammalian target of rapamycin (mTOR) activity drives the process of lysosome reformation, by generating proto-lysosomal structures that extrude from autophagolysosomes and mature to supplement the lysosomal pool and maintain lysosomal homeostasis (Yu *et al.*, 2010). Amino acids that are produced during autophagy-driven proteolysis exit autophagolysosomes through the vacuolar effluxers Atg22, Avt3, and Avt4 which transport them across the autophagolysosomal membrane into the cytosol (Yang *et al.*, 2006).

Lysosomes play a vital role in the process of autophagy, as they enable the degradation of various substrates. They are comprised of a single-lipid bilayer membrane which encapsulates several types of hydrolases (Settembre *et al.*, 2013). Transport proteins in the membrane facilitate the transport of both intra- and extracellular proteins as well as acidification of the lumen and fusion with other structures. Apart from their established role in clearing substrates, lysosomes have other functions including activities related to lysosomal exocytosis and signalling pathways involving nutrient sensing, metabolism and cell growth (Settembre *et al.*, 2013). However, research regarding these alternative roles of lysosomes is still in its early phases. The importance of functioning lysosomes is demonstrated by lysosomal storage diseases (LSDs). LSDs are inherited metabolic

dysfunctions which are caused by mutations in genes encoding proteins that are necessary for lysosomal function e.g. lysosomal membrane or lumen proteins (Settembre *et al.*, 2013). As a result individuals with these disorders display the progressive accumulation of material destined for lysosomal degradation. More than 60 LSDs have been identified, with classification based on which material accumulates in lysosomes. Patients with LSDs frequently display neurodegeneration as well as cognitive decline, suggesting a particularly high neuronal reliance on functional lysosomal clearance (Settembre *et al.*, 2013). The link between disrupted cellular clearance methods and neurodegeneration will be discussed later.

There are more than 30 known genes regulating autophagy in yeast, many with mammalian orthologs (Ravikumar *et al.*, 2010). Atg proteins drive the different processes of autophagy (Mizushima *et al.*, 2010). The autophagosomal membrane is thought to form from intracellular membranous structures such as the endoplasmic reticulum (ER), mitochondria and the Golgi body upon induction by the Beclin-Vps34 complex. Following induction, elongation is facilitated by the actions of two ubiquitin-like reactions (Ravikumar *et al.*, 2010). First, activated Atg12 forms a covalent bond with Atg5, after which the Atg12-Atg5 complex conjugates with Atg16L1. In the second reaction microtubule-associated protein 1 light chain 3 (MAP1-LC3 or LC3) is cleaved to form LC3-I in the cytosol. LC3-I is then conjugated to phosphatidylethanolamine (PE) to form LC3-II via the actions of Atg3 and Atg7. LC3-II is the only known Atg protein to remain associated with the autophagosomal membrane, and as such is a valuable molecular marker for autophagy (Ravikumar *et al.*, 2010). Sequestome 1 (SQSTM1), or p62 is another protein used in this regard, as it is involved in the targeting of poly-ubiquitinated proteins towards autophagolyosomes for degradation (Barth *et al.,* 2010).

Control of autophagy induction and its link to metabolism

Autophagy is tightly linked to cellular metabolism, energy sensing and mitochondrial function. Several different signalling pathways in mammals are involved in regulating autophagy in this context. The first of these is the mTOR pathway, which is the most widely studied (Ravikumar *et al.*, 2010). Many different pathways affect autophagy via their actions on the mTOR complex 1 (mTORC1) consisting of various different proteins (Figure 1.4).

Importantly, it negatively regulates autophagy by phosphorylating ULK-1. Rapamycin binding strengthens the association of mTOR with Raptor, another mTORC1 protein, and inhibits the mTOR kinase activity. On the one hand, the phosphatidylinositol 3-kinase (PI3K) pathway, triggered by insulin binding to its cell surface receptor, acts on mTOR, in the process eithersuppressing autophagy (Ravikumar *et al.*, 2010). Theclass I PI3K product PIP$_3$ activates Akt, thereby inhibiting autophagy. Akt phosphorylates and inactivates the tuberous sclerosis complex (TSC) 1/2, which will lead to mTOR activation. In addition, it inhibits the transcription of autophagy genes. The class III PI3K product, PI-3-P, in contrast stimulates autophagy when its levels increase. Phosphatase and tensin homologue deleted from chromosome 10 (PTEN) stimulates autophagy by inhibiting the PI3K pathway upstream of mTOR (Ravikumar *et al.*, 2010).

Amino acids suppress autophagy through the mTORC1 pathway. Influx of essential amino acids causes their binding to and stimulation of Rag GTPases present on the lysosome associated protein, Ragulator. This recruits mTORC1 to the lysosomal surface and suppresses autophagy (Sarkar, 2013). The phenomenon of macrolipophagy, the regulatory function of autophagy on intracellular lipid stores is another example of substrate-driven control of autophagy. Lipid metabolism and autophagy both provide nutrients during times of nutrient deprivation and share further similarities in their function and regulation (Singh *et al.*, 2009). Autophagy is crucial for lipid droplet breakdown and its inhibition increases lipid storage. Autophagic pathway components facilitate lipid metabolism by associating with lipid droplets during starvation (Singh *et al.*, 2009).

AMPK is a cellular energy sensor which detects changes in the intracellular ATP/AMP ratio. It activates TSC2 directly through phosphorylation, priming it for phosphorylation by glycogen synthase kinase 3 (GSK3) effectively inhibiting mTORC1 (Ravikumar *et al.*, 2010).

Regulation of autophagy can also occur in an mTOR-independent fashion. Several signalling cascades are involved here (Sarkar, 2013). Adenylate cyclase mediates the increase of cyclic AMP (cAMP) by converting ATP activating the PKAsignalling pathway. In turn phospholipase C leads to the the production of inositol triphosphate (IP3) and diacylglycerol (DAG)suppressing autophagy by the release of calcium from the ER and influx through calcium channels. This prevents fusion of lysosomes and autophagosomes, and thus the

maturation of autophagosomes. In addition, PKA can directly phosphorylate and thus modulate the activity of calcium channels, illustrating crosstalk between these two pathways (Marx *et al.,* 2000). Increased calcium also activates calpain, which inhibits autophagy (Sarkar, 2013). Inhibition of nitric oxide synthase (NOS) stimulates autophagy by inhibiting c-Jun N-terminal kinase 1 (JNK1) and its downstream effects. Starvation, in turn, activates JNK1 and autophagy by disrupting the interaction of Bcl-2 and Beclin-2, which normally suppresses autophagy. Pharmaceutical drugs targeting specific proteins in these pathways can be used to induce or inhibit autophagy (Sarkar, 2013).

Recently, acetyl-coenzyme A (AcCoA), a major metabolite generated by fatty acid, protein and carbohydrate catabolism, was identified as an important regulator of autophagy. It has been demonstrated that increasing cytosolic AcCoA inhibits autophagy and decreasing levels induces it (Mariño *et al.*, 2014). The authors found that depleting AcCoA reduced the activity of E1A binding protein p300 (EP300), an acetyltransferase which is required for the suppression of autophagy when high levels of AcCoA are present. They surmise that the acetylation of Atg proteins by EP300 is the mechanism of its action, yet further investigation is required to eliminate other targets of EP300. These data further indicate the strong integration of the autophagy pathway and cellular metabolism.

The brain is uniquely sensitive to stresses that upregulate autophagy. This may be achieved by different conditions including starvation, exercise and treatment with pharmacological
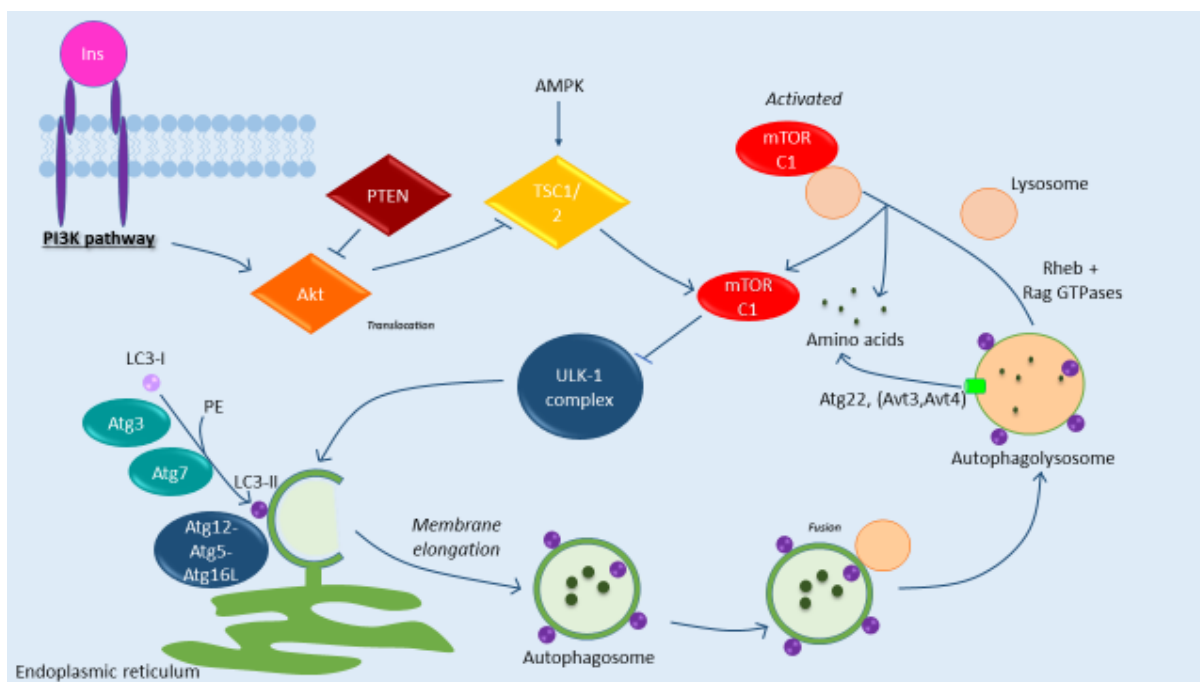
Figure 1.4: Autophagy generates metabolic substrates through continuously recycling lysosomes.

agents such as rapamycin (He *et al.,* 2012a; Kuma *et al.,* 2004; Ravikumar *et al.,* 2004). Neurons treated with 5 nM rapamycin for 1 h demonstrate rapidly induced autophagy as evidenced by a decrease in phosphorylated p70S6 kinase (p70S6K) activation mediated by mTOR when compared to controls (Boland *et al.,* 2008). Decreased mTOR activity was sustained after 6 h and 24 h treatment with rapamycin at the same concentration, with LC3-II levels increased at both measured time points. Majumder *et al.* (2011) elegantly revealed that administering rapamycin (14 mg/kg) in chow to two month old transgenic AD mice across their lifespan induces autophagy in the brain as indicated by decreased p70S6K protein levels. Moreover, autophagy is also induced in transgenic mice that were fed the rapamycin-containing diet for three months from the age of 15 months (Majumder *et al.,* 2011). Exercise is a potent inducer of autophagy in the brain. Rats performing an acute bout of exercise (95 min of treadmill exercise) had significantly increased autophagy markers as assessed by Western blot analysis and GFP-LC3 puncta count in brain slices (He *et al.,* 2012a). Mice subjected to 1 h of treadmill exercise demonstrated a significant upregulation in the conversion of LC3-I to LC3-II as indicated by Western blot analysis as well as increased

GFP-LC3 puncta visible in skeletal muscle, compared to non-exercised littermates (Grumati *et al.,* 2011).

Starvation is a well-documented inducer of autophagy. Kuma *et al.* (2004) demonstrated in a mouse model that autophagy is induced during the early neonatal starvation period, occurring when pups are deprived of the nutrients supplied across the placenta and before they are suckled. The authors analysed primarily GPF-LC3 punctae and amino acid levels in different tissues and identified a marked plasma decrease of amino acids. These data indicate the major physiological role of functional autophagy. Brain tissue levels were not analysed by this group (Kuma *et al.,* 2004). Neurons exposed to serum starvation, grown in glucose containing-medium without amino acids and other growth factors, display autophagy induction as indicated by increased LC3-II protein levels in the presence of the lysosomal inhibitor leupeptin, as well as increased presence of autophagolysosomes (Boland *et al.,* 2008).

Measuring autophagic flux

Different tissues express autophagic activation to different degrees. Mizushima *et al.* (2004) generated a GFP-LC3 mouse to monitor the induction of autophagy in different organs in response to starvation, which allows visualization of autophagic vacuoles (AV). Interestingly, the brain did not show autophagy induction even after 48 h starvation. An important consideration relating to this finding is that purely measuring cellular levels of LC3 is not sufficient to make deductions about autophagy levels as autophagosomal cargo is continuously degraded. It has therefore been proposed that lysosomal turnover be used as marker instead (Tanida *et al.*, 2005; Barth *et al.,* 2010). It has been suggested that the apparent absence of autophagy induction in brain tissue may simply be the expression of an efficient turnover of AV, which will result in the rapid degradation of LC3-II. An example to illustrate the pitfalls of a static measure of autophagy is provided: LC3-II levels will increase either in the case of increased autophagosome synthesis, or if LC3-II degradation is blocked at any stage of autophagy after autophagosome formation (Rubinsztein *et al.*, 2009). Thus, the utilization of lysosomal fusion inhibitors is crucial in order to interpret results related to autophagy activity (Rubinsztein *et al.,* 2009).

Autophagic flux is defined by the extent of autophagic degradation activity, and thus by the rate of measured autophagic degradation (Loos *et al.,* 2014). Various methods for measuring 'autophagy' exist, but only some of them consider changes in autophagosomal numbers over time (Klionsky *et al.*, 2012). Transmission electron microscopy, GFP-LC3 fluorescence microscopy and LC3 detection and quantification are examples of frequently used methods to measure autophagy, most often *in vitro*. *In vivo* methods to measure the autophagic flux of organs is a poorly developed area of research currently, yet it is of great importance as basal autophagy levels, the time course of autophagy induction and the bioavailability of drugs that induce and inhibit autophagy are likely tissue specific. Great care needs to be taken when interpreting autophagy markers (Klionsky *et al.,* 2012). LC3 is the most widely monitored autophagy-related protein and different methods utilize its detection. Western blotting can be performed to detect the ratio of LC3-I to LC3-II, which provides an indication of how efficiently the conversion from LC3-I to LC3-II occurs. However, the pattern of this conversion seems to be cell specific, and related to the type of stress cells are exposed to. Autophagic flux can more accurately be inferred by measuring the difference in LC3-II levels between samples in the presence and absence of autophagy inhibitors (Mizushima and Yoshimori, 2007). Inhibitors include lysosomal protease inhibitors E64d and pepstatin A, as well as bafilomycin A_1 which inhibits the fusion of autophagosomes and lysosomes (Mizushima and Yoshimori, 2007).

It is clear that autophagy is a crucial evolutionary conserved pathway to maintain homeostasis in conditions of nutrient stress, with a particular role in neuronal metabolism. Now that the high ATP demands, substrate preference and metabolic pathways of the brain have been highlighted, the focus will shift to the perturbations in these parameters observed in Alzheimer's disease.

1.3 The Alzheimer's disease brain

In this section the molecular disruptions observed in AD will be discussed first, followed by a summary of how AD and dementia are diagnosed, thirdly the different cell death modes by which neuronal loss occurs will be highlighted, fourthly the role of mitochondrial function in AD followed by disrupted autophagy in AD and finally altered neuronal metabolism in AD will be discussed.

a. __Molecular disruptions present in Alzheimer's disease__

Defective autophagy is a feature of numerous neurodegenerative diseases including AD. The exact nature of the observed dysfunction will be discussed in section 1.3d. The focus will now move to the underlying cause of neurotoxicity in AD. Neurodegenerative diseases include AD, Parkinson's disease (PD) and Huntington's disease (HD). They are each characterized by the accumulation of specific abnormal proteins, such as Aβ and tau in AD, α-synuclein in PD and huntingtin protein in HD, each affecting particular brain regions. Despite the differences in the aetiology of these diseases, they share the symptom of protein aggregation (Swart *et al.*, 2014). Protein aggregation is the association of two or more non-native protein molecules. Aggregation most often occurs with partially folded or misfolded states of proteins (Hartl and Hayer-Hartl, 2009). The $Aβ_{1-42}$ peptide, the predominant peptide present in amyloid plaques, aggregates and forms oligomers, protofibrils and fibrils before being deposited to form plaques (Ahmed *et al.,* 2010). However, this process is not a one-way reaction – fibrils represent a dynamic state of constant breakdown to recycle their composite units to be reassembled (Carulla et al, 2005). The histopathological and molecular presentation of AD will be discussed first before delving deeper into the nature of the aggregates observed.

Two overt hallmarks have been identified post-mortem in AD brains; extracellular senile plaques and intracellular neurofibrillary tangles (NFTs). They were first described in the seminal work of German neuropathologist Aloïs Alzheimer more than a century ago (Alzheimer, 1911). NFTs contain hyperphosporylated tau (Grundke-Iqbal *et al.*, 1986), a protein which functions to stabilize tubulin while senile plaques are comprised largely by amyloid-β (Aβ) peptide (Roher *et al.*, 1996).

Tau is a neutral or slightly basic protein which forms part of the microtubule associated protein (MAP) family (Cleveland *et al.*, 1977). It is a hydrophilic protein which appears as a random coiled structure in solution. It mainly occurs in neurons and functions to stabilize microtubules (Avila *et al.*, 2004). Alternative splicing of exons two, three and ten generates six different isoforms in the central nervous system. AD is classified as the most common of the tauopathies - conditions resulting from abnormal tau levels, processing or mutations

(Avila *et al.*, 2004). Tau is hyperphosphorylated in AD, a reaction catalysed mainly by GSK3 (mainly GSK3β) at the amino acid residues threonine-231, serine-396 or -404. In nonpathological conditions, kinase-mediated phosphorylation of tau causes it to detach from microtubules, which allows for effective axonal transport (Ballatore *et al.*, 2007). Hyperphosphorylation causes tau to dissociate from microtubules and to form aggregated NFTs in the cytosol (Grundke-Iqbal *et al.*, 1986). Tau knockout mice have a deficiency in tau protein which partially delays neurodegeneration as indicated by dentate gyrus volume (De Barreda *et al.*, 2010). GSK3 overexpression is toxic to mice, but tau knockout ameliorates this effect, demonstrating the importance of tau in the pathology of neurodegeneration (De Barreda *et al.*, 2010).

Braak and Del Tredici (2012) delineate AD progression by using a staging model, important for determining disease severity. It encompasses both pre-tangle formation and NFT stages I-VI, each characterized by the extent to which NFTs are present. Immunostaining for abnormal tau (using AT8 antibody) reveals that a variety of brain regions are systematically affected. Vulnerable neurons in the locus coeruleus are affected first, followed by lesions in the entorhinal region of the temporal lobe, with cortical involvement seen only in NFT stages V and VI.
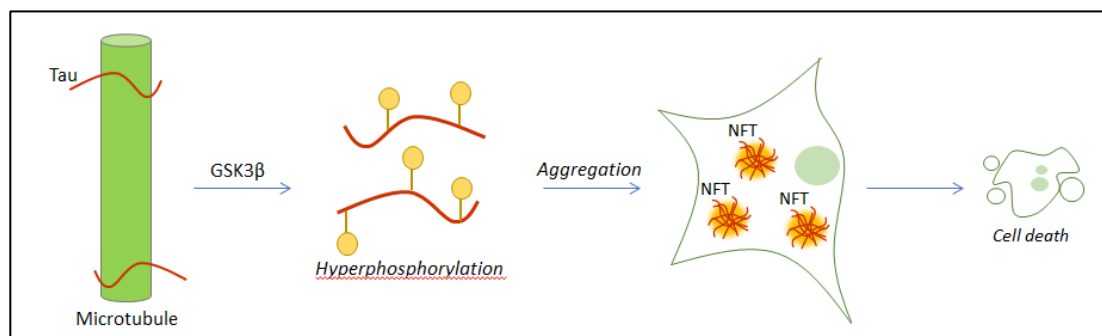
Figure 1.5: Tau hyperphosphorylation leads to neurofibrillary tangle formation.

The second major AD lesion, amyloid plaques, is comprised of Aβ peptide. Aβ is a physiologically occurring peptide derived from the processing of the membrane-spanning amyloid precursor protein (APP) which is present ubiquitously in the plasma and organelle membranes (Sambamurti *et al.*, 1992). The Aβ peptide plays an important role in synaptic physiology; however the precise role of APP is still largely unclear although it is known to be expressed in neurons (O'Brien and Wong, 2011). There are various pathways of APP

processing, and not all of them generate Aβ. APP is synthesized in the ER and Golgi apparatus and then transported along the axon toward the synaptic terminal's cell surface through the trans-Golgi network, where it inserts. The exact intracellular locus of APP processing is an important factor determining whether or not Aβ is produced. APP can be proteolyzed at the cell surface by α-secretase and γ-secretase, which produces an APP ectodomain (sAPPα) which diffuses rapidly. Alternatively, APP can re-enter the cell by being taken up into clathrin-coated pits and transported to endosomes which contain γ-secretase and beta-site APP-cleaving enzyme (BACE), produces the ectodomain sAPPβ, the APP protein intracellular domain (AICD) as well as Aβ. These peptides are released into the extracellular space by endosomes that translocate to the cell surface or are degraded in lysosomes (O'Brien and Wong, 2011). The enzymes governing APP processing have been identified. BACE1 is a transmembrane aspartic protease that cleaves APP at two sites. It is the neuronal β-secretase. Following BACE1 cleavage of APP, its C-terminal fragment (APP-CTF) is cleaved by the γ-secretase complex at one of many sites, situated at residue 40-44 to produce Aβ peptides. The γ-secretase complex is comprised of four proteins, of which one is presenilin 1 (PSEN1) or presenilin 2 (PSEN2). PSEN1 and PSEN2 contain two aspartyl residues which are crucial for intramembranous cleavage, an important function of the γ-secretase complex (O'Brien and Wong, 2011). Cells in which PSEN1 are deleted are characterized by a near complete abolition of autophagy, demonstrating an important function of PSEN1 in the autophagosomal/lysosomal degradation pathway. The PSEN1 holoprotein acts as a chaperone in the ER to facilitate maturation and targeting of the v-ATPase V0a1 subunit to lysosomes (Lee *et al.*, 2010). This subunit is essential for lysosome acidification and the activation of proteases, without which substrates cannot be degraded. These same functions are affected in patients with familial AD caused by PSEN1 mutation, though to a lesser degree.

There has been a change regarding the consensus of which form of the amyloid peptide aggregates, i.e. formation driven by oligomers or fibrillar plaques, and it is not clear which of these is the main agent causing neurotoxicity (Benilova *et al.*, 2012). Even though the exact aetiology of AD remains unknown, aberrant processing of APP and Aβ are unifying factors among different theories (Di Carlo *et al.*, 2010). Recent findings suggest Aβ being responsible for AD-related tau hyperphosphorylation, as the addition of soluble Aβ or

aqueous extract from AD brains stimulates tau phosphorylation at epitopes characteristic of AD *in vitro* (De Felice *et al.*, 2008; Jin *et al.*, 2011). This emphasizes the central role of Aβ in AD. However, it has to be remembered that tau and amyloid proteins are functionally linked as the transport of autophagosomes to lysosomes is dependent on a stable microtubule network (Swart *et al.*, 2014). Additional considerations in Alzheimer's research, apart from proteolytic cleavage pathways involved, are the rate of Aβ production, its removal rate and rate of fibril formation from soluble proteins (Shoji *et al.*, 1992). The rates of protein degradation pathways, such as autophagy, will here play an important role. It is important to identify the level of functioning of these parameters as it will determine neuronal health and thus resistance to cell death.

Oligomers and amyloid fibrils are toxic to cells and contribute to neurodegeneration (Hartl and Hayer-Hartl, 2009). However, literature suggests different sources of toxicity, i.e. either oligomers or fibrils present in amyloid plaques as the main agent responsible for neurodegeneration. Xie *et al.* (2013) demonstrated that plaques cause surrounding oxidative stress and contribute to toxicity and neuronal death in AD. However, the fibril-rich plaques appear not to be a direct cause of AD-associated dementia, rather the increased production of a toxic version of Aβ, the peptide $Aβ_{42}$, is central in the disease progression (Saido, 2013). It has been shown that neuronal cell loss is correlated with oligomeric Aβ load, and not with fibrillar amyloid plaque burden (DaRocha-Souto *et al.*, 2011). In this case 'Aβ load' (oligomers) refers to the percentage the cortex covered by immunostained amyloid deposits and 'amyloid plaque burden' refers to the area occupied by dense plaques staining positive for thioflavin S. Similarly, it has been found that $Aβ_{42}$ oligomers are more toxic than fibrils *in vitro* (Ahmed *et al.,* 2010).

Indeed, various studies have shown that oligomers are more potent inducers of disrupted synaptic function and neural networks than aggregates (Palop and Mucke, 2010). Synaptic function can be measured by the synaptic transmission strength and plasticity, while excitatory synapse transmission can be assessed by monitoring the expression levels of cell surface receptors such as the N-methyl-D-aspartate (NMDA) and A-amino-3-hydroxy-5-methyl-4-isoxazolepropionic acid (AMPA) receptors. It is also significant to note that AD transgenic mice exhibit altered physiology and neurites prior to plaque deposition

(Capetillo-Zarate *et al.*, 2006; Gillardon *et al.*, 2007). Furthermore, Gillardon *et al.* (2007) suggest that the Aβ-induced neurodegeneration is not caused by a simple increase in Aβ levels or plaques but rather the transition of Aβ protein to soluble oligomers or fibrils.

It has been elegantly demonstrated by the Finkbeiner lab (Arrasate *et al.*, 2004) that protein aggregation *per se* is not associated with cell death. In fact, the cells that survived the longest upon mutant huntingtin protein presence were those that also displayed protein aggregates or inclusion bodies. Ross and Poirier (2005) use many lines of evidence to support the theory that aggregates represent a cellular protective mechanism. However, the amount of Aβ deposit in the brains of transgenic mice is correlated to neuronal loss in the CA1 hippocampal subfield. Thus the presence of Aβ, regardless of its form (soluble or aggregated), is considered to be detrimental to neuronal cells (DaRocha-Souto *et al.*, 2011).

AD is classified as either familial or sporadic AD. Familial AD occurs primarily as a result of genetic mutations on chromosomes 1, 14 or 21 (Götz *et al.*, 2011; Hoyer, 2000). These mutations cause autosomal dominant AD that presents early and usually severely. There are
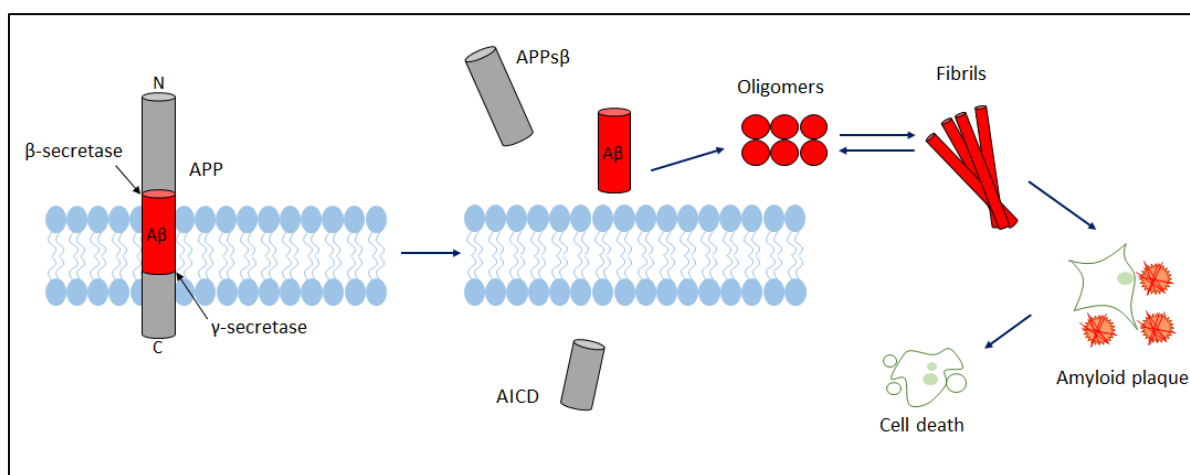
Figure 1.6: Amyloid beta is produced from amyloid precursor protein (APP) and forms toxic aggregates.

32 mutations in genes encoding APP, 179 mutations in PSEN1 and 14 in PSEN2. APP mutations occur around the γ-secretase cleavage site, but it should be noted that the most frequently observed APP mutation occurs adjacent to the BACE1 cleavage site. PSEN mutations cause alternated expression of amino acids in their transmembrane regions

(O'Brien and Wong, 2011). These mutations lead to an important outcome – increased production of $A\beta_{42}$ relative to $A\beta_{40}$. $A\beta_{42}$ is the less soluble and more toxic $A\beta$ species. Only about 1% of AD cases are familial, however. The rest are classified as 'sporadic AD', of which 50-70% are estimated to have a genetic component, however the cause is mostly unknown. Susceptibility genes for sporadic AD include the apolipoprotein E allele (ApoE). The ApoE allele occurs as three variants that encode the proteins ApoE2, ApoE3 and ApoE4. The ApoE4 allele significantly increases the risk of developing AD, with increasing risk for homozygous individuals. ApoE4 binds $A\beta$ less strongly than the other two ApoE proteins, and in individuals with the ApoE4 allele it shows a strong correlation with increased $A\beta$ deposition in the brain (O'Brien and Wong, 2011). In addition to the APP, PSEN1, PSEN2 and ApoE gene mutations or expression patterns discussed, two potential AD susceptibility genes have recently been identified. The function of IGHV1-67 (chromosome 14) is unknown but is most likely involved in immunoglobulin G (IgG) VDJ-type recombinations during lymphocyte maturations. The TP53INP1 gene on chromosome eight encodes a protein that facilitates autophagy-dependent apoptosis via phosphorylating p53 and is involved in cell migration and extracellular matrix adhesion (Escott-Price *et al.,* 2014). Thus disrupted autophagy in the context of apoptotic cell death is implicated in AD. Despite the genetic alterations observed in familial AD, it is impossible to macroscopically distinguish a sporadic from a familial AD brain as both present a similar set of characteristics (Götz *et al.*, 2011). These will now be discussed.

AD researchers face the challenge of multifaceted disease pathology, yet the biggest hurdle is the length of time, often a matter of decades, that separates its cause from functional defects (Saido, 2013). Aging is the main risk factor for developing AD, complicating the process of unravelling its aetiology, as aging is also associated with molecular disruptions that are implicated in AD e.g. oxidative stress, inflammation and mitochondrial damage (Gouras *et al.*, 2010). In aging, there is a loss of brain volume, but the extent is less severe than observed in AD, especially in the hippocampus (Resnick *et al.*, 2003; Frisoni *et al.*, 2010). The free radical theory of aging states that reactive oxygen (ROS) species are responsible for damaging proteins, which accumulate over time (Harman, 1956). Aged cells are less proficient at clearing defective proteins by proteolytic pathways and as a result proteins accumulate and aggregate intracellularly (Martinez-Vicente *et al.*, 2005).

The theme of proteostasis, homeostasis of protein degradation, is hence central and will be discussed in more detail below. The divide between apparent cognitive decline and the molecular disruptions remains a large problem, however, and the means by which AD is currently diagnosed remains challenging and will be investigated first.

b. <u>Dementia and Alzheimer's disease diagnosis</u>

Perhaps the most well-known clinically manifest hallmark of AD is the memory loss associated with dementia. The definition of dementia is the development of cognitive deficits which manifests as memory impairment and disturbances in language use, motor activity, cognition of objects and executive function (Chertkow, 2008). The term 'mild cognitive impairment' (MCI) was created to identify cognitive deficiency in the stage between normal aging and dementia. MCI as separate diagnostic category is seen as a valuable tool because of the possibility to intervene before AD (or other dementia-associated diseases) manifests in the transition from MCI to dementia (Petersen *et al.*, 2014). MCI is not always a precursor to more serious conditions, but it is very often the case, with a rate of conversion to dementia of 50% within five years (Petersen *et al.,* 1999). Recently, the American Psychiatric Association has published a new set of criteria for dementia which includes pre-dementia in the Diagnostic and Statistical Manual for Mental Disorders (DSM-5). Here the stage of cognitive impairment is termed 'mild neurocognitive disorder' (NCD). It shares many features with MCI but includes more expanded criteria that allow clinicians to distinguish subtle features that are present in NCD, but absent in normal aging and dementia. Some characteristics of NCD include 'preserved independence in functional abilities' and 'objective cognitive impairment'. It is implied that neuropsychological testing can be a helpful diagnostic tool. NCD can further be classified as mild or major, and its aetiology can be determined, such as arising from AD, frontotemporal degeneration or Lewy body disorders (Petersen *et al.*, 2014).

AD dementia can be distinguished from so-called 'all-cause dementia' by specific features, outlined by the National Institute on Ageing and the Alzheimer's Association (McKhann *et al.*, 2011). Here it is recommended that AD dementia be subdivided into '(1) Probable AD dementia, (2) Possible AD dementia, and (3) Probable or possible AD dementia with evidence of the AD pathophysiological process'. 'Probable dementia' includes insidious

onset from months to years, a history of worsening cognition, impaired learning and information recall as well as a range of non-amnestic presentations such as impaired executive function. The certainty of diagnosis increases to 'possible AD dementia' with evidence of progressive cognitive decline as reflected by formal neuropsychological tests, and with the presence of genetic mutations in the APP, PSEN1 or PSEN2 genes. Evidence of pathophysiological processes adds another level of certainty. This evidence is based on various biomarkers characteristic of AD, such as Aβ and tau proteins. The focus of this review will hence be on the pathophysiological changes observed in AD. It is important to consider when in the disease pathogenesis the molecular underpinning of these symptoms appear and how cognitive decline correlates with molecular events. Dementia symptoms are observed only late in AD disease progression, during Braak stage V, when clinical diagnosis usually takes place. Thus there is an extended time, possibly decades, during which pathogenic changes take place before diagnosis (Braak and Del Tredici, 2012).

Diagnosing AD can be confusing when one considers the long 'pre-clinical' stage of the disease in which no AD dementia is diagnosable. Sperling *et al.* (2011) developed a model of AD disease progression where the phases of AD are characterized sequentially from 'pre-clinical', 'MCI', and 'dementia' with biomarker presence increasing the risk of developing AD, but not guaranteeing progression to the clinical phases. A particularly powerful model has been proposed by Jack *et al.* (2010) and expanded by Sperling *et al.* (2011) and includes preclinical AD, where the most important biomarkers of AD pathophysiology are shown to increase to abnormal levels in a predictable order until a ceiling is reached. These biomarkers present as reduced presence of $Aβ_{42}$ in the cerebrospinal fluid (CSF) and as increased amyloid tracer retention in PET imaging. Both indicate brain Aβ amyloidosis. PET can also be used to identify decreased FDG uptake with an AD-typical pattern of temporoparietal hypometabolism, a marker for synaptic dysfunction. MRI is used to detect brain atrophy that presents in a specific pattern of neurodegeneration in AD involving the medial temporal lobes, paralimbic and temporoparietal cortices (Sperling *et al.*, 2011).

It is beneficial in a clinical setting to distinguish between stages of severity of AD dementia in order to govern decision-making for treatment. The Clinical Dementia Rating (CDR) has become a standard measure for dementia staging internationally, and evaluates patients'

impairment in six domains: memory, orientation, judgement and problem-solving, community affairs, home and hobbies and personal care, to yield a score that indicates one of five categories (Perneczky *et al.*, 2006). These are: 0 (no dementia), 0.5 (questionably dementia), 1 (mild dementia), 2 (moderate dementia) and 3 (severe dementia). Caregivers are relied upon to provide substantial information necessary to make a diagnosis with CDR, and brief assessment tools, such as the Mini-Mental-State Examination (MMSE) may be more useful in clinical practice. The MMSE involves the patient having to complete tasks and questions such as the time and place that reveal his/her state of cognitive functioning. It usually takes about 10-15 minutes to complete. The final score of the patient will indicate dementia severity, with a score of 30 indicating the best cognitive function, and a score of zero the worst (Perneczky *et al.*, 2006).

As the loss of brain volume and neuronal cell death is responsible for AD dementia, the processes governing cell death and their molecular link with the autophagic machinery will be discussed now.

c. Cell death modalities

Magnetic resonance imaging reveals macroscopic changes present in the AD brain. These typically include an atrophied hippocampus and widened ventricles (Apostolova *et al.*, 2012). Neuronal and synaptic loss occur in parallel with the 'positive' features of protein aggregation, and more recently early changes such as injured dendrites and synapses have expanded the traditional hypothesis of the events leading to AD (Serrano-Pozo, 2011). An overview of cell death mechanisms and their molecular regulation is necessary in order to better contextualize its contribution to neuronal tissue atrophy.

Cell death categorization

Early cell death research used morphological features to identify different cell death modes, as biochemical research methods were less available then (Galluzzi *et al.*, 2012). However, subsequent research has provided evidence that using morphotypes of cell death may hide a great degree of heterogeneity. Nonetheless this approach was favoured by the scientific community until recently, despite the availability of powerful biochemical methods to assess cell death. A 'dead' cell displays either irreversible plasma membrane

permeabilization or has suffered complete fragmentation. Cell death can occur by activation of one of three death modes: apoptosis, necrosis and cell death by autophagy. However, recent developments recommend to move away from this, primarily morphology based, restrictive categorization since a large degree of molecular overlap exists (Galluzzi *et al.*, 2015). Instead, cell death can be classified into two main categories for functional purposes – 'accidental' and 'regulated' cell death. Accidental cell death usually occurs when cells are exposed to severe conditions, usually over a short period of time and probably does not involve a specific molecular machinery (Galluzzi *et al.*, 2015). However, for the purpose of this literature review we will refer to both factors that control cell death, as well as morphological features in order to better connect with previous literature.

Traditional cell death modalities

'Programmed cell death' refers to an established series of events that lead to cell death, such as observed during apoptotic cell death. Apoptosis can be identified morphologically by cell shrinkage, membrane blebbing, nuclear fragmentation and chromatin margination (Lockshin and Zakeri, 2004). It is dependent on a cascade of molecular events, and can be subdivided into the intrinsic and extrinsic apoptotic pathway that culminates in the same execution pathway. The execution pathway is initiated by caspase-3 cleavage which results in DNA fragmentation, cell protein degradation, protein cross-linking, formation of apoptotic bodies and uptake by phagocytic cells following the expression of phagocytic cell receptor ligands. In the extrinsic pathway, transmembrane receptors or death receptors of the tumour necrosis factor (TNF) receptor gene superfamily transmit death signals from the cell surface to intracellular signalling pathways (Elmore, 2007). Death receptors bind their ligands and form cluster interactions with one another. A death-inducing signalling complex (DISC) is formed which triggers the autocatalytic activation of pro-caspase 8, to form active caspase-8. Caspase-8 triggers the execution pathway. The intrinsic apoptotic pathway is triggered by a diverse range of intracellular stimuli that do not act via receptors, but through mitochondria. Signals can act in a negative fashion in the absence of growth factors, hormones and cytokines where there is a loss of apoptosis suppression. Positive signals include toxins, hypoxia, hyperthermia, viral infections, and free radicals. Intrinsic stimuli cause changes in the mitochondrial inner membrane, which triggers the opening of the mitochondrial permeability transition pore (mPTP) and loss of the mitochondrial

transmembrane potential. Two groups of pro-apoptotic proteins, normally sequestered in the intermembrane space, are then released into the cytosol. The first group activates the caspase-dependent mitochondrial pathway and consists of cytochrome c, Smac/DIABLO, and Htr/Omi (Elmore, 2007). Cytochrome c binds and activates apoptotic protease activating factor 1 (Apaf-1) and pro-caspase 9, which forms an apoptosome and in turn activates caspase-9. The second group of proteins is released from mitochondria during apoptosis – a late event in the apoptotic cascade – and consists of apoptosis-inducing factor (AIF), endonuclease G and caspase-activated DNase (CAD). Both AIF and endonuclease G act in a caspase-independent manner and cause changes in DNA such as fragmentation and condensation. CAD is released from mitochondria and translocates to the nucleus. Caspase-3 cleaves and activates CAD which in turn causes DNA fragmentation and advanced chromatin condensation (Elmore, 2007). Poly (ADP-ribose) polymerase (PARP) is also cleaved during apoptosis, to form an 85 kDa protein (Tewari *et al.,* 1995). Apoptotic mitochondrial events are controlled and regulated by members of the Bcl-2 family of proteins, and the tumour suppressing protein p53 also plays an important regulatory role (Elmore, 2007).

Necrosis, in contrast, most often operates in a less controlled fashion where cells swell, leak cytoplasmic contents into the extracellular environment and cause an inflammatory response (Lockshin and Zakeri, 2004). In addition, it was traditionally defined by the absence of apoptosis and autophagic morphological traits. However, more recently, it has emerged that necrosis is less accidental and can occur in a regulated fashion (Galluzzi *et al.*, 2012). Triggers that may induce regulated necrosis include alkylating DNA damage, excitotoxins and death receptor ligation. TNFα binding to the TNF receptor 1 (TNFR) recruits five proteins, including receptor-interacting protein kinase 1 (RIPK1 or RIP1) to its cytoplasmic tails, which provides a docking station for three other proteins. Under certain conditions such as caspase-8 absence, deubiquinated RIP1 can engage with its homolog, RIP3 which activates the execution of necrotic cell death (Galluzzi *et al.,* 2012).

Autophagic cell death is caspase-independent, and cells display many large AV, and an externalization of phosphatidylserine (Lockshin and Zakeri, 2004). However, the existence of this type of cell death has been questioned, and suggested that increased autophagy

29

preceding cell death may rather represent a futile attempt to escape death (Shen *et al.*, 2012). The loss of ATP is a striking feature distinguishing apoptosis and necrosis, as only necrosis is marked by a large decrease in the amount of ATP (Lockshin and Zakeri, 2004).

Recent literature now recommends to rather focus on the factors that control cell death than on characterizing the different cell death modalities. Cellular metabolism is a major role player in determining cellular fate. There is evidence of 'metabolic checkpoints', molecular mechanisms regulating cellular functions in response to metabolic stimuli, that detect changes in the major metabolites, such as the ratios of ATP/ADP and AcCoA/CoA, and that interact with these metabolic signals to initiate downstream events (Green *et al.*, 2014). The effectors of these events are metabolites and metabolic by-products, as well as various enzymes involved in metabolic circuits. Signal transducers are activated in this way, including those involved in initiating cell death. Examples of checkpoints include the mitochondrial checkpoint, the autophagy checkpoint (comprehensively interconnected with other checkpoints), the AcCoA/CoA checkpoint and the p53 checkpoint (Green *et al.*, 2014).

Cell death dynamics

Cellular dynamics is at the heart of cell death decision-making. The point-of-no-return (PONR) is a powerful concept here. A cell's ability to respond to an insult will determine the subsequent cell death mode, with the metabolic state of the cell playing a key role (Loos and Engelbrecht, 2009). The PONR for autophagy occurs earlier in time than that for apoptosis since autophagy induction, above basal levels of autophagy, is the first stress response initiated. Cells have to be most stressed for necrosis to occur. The three death modes are connected ATP-dependently, and autophagy plays both a direct and indirect role in delaying apoptosis and necrosis onset as it can generate ATP (Loos and Engelbrecht, 2009).

Apoptosis is the main cell death pathway involved in AD and neurons treated with Aβ peptide trigger apoptosis *in vitro* (Loo *et al.*, 1993)*.* Moreover, the activation of apoptosis by both the intrinsic and extrinsic pathways, possibly dependent on the form of Aβ protein involved, has been described (Di Carlo, 2010). However, based on the here described

molecular overlap between cell death modalities, it has to be considered in the particular context of a cellular stress response.

d. The role of dysfunctional mitochondria in Alzheimer's disease

Mitochondrial dysfunction is a prominent feature of AD (Reddy, 2009). It constitutes a host of factors such as respiratory chain uncoupling, superoxide radical production, and calcium leakage (Kroemer *et al.*, 1998). It can also be a cause of neuronal death. Mitochondrial dysfunction can lead to cell death in two distinct ways. The first is characterized by activation of the permeability complex, which occurs when environmental factors trigger an increase in mitochondrial membrane permeability. This activates apoptosis by releasing mitochondrial proteins such as cytochrome c and dispersion of the electrochemical gradient present on the inner mitochondrial membrane. The second way is characterized by a bioenergetic state of distress which disrupts cellular function to such an extent that apoptosis or necrosis is triggered (Kroemer *et al.*, 1998).

Aβ and APP can associate with various mitochondrial compartments, including the inner and outer mitochondrial membrane, the intermembrane space and the matrix which may explain the mitochondrial dysfunction observed (Pagani and Eckert, 2011). Aβ may affect components of the electron transport chain (ETC) present on the inner membrane, and TCA cycle enzymes present in the mitochondrial matrix, disrupting normal metabolic as well as antioxidant function. Aβ may also bind to cyclophilin D (CypD), a component of the mPTP which promotes its opening and thus apoptosis. The activity of fission protein Fis1, present on the outer mitochondrial membrane, is enhanced by Aβ, resulting in increased mitochondrial fragmentation (Pagani and Eckert, 2011).

Significant impairment in four functional parameters of mitochondria, i.e. reductive capacity, mitochondrial membrane permeability, ROS and ATP levels, occurs after exposing hippocampal cells to mitochondrial-targeted Aβ (Cha *et al.*, 2012). These detrimental changes are a direct cause of cell death. Aβ's association with mitochondria causes harmful changes in both morphology and function. Morphologically apoptotic features are observed, such as fragmentation, cristae disruption, and mitochondrial swelling (Cha *et al.*, 2012).

31

Calkins and Reddy (2011) exposed hippocampal neurons to Aβ peptide and observed decreased mitochondrial motility as well as fragmented mitochondria (Figure 1.7).

Animal models of AD reveal similar results. In a study of transgenic mice, Robinson *et al.* (2014) demonstrated that deficiency in PSEN1/2 or AICD affects mitochondrial function. Here, PSEN1 regulated peroxisome proliferator-activated receptor-c coactivator 1α (PGC-1α), important for expression of mitochondrial proteins, causing disrupted mitochondrial energy metabolism when mutated.

Multiple researchers have shown that Aβ disrupts mitochondrial dynamics, which causes the equilibrium between fission and fusion to shift and favour fission (Calkins *et al.*, 2011). Protein levels of Drp1, Opa1, Mfn1 and Mfn2 are significantly reduced in AD neurons, while Fis1 protein levels are significantly increased. Although the changes in Opa1, Mfn1 Mfn2 and Fis1 expression are associated with increased fission, Drp1 reduction is linked with mitochondrial elongation, which could lead to an uncertain outcome in mitochondrial dynamics in AD. Furthermore, soluble amyloid oligomers have a detrimental effect on mitochondria – there is an increased mitochondrial fragmentation and altered mitochondrial distribution to a state where the majority of mitochondria are localized in the soma and very few present in the neuronal processes (Wang *et al.*, 2009). This is understandable in light of the fact that fission/fusion proteins control not only mitochondrial morphology but also their intracellular distribution. The same group also identified that overexpressing Drp1 prevented the oligomer-induced synaptic loss, indicating the important role of abnormal mitochondrial dynamics in the process of synapse loss. This finding is of interest as Drp1 overexpression causes predominantly fragmented mitochondria, a condition that seems to be present in AD, but was found to rescue neurons from the abnormal pattern of mitochondrial distribution. This may be understood better when one considers that there is both an abnormal expression pattern of fission and fusion proteins in AD, and that both of these processes occur at a slower rate in AD neurons compared to healthy neurons. Mitochondria spend more time in a state of fission in amyloid oligomer treated cells, which may indicate the reason for the increased fission observed in AD (Wang *et al.*, 2009). These results suggest a dynamic assessment of fission and fusion rate, in order to dissect the mitochondrial function in the context of protein levels.

32

The focus will now shift from altered mitochondrial network features often observed in neurons derived from AD patients to autophagy, which is another crucial intracellular system that is involved in metabolic homeostasis.
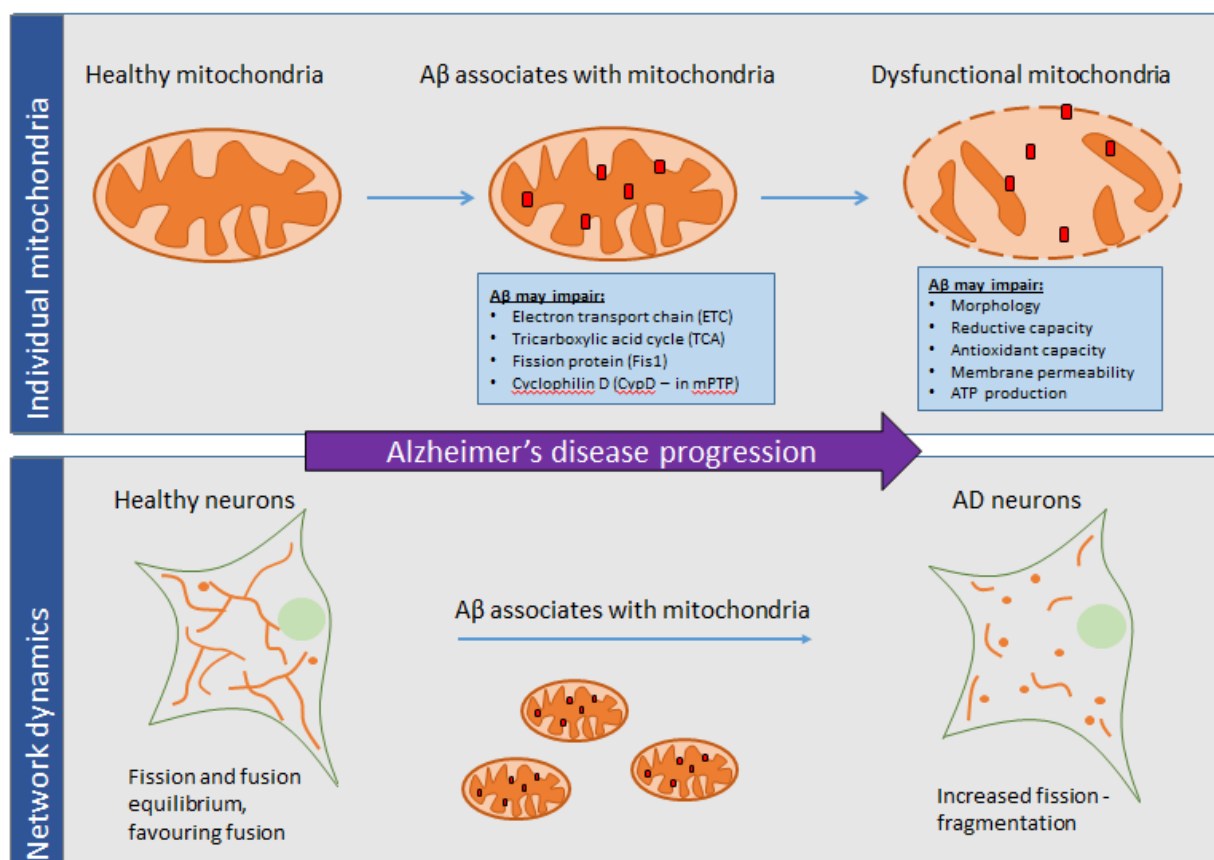
Figure 1.7: Aβ associates with mitochondria and results in increased mitochondrial fission.

e. The role of disrupted autophagy in Alzheimer's disease

Autophagy, a major protein degradation pathway, is usually activated as a first stress response in cells during e.g. nutrient deprivation, but it also serves important homeostatic functions, such as the breakdown of non-functional structures e.g. peroxisomes (Klionsky, 2005). It is also the mechanism by which long-lived proteins are degraded (Nixon and Yang, 2011), an important role in light of the fact that 99% of all cellular proteins are long-lived (Schworer *et al.,* 1981). Disrupted autophagy has been identified as a key factor in neurodegenerative diseases such as PD, HD and AD. In HD, autophagy malfunction occurs as a result of AV not being able to recognize cytosolic cargo, resulting in failure to engulf cargo as demonstrated by studies on a HD mouse model and human HD cells where mutant huntingtin protein (Martinez-Vicente *et al.,* 2010). In PD mutant α-synuclein binds to

lysosomal membrane receptors, probably impairing the uptake and degradation of both α-synuclein and other substrates, thereby contributing to their accumulation (Pan *et al.*, 2008). Elucidating the exact nature of autophagy disruption in AD is complicated as there is conflicting evidence regarding altered autophagy induction (Nixon and Yang, 2011). We will present the major characteristics of this dysfunction below.

Autophagy has become a major focus of current AD research. Disrupted autophagy is recognized as an important event that leads to the characteristic AV accumulation observed in dystrophic neurites (Nixon and Yang, 2011). Fascinating work by Hara *et al.* (2006) demonstrates that the suppression of basal autophagy in mice by preventing Atg5 expression leads to neurodegeneration, and suppression of Atg7 leads to multiple cellular abnormalities (Komatsu *et al.*, 2005). This finding places enormous importance on autophagic dysfunction as a factor in the disease pathogenesis of neurodegeneration, if one considers that neurodegeneration occurs in the absence of mutated proteins in these studies. The authors demonstrate that a loss of autophagy first leads to the accumulation of diffuse abnormal proteins, and then to inclusion body formation in later stages, suggesting that autophagy is primarily responsible for the turnover of diffuse cytosolic proteins under normal conditions (Hara *et al.*, 2006). This validates the theory that inclusion body formation is an adaptive response which occurs when diffuse abnormal proteins overwhelm the process of autophagic clearance.

The implications of defective autophagy are dire; the fact that it is a feature of so many neurodegenerative diseases is not surprising. The autophagic machinery is connected to three major pathways of energy sensing, i.e. the AMPK, mTOR, and protein kinase A (PKA) pathways, which are vital for maintaining cellular energy levels, and thus susceptibility to cell death (Loos *et al.*, 2013).

He *et al.* (2012a) generated mice with a knock-in BCL2 deficit, which resulted in blocked induction of autophagy but not basal levels of autophagy. They identified that mutant mice had an impaired increase in muscle glucose metabolism and also decreased exercise endurance. The metabolic effects of the BCL2 mutation could illuminate these findings; there was a blunted decrease in serum glucose and insulin levels. Thus induced autophagy is necessary for sufficient glucose supply, indicating its profound integration in metabolism.

AD is characterised by severe changes in autophagy. Neurons in the brains of AD patients exhibit swollen neuritic processes - dystrophic neurites - which are filled with AV (Nixon *et al.*, 2005). These represent the various intermediate stages of autophagic degradation and include autophagosomes and endosomes fused with autophagosomes. AV accumulation has been attributed to impaired clearance of AV rather than strong autophagy induction (Boland *et al.*, 2008). Yet upregulated autophagy initiation has been observed in the early stages of AD (Cataldo *et al.*, 1995; Ginsberg *et al.*, 2010). These apparently contradictory scenarios may be understood in terms of disease progression – early in the disease progression increased autophagy induction may represent a compensatory mechanism, but during the later stages, neurons' degradative capacity decrease (Lipinski *et al.*, 2010). It has also been demonstrated that the defect in autophagy is localized at the level of lysosomal degradation, and not in the early steps of autophagosome or autolysosome formation (Nixon and Yang, 2011). PSEN1 mutations, which cause early-onset AD, result in disrupted lysosome acidification, which provides strong evidence for defective proteolysis in AD (Nixon and Yang, 2011).

Genomic analysis has revealed the underlying mechanisms governing the disrupted autophagy characteristics of AD (Lipinski *et al.*, 2010). Specifically, ROS are identified as mediators of the type III PI3 kinase activity – an important upstream regulator of autophagy initiation. Lysosomal dysfunction caused by Aβ is independent of ROS, however. Proteomics has revealed that PSEN1 and nicastrin are found in the lysosomal membrane. These proteins both form part of the γ-secretase complex and are involved in intramembrane proteinolysis and are associated with AD (Schröder *et al.,* 2010). This provides additional evidence for lysosomal autophagy dysfunction in AD.

The molecular connection between autophagy and Aβ peptides is of vital importance in understanding disrupted autophagy in AD. Tian *et al*. (2013) demonstrated that an LC3-receptor mediated reaction is responsible for the shuttling of the APP-CTF from the endocytic pathway to autophagosomes for degradation via autophagy. They identified that adaptor protein 2 complex which plays a role in chlathrin-mediated endocytosis functions as an LC3 receptor and is likely required for APP-CTF degradation by autophagy (Tian *et al.,* 2013). This result supports the concept of targeted elimination of cargo by autophagy, an

emerging theme in recent research, and, more specifically identifies a possible mechanism by which autophagy degrades Aβ.

Amyloid homeostasis may be greatly dependent on autophagy. Beclin-1 levels are reduced in the brains of AD patients and result in reduced neuronal autophagy (Pickford *et al.*, 2008). Beclin-1 plays an important role in autophagy as it binds with and promotes the activity of Vps34 (Pickford *et al.*, 2008), a class III PI3 kinase imperative for autophagosome formation (Jaber *et al.*, 2012). Beclin-1 deficiency disrupts autophagy, modulates APP metabolism and leads to both intra- and extracellular Aβ deposits in mice (Pickford *et al.*, 2008). Furthermore, the reduction in beclin-1 observed in the AD brain seems to be correlated with disease severity – patients with amnestic MCI (which could be considered early, prodromal AD) had a 30% reduction in beclin-1 levels compared to age-matched controls, while patients with severe AD had a 70% reduction in beclin-1 levels compared to control (Pickford *et al.*, 2008). Thus beclin appears to be involved in the gradual autophagic failure associated with AD progression. Aβ accumulation may overwhelm the autophagic system which plays a 'clean-up' role in this situation and may clarify the many AV observed histologically (Cataldo *et al.*, 1995). However, autophagy also plays a direct role in the production of Aβ as AV contain APP and amyloid producing enzymes, as demonstrated using APP transgenic mice (Yu *et al.*, 2004). Indeed, autophagy and the endocytic pathway are heavily involved in the processing of APP and Aβ generation. The combination of increased formation of vacuoles containing Aβ, combined with the reduced clearance facilitates Aβ accumulation observed in AD (Nixon, 2007). Autophagy regulates Aβ peptide levels (Vingtdeux *et al.,* 2011; Spilman *et al.,* 2010), and it has been demonstrated that inducing autophagy can slow AD progression in mice models (Yang *et al.*, 2011; Spilman *et al.*, 2010). Thus, increasing autophagy holds promise as a therapeutic target.

Activating autophagy can reduce both Aβ levels and AD occurrence *in vivo*, demonstrating its validity as a therapeutic target (Spilman *et al.*, 2010). However, timing is a crucial component when considering the manipulation of autophagic flux as a therapeutic strategy. It would be optimal to increase autophagy at early stages of the disease, when the degradative capacity of cells is more likely to be intact. This would aid the inherent machinery in cells that clear defective proteins. Enhancing autophagy later in disease could be not only counter-productive, but also dangerous as this period is characterized by

reduced proteolytic abilities and extensive AV accumulation. Doing so could potentially exacerbate the AV load and may accelerate neuronal cell death. It is hence very important to characterize autophagic flux and autophagy status in *in vitro* and *in vivo* models. It would be most useful to determine the level of autophagic flux in AD patients. The scientific tools to achieve this are still lacking, yet the importance of an 'autophagometer' has been outlined (Rubinsztein *et al.,* 2009). If implemented, decreased autophagic flux could potentially be identified even before dementia manifests. The deficit could then be treated according to flux deviation in patients. Currently, major neuronal loss precedes the onset of disease manifestation. This emphasizes the therapeutic focus on prevention, as opposed to the mere management of symptoms.

f. <u>Altered neuronal metabolism in Alzheimer's disease</u>

The fact that cellular energetics and survival are closely linked warrants a closer assessment of the metabolic changes that occur in the AD brain and how metabolism influences AD susceptibility. Energetic substrates are inextricably linked to cellular functioning. Indeed, it is not only a lack of a balanced supply of substrates which may be detrimental to cells, but also the type of substrate being metabolized.

There is disrupted energetic substrate supply in AD and cerebral glucose metabolism is reduced by 20-40% in sporadic AD (Hoyer, 2000). Moreover, decreased hippocampal glucose metabolism in AD mice has been observed, which occurs concomitantly with impaired spatial memory and neuronal cell loss (Sadowski *et al.*, 2004). Decreased glucose transport may cause this decrease, and it is an widely observed effect found in both normal and triple transgenic (3xTg-AD) mouse brains which harbour mutations in PSEN, APP and tau (Ding *et al.*, 2013).

In patients with MCI, brain volume loss due to AD can be detected in the hippocampus, entorhinal cortex and parahippocampal gyrus (Mosconi, 2005). Structural MRI studies have revealed that the medial temporal lobe is the earliest affected brain region in AD. Furthermore, the transition to dementia can be predicted by changes in the lateral temporal lobe. FDG-PET imaging has demonstrated that reduced glucose metabolism in the parieto-temporal, frontal and posterior cingulate cortices is indicative of AD (Mosconi, 2005). This

method has 90% sensitivity in identifying AD, although it is not able to differentiate AD from other dementias.

Metabolomics has revealed that 154 metabolites in plasma and 150 metabolites in CSF were significantly altered in AD patients compared to control subjects (Trushina *et al.*, 2013). In addition, 40 canonical pathways in plasma and 30 in CSF were significantly altered in the AD subjects. Cholesterol and sphingolipid transport was the most affected pathway in both CSF and plasma samples, and in the CSF aspartate and aspargine metabolism as well as the TCA cycle were among the top four altered pathways. Not surprisingly, the number of affected pathways was found to increase with disease severity, emphasising the importance of healthy metabolism for delaying disease progression.

A poor diet and lack of physical exercise increases the risk of developing AD. In contrast, it has been demonstrated that elders without dementia who followed a Mediterranean-type diet, i.e. a diet rich in cereals, legumes, fish, fruits and vegetables as well as monounsaturated fats, had a decreased risk for developing AD over a mean period of 5.4 years of follow-up. Their odds improved even further when physically active, with more physical activity being associated with a lowered risk for developing AD. When the factors of diet and physical exercise were considered together in the same model, a statistically significant association with AD incidence was found (Scarmeas *et al.*, 2009).

Longitudinal (Janson *et al.*, 2004) and epidemiological studies (Peia *et al.*, 2002) support the relationship between AD risk and glucose metabolism disorders. Type 2 diabetes mellitus (T2DM) has been identified as a risk factor for developing AD (Vagelatos and Eslick, 2013) and altered brain metabolism is observed in AD patients soon after clinical symptoms manifest, alterations which have features reminiscent of T2DM such as impairments in glucose handling and energy metabolism (Bosco *et al.*, 2011). Furthermore, these changes are proposed to occur *before* symptoms manifest, casting AD as a particular type of 'brain diabetes'. Insulin and insulin-like growth factor-1 (IGF-1) can bind to receptors expressed ubiquitously, including in the brain. Binding to their respective receptors in the brain facilitates important functions such as neuronal survival, energy homeostasis and memory (Bosco *et al.*, 2011). The insulin signalling pathway is initiated by insulin binding the insulin receptor in the plasma membrane, which causes its autophosphorylation, in the process

activating its tyrosine kinase activity (Liu *et al.,* 2011). This causes the recruitment and phosphorylation of a variety of substrates including insulin receptor substrate-1 (IRS-1). IRS-1 also binds various substrates, notably PI3K, which leads to the phosphorylation and activation of 3-phosphoinositide-dependent protein kinase-1 (PDK1) which in turn activates Akt. Insulin induces the upregulation of the insulin degrading enzyme (IDE) which acts in a feedback mechanism in hippocampal neurons to control insulin signalling (Zhao *et al.,* 2004). IDE levels and activity are decreased in AD and are associated with increased levels of Aβ, demonstrating the importance of insulin signalling control in preventing AD (Figure 1.89). It is important to note that Akt phosphorylates GSK3β, thereby deactivating its activity. Thus a decrease in insulin signalling contributes to exacerbated tau hyperphosphorylation via GSK3β activity (Liu *et al.,* 2011).

Brain glucose uptake occurs at specific regions such as the hippocampus through the actions of glucose transporters. It has been shown, however, that there is a reduced uptake of glucose in the brains of animals with T2DM. A similar theme emerges with AD. Insulin levels are lower in the CSF of AD patients and IGF-1 receptor expression is diminished dependent on disease severity. IGF-1 resistance seems likely, as an increase in serum IGF-1 is seen in early AD, but IGF-1 mRNA levels are reduced in severe AD (Bosco *et al.*, 2011). Moloney *et al.* (2010) describes similar results: despite increased expression of IGF-1 receptor levels in AD, a significantly reduced number of neurons expressed the receptor. The insulin receptor also reflects this pattern, as despite increased expression levels, the receptors were found to be concentrated intracellularly in AD neurons as opposed to distributed throughout the soma and dendrites. Amyloid may be the causative factor of these disruptions - Aβ was found to target the insulin receptor, to interfere with its signalling and to alter its responsiveness (Townsend *et al.*, 2007; Lee *et al.,* 2009).

Other research supports the notion that a diabetic milieu causes AD pathophysiology. Trudeau *et al.* (2010) has shown that cells grown in high glucose (30 mmol/L) medium were characterized by mitochondria with disrupted morphology. 3xTg-AD mice and sucrose-fed mice presented similar mitochondrial disruptions, reflecting the link between T2DM and AD, and highlighting the risks of a high sugar diet (Carvalho *et al.*, 2012). Moreover, altered insulin signalling is implicated in Aβ-mediated tau hyperphosphorylation via GSK3β

(Tokutake *et al.*, 2013; Hong and Lee, 1997). The exact mechanisms involved are not yet clearly understood, however.

Modern diets have protected most members of urbanized communities from starvation, yet the resulting overnutrition is increasing the burden of health globally, and is leading to the development of not only obesity, diabetes and cardiovascular disease (Chopra *et al.*, 2002) but is also associated with the risk of developing AD, due to the inflammatory milieu that exists in obesity (Businaro *et al.*, 2012). In sharp contrast, dietary restriction is one of the few interventions that extend lifespan in model organisms including primates (Fontana *et al.*, 2010; Colman *et al.,* 2014). This may be the result of the resistance to oxidative stress, reduction in molecular damage, reduced occurrence of cancer and cardiovascular disease (Fontana *et al.*, 2010). Caloric restriction leads to an increase in circulating ketone body levels (Knopp *et al.*, 1991), demonstrating the physiological impact of nutrient deprivation and ketone bodies. This deserved further attention and will form part of this thesis.
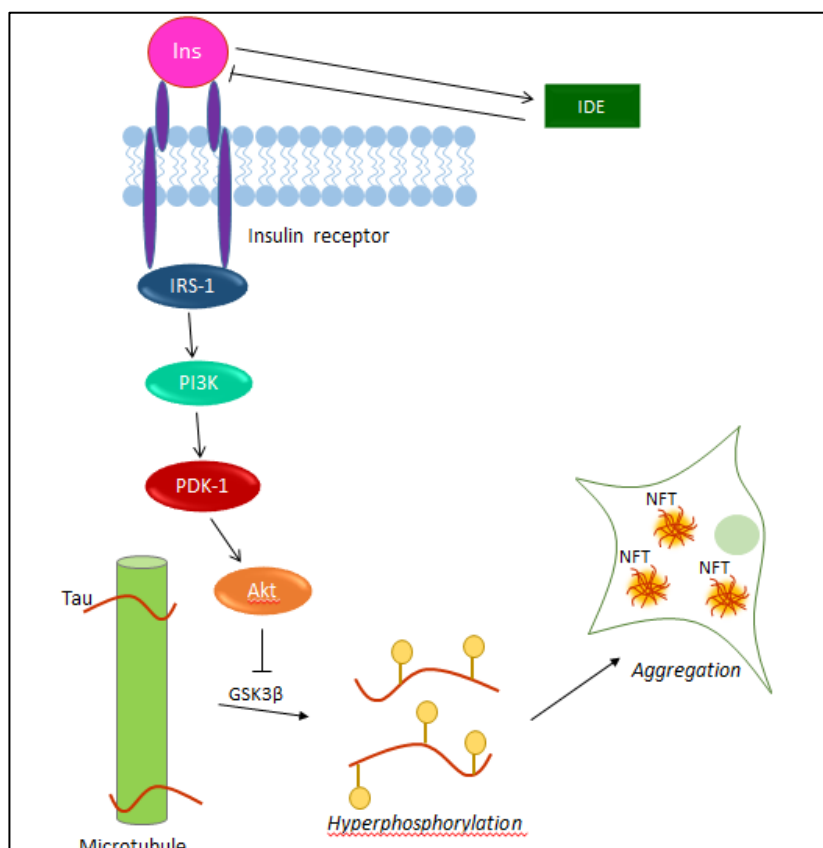
Figure 1.8: Decreased insulin signalling leads to tau hyperphosphorylation.

g. Experimental models in Alzheimer's disease research

Genetically altered mouse strains often serve as powerful animal models of AD. Knowledge of susceptibility and causative genes has allowed for the generation of different mouse strains with AD symptoms. Commonly used systems include the Tg2576 strain which overproduces APP and 3xTg-AD mice (Morrissette *et al.*, 2009).

The use of transgenic mice offers the valuable opportunity to gather information about the physiological and *in vivo* function of expressed genes and their gene-products. This aspect is especially powerful for investigating of early pathogenic changes at the molecular level, as only late stages of the disease are accessible in humans due to *post mortem* tissue analysis (Van Leuven, 2000). A major limitation of these mice models, however, is that they only mimic the rare familial forms of AD; and not sporadic AD which accounts for most cases (Morrissette *et al.*, 2009).

It is also possible to move beyond amyloid-based manipulation in AD models. The physical conditions present during neurodegeneration can be represented in both *in vivo* and *in vitro* models. It is known that inflammation occurs in the AD brain as the result of amyloid plaques. Microglia and other inflammatory cells are found in abundance in plaque-rich areas as well as high levels of ROS which damages neurons and leads to oxidative stress (Johnstone *et al.,* 1999). Paraquat (1,1'-dimethyl-4,4'-bi-pyridinium) is a broad-spectrum herbicide used in the field of neurodegeneration research to induce neuronal cell death as it causes oxidative stress (McCormack *et al*., 2005). Although paraquat results in selective neurodegeneration in the substantia nigra, it has a host of effects on neurons that makes it suitable for neurodegeneration research in general. Its toxic effects are attributed to its redox cycling abilities, producing superoxide radicals and depleting reducing equivalents such as NADH, which can induce lipid peroxidation (Bus and Gibson, 1984). This mechanism of action is supported by McCormack *et al*. (2005) who observed that ferritin transgenic mice, able to prevent iron-catalyzed oxidative reactions, were protected from paraquat-induced cell death and had unchanged levels of lipid peroxidation, as evidenced by 4-HNE staining. McCarthy *et al.* (2004) demonstrated that apoptosis is probably the cell death mode involved as indicated by morphological and biochemical changes in human neuroblastoma cells treated with paraquat. In addition, paraquat causes a decrease in ATP

production, which indicates impaired mitochondrial functioning, as well as an increase in the mitochondrial ROS generation. Gliosis occurs as a result of paraquat exposure, as indicated by the microglial and astrocytic activation (McCormack *et al*., 2002). Thus, the oxidative stress caused by damaged neurons can effectively be mimicked *in vitro* by treating cells with the herbicide paraquat.

1.4 Therapeutic interventions

a. <u>Current treatment interventions and trends in research</u>

Despite major efforts in research into AD, no effective disease modifying intervention to treat it exists. There are treatment options available to ameliorate symptoms, however, and new treatment avenues are being explored.

AD patients are commonly treated with drugs to control behavioural changes such as depression or psychosis. The use of these drugs has associated risks, including increased mortality in elders with dementia (Honig and Boyd, 2013). Here, we provide a brief overview of the therapies currently available, and thereby indicate the disconnect between treatment intervention and cellular pathology. This pathology eventually leads to neuronal cell death and outwardly manifests as first MCI and then AD dementia (Apostolova *et al.,* 2012).

<u>Neurotransmitter based therapies</u> are primarily aimed at addressing the cholinergic defect, the loss of cholinergic neurons present in AD (Whitehouse *et al.*, 1982). Four acetylcholinesterase inhibitor drugs were approved in the United States of America between 1993 and 2001, however since then the use of the first acetylcholinesterase inhibitor, tacrine hydrochloride, has declined due to its side effect of hepatic toxicity. Donepezil hydrochloride is commonly prescribed, and is used in a once daily dose. Newer approved acetylcholinesterase inhibitors are rivastigmine tartrate and galantamine hydrobromide. Memantine hydrochloride functions as an NMDA antagonist to reduce excessive excitatory activity (Honig and Boyd, 2013). Excitotoxicity, the excessive exposure to the neurotransmitter glutamate or overactivation of its receptor (one of which is the NMDA-type receptor) results in excessive calcium influx which can injure neurons and contributes to neuronal death (Lipton, 2004). Despite the fact that these drugs have resulted in cognitive, behavioural and functional improvements, the beneficial effects are limited. Furthermore, they are only symptomatic treatment and may cause a variety of side

effects (Honig and Boyd, 2013). Neurotransmitter-based pharmacological agents are the only drugs being prescribed to patients today (Chou, 2014). However, many other therapeutic interventions are being tested on the grounds of encouraging preliminary results.

Immunotherapy refers to applying a vaccine approach to reduce amyloid depositions. This treatment method has received attention since 1999 when reduced amyloid deposition was described in transgenic mice overproducing APP (Schenk *et al.,* 1999). Early human clinical trials generated conflicting results, with some patients displaying autoimmune reactions, while others exhibited improved cognition and amyloid clearance (Morgan, 2011). Passive immunotherapy investigations showed a similar trend of increased amyloid clearance, but with the side effect of micro-haemorrhages and increased vascular amyloid deposition. Later, cases of vasogenic oedema were reported. Several clinical trials have reached phase three testing, however the adverse effects prevent its use as a treatment in the near future (Morgan, 2011).

Physical exercise exerts beneficial effects in AD transgenic mice. This includes behavioural improvements such as ameliorated cognitive impairment as well as a protective effect against synaptic changes and oxidative stress (García-Mesa *et al.*, 2011). Rats exposed to long-term exercise in the form of 30 min treadmill exercise per day demonstrated decreased tau and GSK3β activation in the hippocampus (Bayod *et al.,* 2011). Recently, it was found that acute exercise causes a two-fold increase in GFP-LC3 positive puncta in wild-type mice (He *et al.*, 2012a), highlighting the role of autophagy in glucose regulation, and its importance for mediating some of the benefits of exercise.

Rapamycin is an antibiotic that can be used to induce autophagy in the brain by inhibiting mTOR. mTOR hyperactivation parallels amyloid an tau pathology in transgenic AD mice (Caccamo *et al.,* 2010), while rapamycin administration decreases brain levels of amyloid deposition and defective tau (Caccamo *et al.,* 2010; Spilman *et al.,* 2010). The benefits of rapamycin extended to improved cognition in transgenic mice (Caccamo *et al.,* 2010; Spilman *et al.,* 2010). However, targeting mTOR has complications as its substrates control many cellular processes such as the regulation of protein synthesis, mitochondria and lipid

metabolism (Bové *et al.*, 2011). Rapamycin is also immunosuppressive and is even considered a classical drug used for this purpose (Matsue *et al.*, 2011).

Treatment	Class/description	Mechanism of action	Status
Donepezil hydrochloride	Acetylcholinesterase inhibitor	Reduces excitotoxicity	Approved, used clinically (Honig and Boyd, 2010)
Rivastigmine tartrate	Acetylcholinesterase inhibitor	Reduces excitotoxicity	Approved, used clinically (Honig and Boyd, 2010)
Galantamine hydrobromide	Acetylcholinesterase inhibitor	Reduces excitotoxicity	Approved, used clinically (Honig and Boyd, 2010)
Memantine hydrochloride	NMDA receptor antagonist	Reduces excitotoxicity	Approved, used clinically (Honig and Boyd, 2010)
Immunotherapy	Aβ vaccine	Targeted amyloid clearance	Clinical trials (Morgan, 2011)
Physical exercise	Behavioural intervention	Upregulated autophagy	Research (He *et al.*, 2012a; García-Mesa *et al.*, 2011)
Rapamycin	mTOR inhibitor	Upregulated autophagy	Research (Caccamo *et al.*, 2010)
Rilmenidine	Unknown	Upregulated autophagy	Research (Rose *et al.*, 2010)

Table 1: Current and developing treatment interventions for Alzheimer's disease

<u>Rilmenidine</u> was recently identified as a potential drug for the treatment of neurodegeneration by a screening of US Food and Drug Adminstration (FDA) approved drugs. This follows the finding that rilmenidine, a drug prescribed for hypertension, could attenuate toxicity in a mouse model of Huntington's disease, possibly by activating autophagy in an mTOR-independent fashion (Rose *et al.*, 2010). However, the research is still in its early phases, no results of rilmenidine-based intervention in an AD model exist yet.

b. **The ketogenic diet and neurodegenerative diseases**

Early reports indicate that specific diets increase the risk for developing AD. A study of a community's fat intake revealed that high intake of saturated or *trans*-unsaturated fats increased the incidence of AD, while unsaturated fat intake served a protective role (Morris *et al.*, 2003). In addition high energy and dietary saturated fat in old age are considered high risk factors for AD (Grant, 1999). The Rotterdam study, which aimed to assess the causes of disease incidence and progression in the elderly (people aged 55 to 106 years), is an example (Hofman *et al.*, 1991). Kalmijn *et al.* (1997) investigated the relationship between dietary fat and cholesterol consumption and the risk of dementia in participants of the Rotterdam study. They suggest a borderline significant association between high saturated fat (p=0.66) and cholesterol (p=0.40) intake and the risk of dementia and refer to the fact that this type of diet is associated with cardiovascular disease, which increases the risk of developing dementia. Thus there is a definitive role for a high calorie diet and metabolic disruptions in AD pathogenesis.

In contrast, evidence indicates that ketosis is protective against dementia, as will be discussed below. Prolonged fasting, diabetic ketoacidosis and following a ketogenic diet (KD) cause production of ketone bodies. KDs are characterised by very low carbohydrate content and increased fat and protein intake, with fat intake commonly providing 80% of dietary calories (Beckett *et al.*, 2013). 'Ketosis' is indicated by an increase in measurable ketone bodies in circulation, specifically elevation of beta-hydroxybutyrate (β-OHB) and acetoacetate (Veech *et al.*, 2001). Physiological ketosis (in contrast to pathological diabetic ketoacidosis) occurs after 3-4 days of no carbohydrate consumption, which leads to the overproduction of ketone bodies from fatty acids (Paoli *et al.,* 2013). AcCoA is synthesised from ketone bodies as an energetic substrate which can enter the TCA cycle (Paoli *et al.*,

2013). Humans are, as far as is known, the only species that reaches plasma β-OHB levels above 5 mM/L –possibly an evolutionary conserved mechanism of relying on ketone bodies for 'brain fuel' during times of starvation. Basal blood β-OHB levels range from 0.01-0.03 mM (Grey *et al.*, 1975) while the average plasma concentration of β-OHB in human adults is 4-7 mM/L after two weeks of fasting (Cahill, 2006).

Ketone bodies are produced by the liver. Three ketone bodies exist: acetone, acetoacetate, and β-hydroxybutyrate (Prins, 2008). Only β-OHB and acetoacetate are used as metabolic fuel sources, and are produced by the partial oxidation of fatty acids (Cahill, 2006). β-OHB is the primary circulating ketone body and increased concentrations are observed four to seven days after fasting (Grey *et al.*, 1975). Plasma β-OHB levels can increase four- to fivefold after two days of fasting or following a KD, with a remarkable 13 fold increase in its cerebral uptake (Prins, 2008). Ketone bodies replace glucose as the brain's main metabolite during ketosis (Owen *et al.*, 1967). They cross the blood-brain barrier by using monocarboxylate transporters (MCTs), where they are metabolised by three enzymes and then enter the TCA cycle (Prins, 2008).

In recent years, there have been increasing reports of KDs improving various disease conditions. Epilepsy was treated successfully with the KD for many decades, and is today an established part of an integrative approach to managing epilepsy, together with anticonvulsant drugs (Kossoff, 2011). The therapeutic use of the KD for epilepsy paved the way for research into other neurological diseases, and the KD has received increasing attention from researchers in the neurodegeneration field.

Administering a KD (60% fat) was found to protect against motor neuron death in a mouse model of amyotrophic lateral sclerosis (ALS; Zhao *et al.,* 2006). In addition, it was found that KB promotes ATP production in ALS mice – ATP concentration was increased in mitochondria isolated from mutant mice when treated with ketone bodies, with mitochondria showing an increased ATP synthesis rate compared to diseased controls (Zhao *et al.*, 2006).

Cheng *et al.* (2009) induced PD in rats by administering 6-hydroxydopamine (6-OHDA) and investigated the effects of a KD (composed of 90,7% fat) on dopaminergic neurons. They revealed that the KD protected against 6-OHDA neurotoxicity and corrected the decreased dopamine levels and its metabolite dihydroxyphenylacetic acid found in PD rats. Levels of the antioxidant glutathione are decreased in PD rats, and administration of a KD inhibited this decrease. The authors conclude that this mechanism was responsible for the neuroprotective effects of the KD observed. In a human feasibility study, PD patients that followed a 'hyperketogenic diet' (4 parts fat to 1 part carbohydrate-protein mixture) for four weeks had improved Unified Parkinson's Disease Rating Scale scores, however a placebo effect was not ruled out (VanItallie *et al.*, 2005).

In a study of HD mice fed a KD, researchers identified delayed onset of significant weight loss in KD fed mice. This is an important improvement, considering that higher body weight is correlated with slow HD progression (Ruskin *et al.*, 2011). Taken together, the evidence presented here demonstrates the versatility and efficacy of using the KD, or KB to treat neurodegenerative diseases. AD is no exception, as will be discussed next.

c. Ketone bodies as Alzheimer's disease adjuvant therapy

Differences may exist in the efficacy of utilizing ketone bodies under normal and diseased conditions. Indeed, there is a loss of utilization efficiency in AD. AD patients report a higher incidence of seizures (Palop and Mucke, 2009) possibly because the homeostasis of both neuronal circuits and mitochondrial functioning is affected (Kapogiannis *et al.*, 2011). Thus it became feasible to use KD as a treatment for AD as it is also a neurodegenerative disease featuring disrupted synaptic transmission as a result of Aβ toxicity (Calkins and Reddy, 2011).

In the hippocampus of non-transgenic female mice KB were transported and utilized as an alternative fuel (Ding *et al.,* 2013). In 3xTg-AD mice, however, only three month old mice showed a ketogenic phenotype, after which the use of ketone bodies declined, indicating that mice with advanced disease were not able to utilize ketone bodies, and thus were

denied the benefits of switching to ketone metabolism as an adaptive response (Ding *et al.*, 2013).

Samoilova *et al.* (2010) demonstrated that exposing hippocampal cultures to a chronic concentration of 10 mmol/L of ketone bodies in conjunction with low glucose was neuroprotective, as indicated by attenuated cell death after ischemia and glucose deprivation, but not against the seizure-type hyperexcitability responsible for neuronal damage during metabolic insults. Arakawa *et al.* (1991) demonstrated that ketone body administration can act as a substitute energy source for glucose. They revelaed that ATP levels were significantly increased after two hours of treatment in brain slices treated with glucose-free medium and medium containing ketone bodies only.

In a study of mice carrying the 'London' (APP/V717I) mutation, which leads to early and significantly increased brain Aβ levels, Van der Auwera and colleagues (2005) revealed decreased Aβ deposition in the brain after only 43 days following a KD. Beckett *et al.* (2013) did not find a decrease in Aβ levels in mice with knock-in mutations of the APP and PSEN1 genes fed a KD for one month, despite motor improvements. Both of these groups used young mice (three and 1-2 months old, respectively) and fed the mice similar chow composed of 79% fat, hence these results are conflicting.

Recently, C57/BL6 double transgenic mice, which exhibit age-dependent Aβ plaque aggregation, administered an esterified form of β-OHB for 2.5 months promoted spatial learning and working memory, as indicated by Morris water maze results (Zhang *et al.*, 2013). In addition to these cognitive improvements, the authors described a multitude of other beneficial effects. There was a decrease in Aβ deposition in the hippocampus which, remarkably, was more effective than the approved AD drug, donepezil. β-OHB administration decreased apoptotic cell death in glucose-deprived cells, possibly due to its protective effects on mitochondria; ketone body treated groups showed stabilized mitochondrial membrane potential, increased ATP levels and an increased reductive state (Zhang *et al.,* 2013).

 A randomized double-blind placebo-controlled clinical trial in which mild-to-moderate AD patients were given an oral ketogenic substrate caused a significant improvement in cognitive performance (Henderson *et al.*, 2009). Similarly, Reger *et al.* (2004) found that increasing serum β-OHB levels of patients suspected of having AD (as indicated by the National Institute of Neurological and Communicative Diseases and Stroke/Alzheimer's Disease and Related Disorders Association's or NINCDS/ADRDA criteria and positive for the ApoE4 allele) by medium-chain triglyceride administration resulted in improved Alzheimer's Disease Assessment Scale (ADAS-cog) scores, a test consisting of 11 subscales which measure various cognitive abilities including memory, language and praxis skills (Benge *et al.*, 2009). Interestingly, the ameliorative effects of KB on AD symptoms seem to be dependent on the patients' ApoE genotype. Cognitive improvements are more marked in or even limited to patients without ApoE4 allele in many studies (see Reger *et al.*, 2004; Henderson *et al.*, 2009). In a retrospective study, eight AD patients on standard pharmacological treatment were given the medium chain triglycerid caprylic triglyceride to induce ketosis (Maynard and Gelblum, 2013). Caprylic triglyceride administration seemed to slow disease progression and some patients had cognitive improvements.

It can be concluded from the above literature that ketone bodies can indeed bring about substantial improvement in AD-related neuropathology. KB successfully ameliorate both molecular disruptions and cognitive deficits present in AD. Despite the encouraging results demonstrated by administering ketogenic agents or diets, however, it is unknown what effects ketone body administration has regarding autophagic flux, mitochondrial network morphology and function, intracellular ATP levels and localization and the extent of apoptotic cell death. Furthermore, it remains unknown where intracellular ATP localizes in neurons and it would be beneficial to assess its association with cell compartments like mitochondria in order to better understand ATP demand and AD-related metabolic failure.

1.5 Aims and hypothesis

Aims

Therefore our aims are to assess the effects of beta-hydroxybutyrate under basal conditions and in an injury-induced model. Specifically we aim to assess the following parameters:

1. Paraquat-induced neuronal cell death

2. Autophagic flux

3. Mitochondrial network morphology

4. Intracellular ATP concentrations and localization in neurons

Hypothesis

We hypothesize that beta-hydroxybutyrate will protect cells from paraquat-induced neurotoxicity, by increasing ATP levels through increasing autophagic flux.

Chapter 2: MATERIALS AND METHODS

2.1 Reagents and consumables
2.1.1 Cell line and general consumables

GT1-7 cells, mouse neuronal cells of hypothalamic origin, were provided by Dr. Kinnear, Tygerberg, University of Stellenbosch (Mellon *et al.,* 1990). Dulbecco's modified Eagle's medium (DMEM, 41965062), PenStrep antibiotic (15140122) and trypsin (25200072) were purchased from Life Technologies. Fetal bovine serum (FBS, FBS-GI-12A) was supplied by Capricorn Scientific and 15 and 50 ml Falcon tubes were purchased from SPL Life Sciences (EF4661 and EF4663). 0.5 and 2 ml Eppendorf tubes were purchased from Citotest (4610-1821) and Axygen Scientific (311-10-051), respectively. 25 cm^2, 75 cm^2, and 175 cm^2 non-pyrogenic polystyrene cell culture flasks were purchased from Nest Biotechnology (707001, 708001 and 709001). 10 ml serological pipettes were acquired from Biocom Biotech (PN10E1) and NUNC 8-well chambered coverglass dishes (155411) were purchased from Thermo Scientific and 48-well plates from SPL Life Sciences (30048). 35 mm culture dishes were supplied by Falcon (353001). White 96-well plates (3912) for use in the ATP luminescence based assay were supplied by Corning Costar as well as cryogenic vials (430488).Dimethyl sulfoxide (DMSO) was supplied by Sigma-Aldrich (D2650).

2.1.2 Treatment reagents

DL-β-Hydroxybutyric acid sodium salt (H6501) and paraquat (methyl viologen dichloride hydrate, 856177) were purchased from Sigma-Aldrich and bafilomycin A$_1$ from LKT Laboratories (B0025). All reagents were prepared as stock concentration using dH$_2$O (paraquat) or sterile PBS (ketone bodies and bafilomycin) as a solvent.

2.1.3 Western blot reagents

Bradford reagent was made up using Brilliant Blue G (27815) from Sigma-Aldrich. Bovine serum albumin (BSA, 10735078001) was obtained from Sigma-Aldrich. Gels were cast using the TGX FastCast Acrylamide kit (12%, 50 μL wells) and Trans-Blot Turbo Transfer packs (Midi format, PVDF 0.2 μm) both purchased from Bio-Rad (161-0175 and 170-4157). An ECL (enhanced chemiluminescence) kit containing peroxide and luminol/enhancer reagents was purchased from Bio-Rad (170-5061). Tween 20 (P1379) and sodium hydroxide (NaOH,

S5881) were purchased from Sigma-Aldrich. The following phosphatase and protease inhibitors were purchased from Sigma-Aldrich: Aprotonin (A1153), Leupeptin (L2884), Pepstatin A (P5318), Benzamidine (B6506), PMSF (93482) and Na_3VO_4 (S6508). BLUeye prestained protein ladder was obtained from GeneDirex (PM007-0500).

2.1.4   Antibodies

Antibodies were purchased from Cell Signaling and produced in rabbit unless otherwise specified. Primary antibodies against BACE (55606S), APP/beta-Amyloid (anti-mouse, 2450S), cleaved PARP (9541S), LC3B (2775) SQSTM1/p62 (ab56416) and GAPDH (5174) were used. The secondary antibodies anti-rabbit IgG HRP (7074S) and anti-mouse IgG HRP (7076S) were acquired from Abcam.

2.1.5   Fluorescent probes

The above indicated primary antibodies for BACE, APP and APP/beta-Amyloid were used for fluorescence microscopy. Secondary antibodies AlexaFluor 488 donkey anti-mouse (A21202) and AlexaFluor 568 donkey anti-rabbit (A10042) were purchased from Cell Signaling. Hoechst 33342 (14533) was supplied by Sigma-Aldrich.

2.2   Experimental procedures

2.2.1   Tissue culture of GT1-7 neuronal cells

GT1-7 cells were cultured at 37 °C within a humidified atmosphere in a 5% CO_2 incubator in 1X DMEM supplemented with 10% fetal bovine serum and 1% PenStrep. Cells were stored in a liquid nitrogen cell tank in 1 ml cryovials containing approximately 1 X 10^6 cells, in 90% FBS with 10% DMSO.

2.2.2   Thawing and culturing of cells

Frozen cells were thawed by immersing the cryovile in a bead bath at 37 °C. Cryovile contents and 1 ml pre-warmed medium were transferred to a sterile 15 ml Falcon tube using a sterile pipette tip (P1000 micropipette) and centrifuged (Eppendorf centrifuge 5804R) at 1500 rpm for 3 min at room temperature after which the supernatant was discarded. The pellet was resuspended in 1 ml pre-warmed medium using a sterile pipette

tip (P1000 micropipette) and transferred to a sterile 25 cm^2 flask containing 4 ml pre-warmed medium. The culture medium was changed every 48 hrs for the duration of the culturing procedure. Cells were subcultured at 80% confluency.

2.2.3   Subculturing and seeding of cells for experiments

Medium was removed using a 5 ml serological pipette after which trypsin was added to the cell monolayer and the flask placed in an incubated cell shaker (MRC) for 4 min. Cells were viewed under an inverted microscope (Olympus CKX31) to ensure their dissociation from the flask surface and were transferred to a sterile 15 ml Falcon tube using a sterile 10 ml serological pipette. FBS-supplemented medium constituting double the volume of trypsin used was added using a 10 ml serological pipette to deactivate the trypsin. The cell suspension was centrifuged at 1500 rpm for 3 min at room temperature after which the supernatant was discarded and the cell pellet resuspended in 1 ml medium using a sterile pipette tip (P1000 micropipette). A Neubauer Improved haemocytometer (Marienfeld) was used to count cells for seeding into the appropriate dish or for subculturing. Cells were used to a maximum passage number of 24.

2.2.4   WST-1 assays

2.2.4.1   WST-1 assay to determine viability

For determining cell viability cells were seeded at 80 X 10^3 cells per well in 48 well plates and incubated (37 °C, 5% CO$_2$) until 80% confluency was reached (approximately 24 hrs). Ketone body salt (DL-β-Hydroxybutyric acid sodium salt) was diluted in medium to obtain concentrations of 1.5 mM, 3 mM, 6 mM and 12 mM to assess for potential toxic effects at high concentrations and to determine the optimal concentration to use for further experiments. Cells treated with medium only served as the control. Following incubation with the various treatments, 10 µl WST-1 cell proliferation reagent (AB155902, Abcam) and 190 µl fresh medium was added to each well and plates were incubated in light protected conditions for 2 hrs. WST-1 is an indicator of mitochondrial reductive activity of living cells, and is analogous to the widely used MTT assay which is accepted as a measure of cell survival. The assay is based on the reduction of tetrazolium salts to formazan by cellular enzymes (Berridge *et al.*, 1996). After incubation, plates were placed on an oscillating bellydancer (Stovall Life Sciences) for 1 min to allow mixing of well contents. The

absorbance values of the supernatant were read at 490 nm using a microplate reader (EL800, Bio-Tek instruments). The relative mitochondrial reductive capacity of cells was calculated as a percentage of control. Three independent experiments were performed for each condition with a mimimum of eight technical repeats for each treatment group.

2.2.4.2   WST-1 assay to determine viability following paraquat and ketone body treatment

After seeding cells as described (section 2.2.4.1) cells were treated with a defined range of paraquat concentrations (10 µM – 5 mM) for 24 hrs to determine a suitable concentration that achieves approximately 50% cell death, to be used in the following experiments. Untreated cells served as the control. The WST-1 assay was completed as in section 2.2.4.1. After determining a suitable concentration (600 µM), the following treatment groups were assessed: Control, paraquat, ketone bodies (6 mM), and paraquat + ketone bodies (600 µM and 6 mM, respectively). Cells were treated for 24 hrs after which the WST-1 assay was completed as described above.

2.2.5   Tetramethylrhodamine ethyl ester (TMRE) treatment

2.2.5.1   Sample preparation and TMRE treatment

GT1-7 cells were seeded into 8-chamber plates at a density of 30×10^3 cells per well. Cells were allowed to adhere overnight at 37 °C and in a 5% CO_2 atmosphere after which growth medium was refreshed. Medium was removed and replaced with medium containing 500 nM tetramethylrhodamine ethyl ester (TMRE; Abcam ab113852) to visualize mitochondria in living cells. TMRE is a membrane potential-dependent fluorochrome that stains mitochondria with polarized, intact membranes as described by Hanley *et al.* (2002). Hoechst 33342 was added to wells (1:200 in medium) prior to imaging to counterstain nuclei.

2.2.5.2   Live cell imaging of mitochondria

Cells were transferred to a wide field inverted microscope (Olympus IX81, Olympus Corporation, Tokyo, Japan) equipped with a Xenon-Arc burner (Olympus Biosystems GMBH, Hamburg, Germany) light source surrounded by an incubator chamber (37 °C; 5% CO_2 atmosphere). An F-view-II cooled CCD camera (Soft Imaging Systems, Olympus Corporation,

Tokyo, Japan) was mounted on the microscope. The TxRed excitation filter was used to capture images of polarized mitochondria and the DAPI excitation filter for the acquisition of nuclei. Emission was collected with a UBG triple-bandpass emission filter cube (Chroma) and images were captured and edited using Olympus Cell^R (Hamburg, Germany) software.

2.2.6   Mitochondrial morphological assessment

GT1-7 cells were stained with the mitochondrial marker TMRE and imaged as described above. Raw images were converted to an 8-bit format using ImageJ software. The 'Convolve' and 'Gaussian blur' filters were utilized and thresholds adjusted to enhance the mitochondrial signal suitable for image analysis. The particles were analysed and the average mitochondrial count per group calculated based on all the mitochondria counted in five different cells in five respective micrographs. The mitochondrial morphological characteristics were quantified according to two parameters: aspect ratio, which indicates the length of mitochondria (ratio between the major and minor axes of mitochondria), and form factor, which indicates the degree of branching (Pm2/4πAm) where 'Pm' is the length of the mitochondrial outline and 'Am' is the mitochondrial area (Mortiboys *et al.,* 2008).

2.2.7   FRET-based ATP indicator

2.2.7.1   Transfection with ATeam construct

GT1-7 cells were seeded into 8-chamber dishes at a density of 30 X 10^3 cells per well. Cells were allowed to adhere overnight at 37°C and in a 5% CO_2 atmosphere after which growth medium was refreshed. A FRET-based ATP indicator, targeted to mitochondrial ATP, ATeam 1.03 (Imamura *et al*., 2009) was used to identify the intracellular localization of mitochondrial ATP. The transfection procedure was performed by adding a solution containing 400 ng DNA, 1 µl lipofectamine (Invitrogen), 20 µl serum-free medium, and 1.6 µl P3000 transfection reagent (Invitrogen) to each well containing 300 µl fresh growth medium and incubating cells (37°C; 5% CO_2 atmosphere) for 1 h. Growth medium was subsequently refreshed and cells incubated for 48 hrs prior to imaging. Treatment groups were exposed to their respective treatment solutions 24 hrs prior to imaging.

2.2.7.2 Fluorescence microscopy of intracellular ATP in live cells

Cells were transferred to a wide field inverted microscope as described above (2.2.5). A minimum of 15 transfected cells were acquired per group using a 100X magnification. Micrographs were captured using the CFP and YFP excitation and emission filters. In brief, the donor was acquired by using CFP excitation and emission, the FRET channel was acquired by using CFP excitation and YFP emission, while the YFP channel was acquired by using YFP excitation and emission. The FRET analysis function (ratio: FRET channel and CFP channel) of the Cell^R program was utilized to generate the FRET image displaying ATP derived signal and a 'ColdWarmHot' lookup table (LUT) was employed to indicate emission intensity.

2.2.8   ATP analysis

Cells were seeded in 35 mm culture dishes at a density of 1 X 10^6 cells per dish and grown under standard culturing conditions until 90% confluent. Medium was transferred to sterile 1 ml Eppendorf tubes (in the case of the paraquat treatment groups) and centrifuged to ensure non-adherent cells were included for ATP harvesting. At this stage cells were trypsinized by adding 1 ml trypsin per dish and by placing samples in a shaking incubator for 4 min. Culture dish contentswere centrifuged in sterile 1 ml Eppendorf tubes at 10 000 rpm at 4 °C for 3 min, the supernatant discarded and the pellet resuspendedin cold PBS. The centrifugation step was repeated and the pellet subsequently resuspended in 50 µl ice cold lysis buffer containing 100 mM Tris-HCl and 4 mM EDTA (pH 7.75) as previously shown (Essman *et al.* 2003). 150 µl boiling lysis buffer was added to the cell suspension and kept at 99 °C in a water bath for 2 min. Samples were then centrifuged for 3 min at 10 000 rpm (4 °C) after which the supernatant containing ATP was collected in fresh Eppendorf tubes and stored at -20 °C until further analysis.

A luminometer (Glomax, Promega) was used to measure sample luminescence. 50 µl of ATP-containing supernatant and 50 ul of rL/L reagent (Enliten ATP assay FF2000, Promega) were added to white 96-well microtiter plates according to the manufacturer's instructions and luminescence signal was acquired. A standard curve was produced according to the manufacturer's protocol.

2.2.9   Flow cytometry

2.2.9.1   Tetramethylrhodamine ethyl ester (TMRE) intensity

Cells were seeded in T-25 flasks at a density of 2 X 10^6 cells per flask and grown to approximately 75% confluency. Following treatment with paraquat and ketone bodies, cells were trypsinized by incubating cells with pre-warmed trypsin for 4 min until cells detached, centrifuged for 3 min at 1500 rpm and then resuspended in 1 ml warm sterile PBS. Unfixed cells were incubated with 1 µM TMRE for 30 min at 37 °C and immediately analysed. Carbonyl cyanide m-chlorophenylhydrazone (CCCP, Sigma, C2759) was used as a positive control using a concentration of 5 µM. An unstained control sample was acquired in order to set the photomultiplier tube (PMT) voltages. Flow cytometry (BD FACSAria I) was used to analyze samples by collecting a minimum of 10 000 cells using a 488 nm laser and 610LP, 616/23BP emission filters. Fluorescence intensity signal was obtained by using the geometric mean of the intensity histogram.

2.2.9.2   ROS assessment

2',7'-Dichlorofluorescein (DCF) was used to evaluate generic ROS. Cells were seeded and treated as mentioned in 2.2.9. Unfixed cells were incubated with 50 µM DCF for 10 min at 37 °C and immediately analyzed. H_2O_2 was used as a positive control, using 100 µl in the cell suspension. An unstained control sample was acquired to set the PMT voltages. A flow cytometer (BD FACSAria I) was used to analyze samples by collecting a minimum of 10 000 cells using a 488 nm laser and 502LP, 530/30BP emission filters. Fluorescence intensity signal was obtained by using the geometric mean of the intensity histogram.

2.2.10   Transmission electron microscopy (TEM)

2.2.10.1   Sample preparation

GT1-7 cells were seeded in T-25 flasks at a density of 1.5 X 10^6 cells per flask and were grown to approximately 90% confluency. Four groups were assessed: Control, paraquat, ketone bodies and paraquat + ketone bodies. Two flasks per group were seeded. Following 24 h treatment, 2 ml trypsin was added to each flask and incubated for 4 min. Cell suspensions were transferred into 15 ml Falcon tubes, each containing 8 ml FBS-supplemented growth medium, according to treatment group. Tubes were centrifuged at 1500 rpm for 3 min at 37 °C. The supernatant was discarded and the cell pellet resuspended

in pre-warmed 1 X PBS to remove remaining trypsin and medium. The centrifugation step was repeated, the PBS discarded and the cell pellet resuspended in 1 ml 2.5% glutaraldehyde, after which tubes were centrifuged at 1500 rpm for 3 min at 37 °C. Samples were transported to Tygerberg Hospital where TEM analysis was completed by the National Health Laboratory Services.

2.2.10.2   Processing, sectioning and imaging of samples

Samples were sectioned into 1 mm sections using a dissecting microscope and rinsed in phosphate buffer. Samples were incubated in 3% osmium tetroxide for 1 h and subsequently kept in a 10% formalin solution to reduce the osmium tetroxide. Samples were then transferred to an automated tissue processer, and immersed in a sequence of solutions according to the following protocol:

1. 15 min in 10% uranyl acetate

2. 10 min in 70% ethanol

3. 10 min in 70% ethanol

4. 20 min in 10% uranyl nitrate

5. 15 min in 100% ethanol

6. 20 min in 100% ethanol

7. 30 min in 100% ethanol

8. 90 min in a 1:1 solution of 100% ethanol and Spurr's resin

9. 60 min in Spurr's resin

10. 60 min in Spurr's resin

Samples were subsequently embedded into gelatin capsules overnight at 60 °C after which they were cut into 200 nm sections using a Leica EM UC7 ultramicrotome. Sections were stretched with chloroform and placed onto copper grids. Images were captured using a JEOL JEM 1011 transmission electron microscope and the iTEM soft imaging analysis program. TEM images were qualitatively analyzed.

2.2.11 Bafilomycin A$_1$ and ketone body treatment for Western blot analysis of LC3, p62, APP, Aβ and BACE

Bafilomycin A$_1$ is an antibiotic that is often used to inhibit the process of autophagy as it is a specific inhibitor of the H$^+$-ATPase (V-ATPase) enzyme (Klionsky *et al,.* 2008). Treatment inhibits the acidification of lysosomes and endosomes and thereby blocks the fusion of lysosomes with autophagosomes. Cells were seeded into T-25 flasks at a density of 1.5 X 10^6 cells per flask. Flasks were divided into four treatment groups: Control, control + bafilomycin, ketone bodies, ketone bodies + bafilomycin. 400 nM bafilomycin diluted in medium was used and cells treated after reaching 80% confluency. Respective groups were treated with pre-warmed supplemented medium for 24 hrs, after which fresh medium in the presence or absence of bafilomycin was added and cells incubated for a further 2 hrs. Both of the ketone body groups were treated with pre-warmed FBS-supplemented medium containing 6 mM dissolved β-OHB for 24 hrs. Medium was refreshed with DMEM growth medium in the presence or absence of bafilomycin and flasks incubated for a further 2 hrs.

2.2.12 Determining intracellular distribution of APP, Aβ and BACE

2.2.12.1 Staining of APP, Aβ and BACE

Cells were seeded into NUNC chamber dishes and treated with bafilomycin and ketone bodies as described above. After treatment, growth medium was aspirated and cells were rinsed with pre-warmed 1X PBS. 200 µl of ice cold methanol-acetone (1:1) was added per well and cells incubated at 4 °C for 10 min. Fixative was removed and cells allowed to airdry for 20 min. Wells were rinsed with 1X PBS and cells were blocked with 100 µl FBS per well for 20 min at room temperature. After removing the serum, each well was incubated for 90 min with 50 µl of a mixture of APP primary antibody (mouse; 1:50) and beta-site APP cleaving enzyme (BACE) primary antibody (rabbit) (1:100) made up in 1X PBS or a mixture of APP and beta-amyloid (Aβ) primary antibody (rabbit; 1:100) made up in PBS. Wells were carefully rinsed with 400 µl PBS and incubated with 50 µl of a mixture of AlexaFluor 488 donkey anti-mouse IgG (for APP) and AlexaFluor 568 donkey anti-rabbit IgG (for BACE or Aβ) for 30 min at room temperature in a humidified, light-protected environment. 50 µl of Hoechst 33342 (1:200 in PBS) was added to wells to counterstain nuclei and incubated for a further 10 min at room temperature in a humidified, light-protected environment. Wells

were rinsed three times with 400 µl PBS and subsequently mounted by using fluorescent mounting medium (S302380, Dako). Cells were imaged immediately.

2.2.12.2 Fluorescence microscopy of APP, Aβ and BACE

Cells were transferred to a wide field inverted microscope as described above (2.2.5). 15 transfected cells were imaged per group at a 100X magnification. Three excitation filters were used to capture images: TxRed for Aβ and BACE and FITC for APP. Emission was collected with a UBG triple-bandpass emission filter cube (Chroma) and images were captured and edited using Olympus Cell^R (Hamburg, Germany) software.

2.2.13 RIPA buffer extraction of protein

Radio-immunoprecipitation (RIPA) buffer contains various ingredients to facilitate protein extraction from cells and includes protease inhibitors and phosphatase inhibitors. RIPA buffer contains phenylmethylsulfonyl fluoride (PMSF), aprotonin, leupeptin, benzamidine, activated sodium orthovanadate (Na_3VO_4) and sodium fluoride (NaF). Each T-25 cell culture plate was rinsed three times with cold PBS and 50 µl cold RIPA buffer was added. The cell monolayer was scraped with a sterile cell scraper and lysates transferred to sterile Eppendorf tubes. Lysates were homogenized by sonicating at a frequency of 3 Hertz (Misosonix S-4000) on ice for a total of four seconds with a 2 sec interval after each second of sonication. Tubes were kept on ice at 4 °C for approximately 2 hrs until the lysates had a clear appearance. Subsequently lysates were centrifuged at 8000 rpm for 10 min at 4 °C, aspirated and transferred into fresh sterile Eppendorf tubes and stored at -20 °C until further analysis.

2.2.14 Western blot analysis of APP, Aβ, BACE, LC3, p62 and cleaved PARP

2.2.14.1 Bradford protein quantification

Bradford reagent was prepared in a working solution by using Coomassie Brilliant Blue G-250 (27815, Sigma), 95% ethanol, phosphoric acid and dH_2O (Bradford, 1976). BSA 0.2 mg/ml stock solution was prepared at a range of concentrations by dilution in dH_2O (see Table 2). 5 µg of protein was added to 95 µl dH_2O and vortexed. 900 µl Bradford working solution was added to all tubes and allowed to incubate for 5 min at room temperature in the dark. Standard and experimental samples were prepared in duplicates. A

spectrophotometer (Cecil CE 2021) was used to measure absorbance at a wavelength of 595 nm. Microsoft Excel was used to produce a standard curve of protein concentration against absorbance values from which the protein concentrations of experimental samples was determined.

Concentration (µg/ml)	Volume of BSA (µl)	Volume of dH$_2$O
0 (Blank)	0	100
2	10	90
4	20	80
8	40	60
12	60	40
16	80	20
20	100	0

Table 2: BSA preparation for Bradford standard curve.

2.2.14.2   Sample preparation

A stock solution (5 ml) of Laemmli's loading buffer was prepared by diluting 1 ml Tris-HCL (0.5M; pH 6.8), 0.8 ml glycerol, 1.6 ml of 10% SDS (sodium dodecyl sulfate), and 0.4 ml of 0.05% bromophenol blue in dH$_2$O. A working solution of Laemmli's loading buffer was prepared by adding 150 µl of β-mercaptoethanol (161-0710, Bio-Rad) to 850 µl of Laemmli's loading buffer followed by vortexing. The appropriate volumes of protein samples were added to Eppendorf tubes so as to obtain 50 µg of each protein sample per tube. The appropriate volume of Laemmli's loading buffer (⅓ of the protein volume) was added to each sample. Samples were boiled for 5 min at 95 ˚C, vortexed, centrifuged, and placed on ice immediately.

2.2.14.3   Sodium-dodecyl-sulfate-polyacrylamide gel electrophoresis (SDS-PAGE)

Precast Mini-Protean SDS-PAGE gels were firmly secured onto an electrode assembly and placed inside a Mini-Protean Tetra cell tank. 1X running buffer was used to fill the buffer chamber and to rinse gel wells using a syringe. 7.5 µl of protein ladder was loaded into the first well and the prepared samples were loaded at their respective volumes into remaining

wells. The electrode assembly was connected to a power supply (Bio-Rad Power Pac 1000) and proteins were separated at 120 V for approximately 60 min. A Trans-Blot Turbo transfer pack and a Bio-Rad Trans-Blot turbo transfer system were used to transfer proteins for 10 min from the gel to a PVDF (polyvinydilene difluoride) membrane. The membrane was blocked in 5% non-fat milk in 1X TBS-T (Tris-buffered saline and 1% Tween 20) for 2 hrs to reduce non-specific binding, rinsed 3 X 5 min in 1X TBS-T, and incubated in primary antibodies (1:1000 in TBS-T) overnight on a rotator at 4 ˚C. After rinsing the membrane in 1X TBS-T for 3 X 5 min, it was incubated in anti-rabbit HRP-linked secondary antibody (anti-rabbit or anti-mouse; 1:5000 in TBS-T) for 60 min at room temperature on a roller mixer (Stuart SRT9) followed by a washing step of 3 X 5 min in 1X TBS-T. 1 ml of ECL reagent (peroxide buffer and enhancer solution prepared in a 1:1 ratio) was added to the membrane and protein signal and band intensities were detected using a Bio-Rad Chemidoc MP imaging system equipped with Image Lab software (version 4.1).

2.2.14.4   Loading controls

Glyceraldehyde 3-phosphate dehydrogenase (GAPDH) was used as a loading control for all Western blots. Membranes were stripped with 0.2 M NaOH in dH_2O for 5 min and washed 3 X 5 min with dH_2O. Membranes were blocked in 5% non-fat milk for 2 hrs, incubated in GAPDH primary antibody (1:1000) and incubated overnight on a rotator at 4 °C. Membranes were incubated with HRP-linked anti-rabbit secondary antibody (1:5000) for 1 h, washed 3 X 5 min with 1 X TBS-T and developed and imaged as described above.

2.2.15   Statistical analysis

Statistical analysis of all quantifiable data was performed using Prism 5 software utilizing a one-way ANOVA with a Bonferroni post-hoc test. A p-value < 0.05 was considered significant. Results are indicated as mean ± standard error of mean.

Chapter 3: RESULTS

SECTION 1: Ketone bodies and autophagy under basal conditions

In order to unravel the role of autophagy in neurodegeneration, two aspects were investigated. Firstly, autophagy and specific candidate proteins were assessed under basal conditions, in the presence and absence of ketone bodies, in order to assess the role of ketone bodies and autophagic flux on the clearance of candidate proteins that are implicated in proteotoxicity. Secondly, neurotoxicity was induced in order to assess the potential protective role of ketone body supplementation in the context of neuronal cell death. Accordingly, the first section of this chapter will focus on the results regarding the effects of ketone bodies on autophagy and amyloid processing. In the second section we will focus on the results that assess the role of ketone bodies on paraquat-induced neuronal injury.

3.1.1 The effect of ketone body treatment and basal autophagy on ATP concentration

A luciferase-based ATP assay was employed to measure total intracellular ATP levels following the treatment with bafilomycin A_1, an inhibitor of lysosomal fusion, in the presence and absence of ketone bodies. There was no significant difference in detected ATP levels between treatment groups (Figure 3.1.1). Measured concentrations per group were indicated as control [2.62 ± 0.2 pM], control + bafilomycin [2.7 ± 0.2 pM], ketone bodies [2.8 ± 0.2 pM] and ketone bodies + bafilomycin [2.5 ± 0.1 pM].
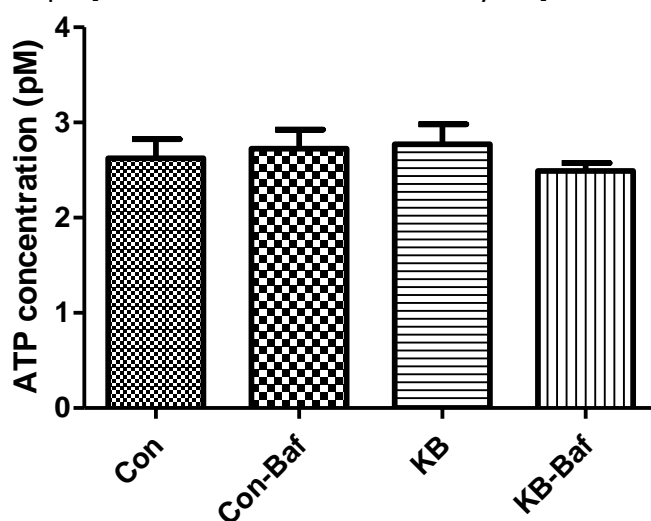

Figure 3.1.1: Total ATP concentration under basal conditions. ATP concentration (pM) in GT1-7 cells indicating control (Con), treatment with bafilomycin (Con-Baf: 4 hrs 400 nM), ketone bodies (KB: 24 hrs 6 mM) or bafilomycin and ketone bodies (KB-Baf: 24 hrs 6 mM + 4 hrs 400 nM), (n=6).

3.1.2 The effect of ketone body treatment and basal autophagy on ATP distribution

Cells were transfected with an ATP indicator, ATeam (Imamura *et al.,* 2009), that utilizes FRET allowing generation of an image of mitochondrial-targeted ATP within cells. GT1-7 cells were treated with bafilomycin A_1 and ketone bodies to determine their effect on the intracellular ATP distribution profile. Here, regions with high signal intensity would indicate areas with a locally high ATP concentration. Micrographs display a discernible pattern of ATP distribution of ATP within cells (Figure 3.1.2a), with the presence of 'hotspots' revealed by using a lookup table (Figure 3.1.2b). In control cells, many small hotspots, occurring throughout the cytoplasm are visible, suggesting a relatively homogenous distribution of ATP across the cell. The distribution is diffuse in comparison to the other groups, where larger hotspots can be observed in different regions of the cells.

It appears that the inhibition of autophagy leads to an increased ATP-derived emission (Figure 3.1.2a Con-Baf and KB-Baf), suggesting that functional autophagy is important for local ATP generation. The same is observed upon ketone body exposure. The image data suggests that exposure to ketone bodies and bafilomycin further changes the ATP distribution profile to a large region of localized signal.

These data suggest that, although total ATP concentration remains unchanged, ATP distribution is being affected by the ketone body treatment. Inhibition of autophagy shows a similar pattern, indicating localized changes in ATP demand.

The ATP distribution within the complete cellular mitochondrial network, instead of distribution within single mitochondria was assessed, as the ATeam construct was mitochondrially targeted.

	CFP-Don	YFP-Acc	FRET	Don/FRET LUT
Con				
Con-Baf				
KB				
KB-Baf				
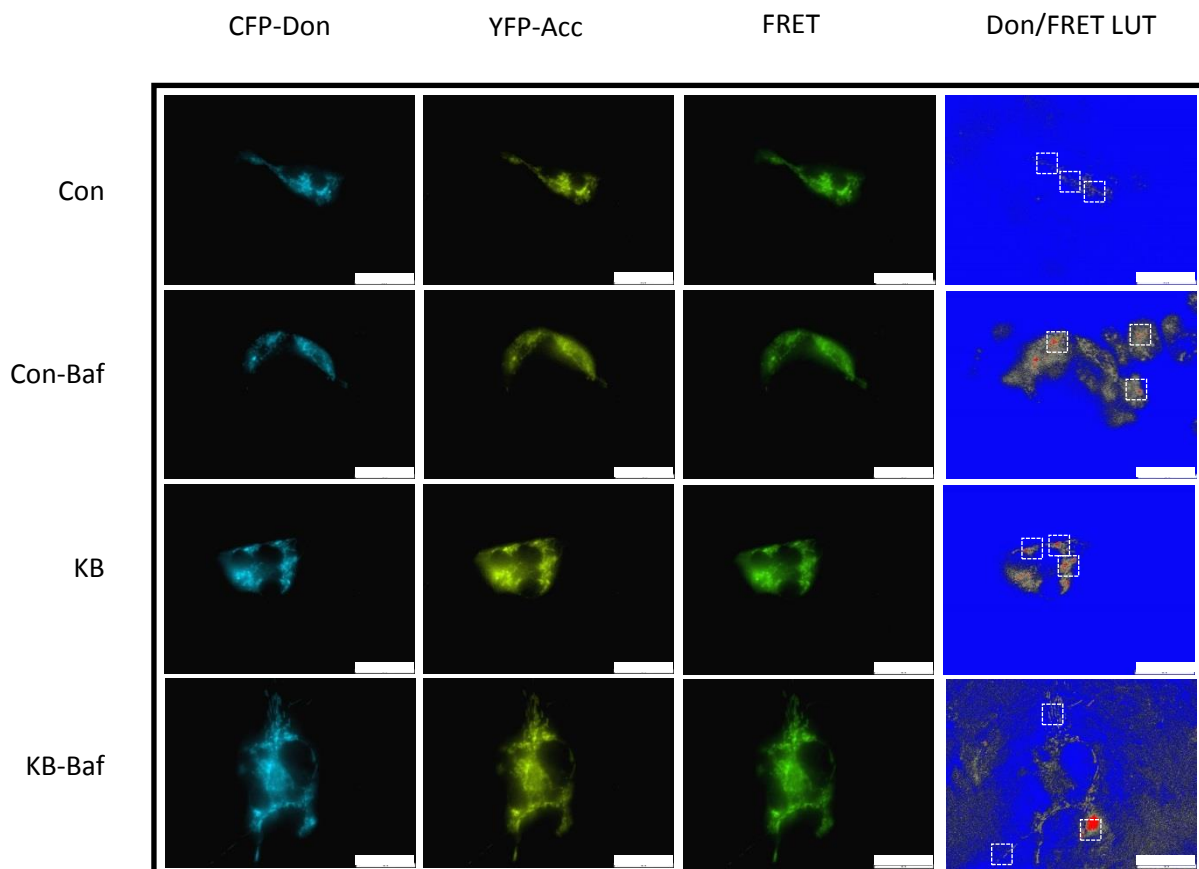
Figure 3.1.2a: Representative fluorescent micrographs of cells transfected with the ATeam ATP indicator under basal conditions. Micrographs display control (Con), control + bafilomycin (Con-Baf: 4 hrs 400 nM), ketone bodies (KB: 24 hrs 6 mM) or bafilomycin and ketone bodies (KB-Baf: 24 hrs 6 mM + 4 hrs 400 nM) treatment groups. The panels show images of the FDonor channel, FAcceptor channel, the FRET channel and a lookup table of images generated by the ratio FFret/FDon. 100X magnification. Scale bar = 20 µm.

	ROI 1	ROI 2	ROI 3

Figure 3.1.2b: Selected regions of micrographs displayed in Figure 3.1.2a indicating ATP distribution and distinct 'hotspots' generated by the ratio of FFret and FDon and processed using a lookup table. Scale bars = 4 μm.

3.1.3 The effect of basal autophagy and ketone body treatment on APP, BACE and Aβ levels

Western blot analysis was performed to assess whether protein degradation through autophagy under basal conditions and ketone body s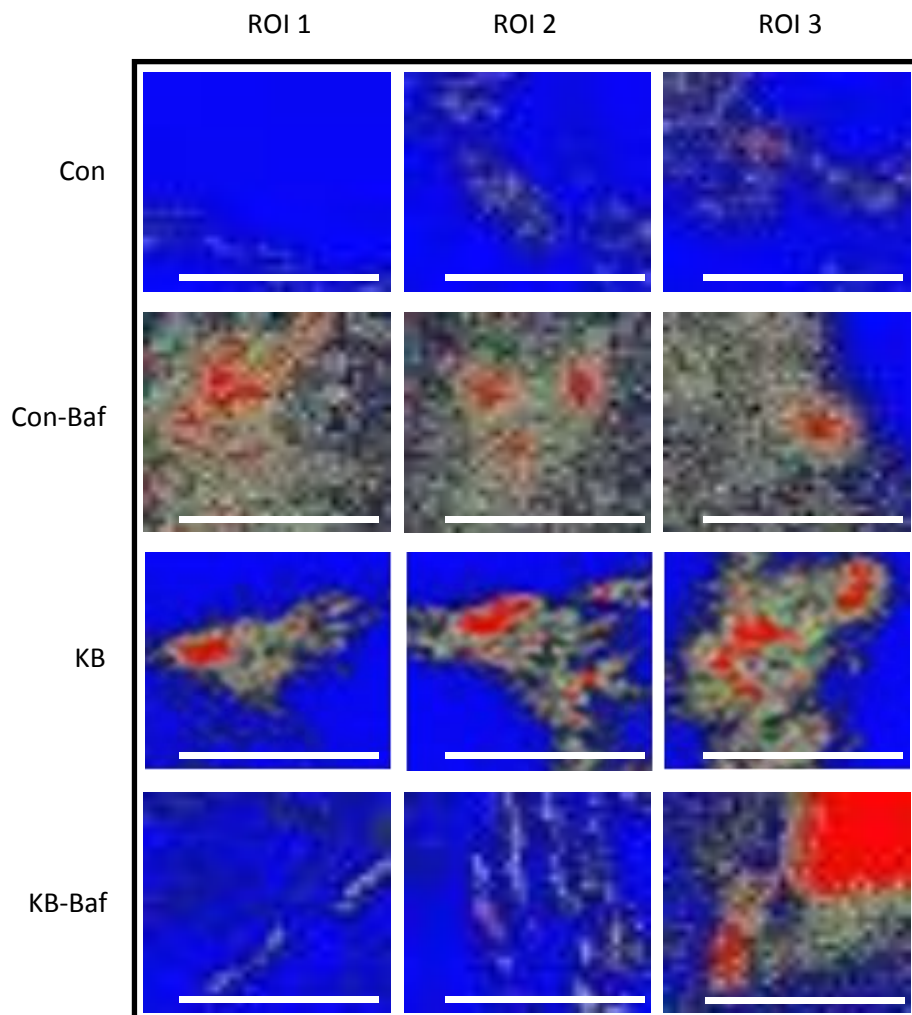upplementation have an effect on the expression levels of three key proteins involved in amyloid processing; amyloid precursor protein (APP), beta-site APP-cleaving enzyme (BACE) and amyloid beta (Aβ) (O'Brien and Wong, 2011). Here, the utilization of bafilomycin would allow determining whether respective proteins are targeted and cleared by the autophagic system under basal conditions. A protein that is cargo for autophagy would accumulate upon bafilomycin treatment. No significant changes were observed in the expression levels of APP or BACE, however strong trends can be observed. Relative expression of APP compared to control (Figure 3.1.3a) was increased with bafilomycin treatment [122.6 ± 27.5%], decreased in the presence of ketone bodies [90.7 ± 12.6%] and appear increased when cells were co-treated with bafilomycin and ketone bodies [137.1 ± 49%]. BACE is the protease responsible for cleaving APP at the +1 and +11 sites of Aβ. BACE expression levels (Figure 3.1.3b) was increased with bafilomycin treatment [186 ± 63.6%], decreased with ketone body treatment [93.3 ± 5.6%] and remained unchanged upon co-treatment with bafilomycin and ketone bodies [98.3 ± 39.5%]. In contrast, Aβ expression levels were significantly decreasedwhen exposed to bafilomycin compared to control and cells treated with ketone bodies (Figure 3.1.3c). This was the case for both in the Con-Baf and KB-Baf groups. Taken together, the results, albeit not significant in this scenario, strongly suggest that these candidate proteins are cleared under basal conditions through autophagy.

These results indicate that both APP and BACE are targeted by the autophagic machinery, serving as substrates for protein degradation through autophagy. The significant reduction in Aβ levels observed when autophagy is inhibited would suggest that autophagy is involved in the production of amyloid beta from its precursor.
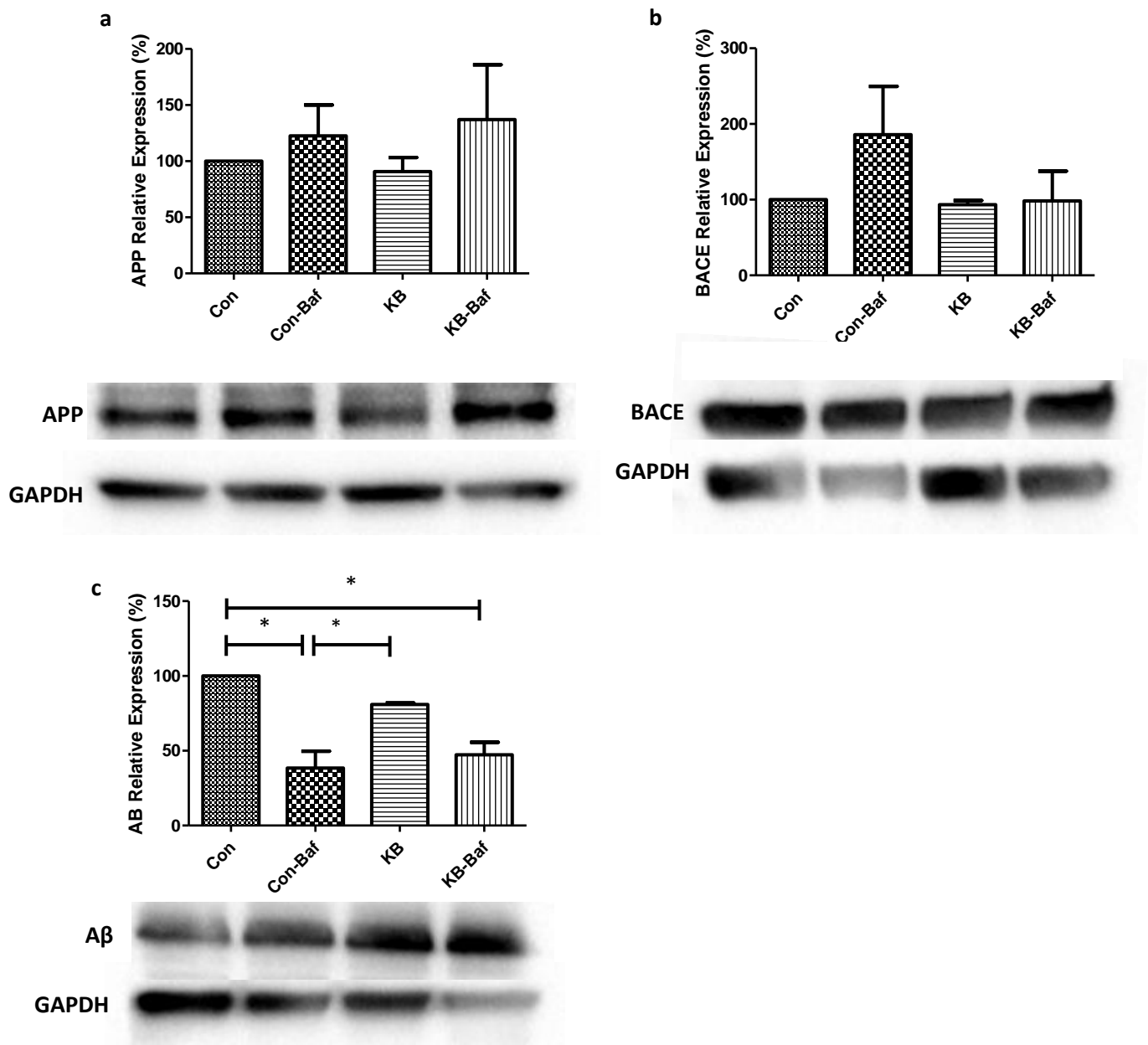
Figure 3.1.3: Relative expression levels of amyloid processing proteins according to the following groups: Control (Con), control + bafilomycin (Con-Baf: 4 hrs 400 nM), ketone bodies (KB: 24 hrs 6 mM) or bafilomycin and ketone bodies (KB-Baf: 24 hrs 6 mM + 4 hrs 400 nM). **a**: No significant differences in APP protein levels are observed. A non-significant trend for increased APP protein with bafilomycin treatment in the presence and absence of ketone bodies is observed, (n=4). **b**: No significant differences in BACE protein levels are observed. A non-significant trend for increased BACE protein with bafilomycin treatment in the presence and absence of ketone bodies is observed, (n=3) **c**: Bafilomycin causes a decrease in Aβ in the absence (*p<0.05) and presence of ketone bodies (*p<0.05) compared to control and ketone bodies with bafilomycin treatment alone (*p<0.05), (n=3). Representative blots are displayed.

68

3.1.4 The effect of ketone body treatment on autophagic flux

Western blot analysis of p62 and LC3 was performed to determine whether ketone body treatment impacts autophagic flux. p62, also known as SQSTM1, is a protein often used as a marker for selective autophagy, as it is involved in the targeting of poly-ubiquitinated proteins towards autophagolyosomes or degradation (Barth *et al.,* 2010). LC3-II is present on the autophagosomal membrane and the relative expression levels of LC3-II as well as LC3-II levels following treatment with a lysosomal inhibitor are widely used to assess autophagy (Mizushima *et al.,* 2010). No significant differences in p62 expression levels were observed (Figure 3.1.4a); however, a strong trend for decreased expression levels was observed with ketone body treatment [78 ± 17.5%], suggesting an increase in the clearance of p62 and hence, autophagic flux. In addition, a slight decrease with bafilomycin and ketone bodies co-treatment [84.8 ± 17.5%] was observed. Bafilomycin treatment had no effect [96.9 ± 14.1%]. No significant differences in LC3-II expression levels were observed, however there was a trend for increased expression in the control condition treated with bafilomycin, compared to control [145.6 ± 10.9%], indicating that autophagosomes indeed accumulate upon bafilomycin treatment.
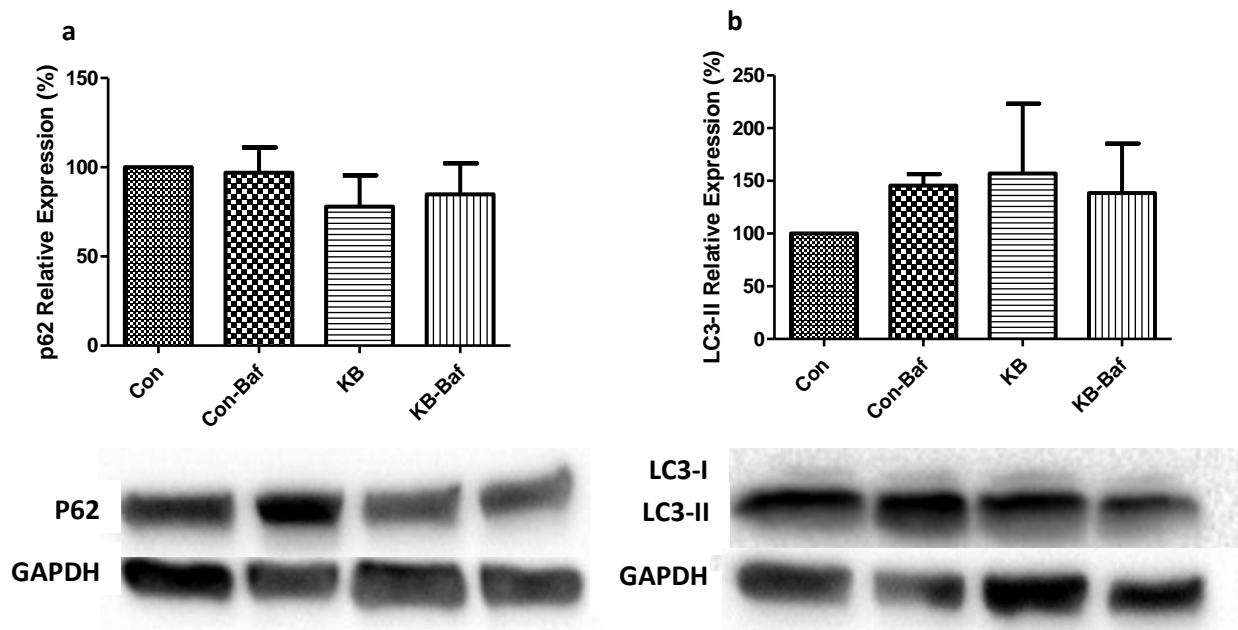
Figure 3.1.4: Relative expression levels of p62 and LC3 protein levels following treatment with medium (Con), bafilomycin (Con-Baf: 4 hrs 400 nM), ketone bodies (KB: 24 hrs 6 mM) or bafilomycin and ketone bodies (KB-Baf: 24 hrs 6 mM + 4 hrs 400 nM) **a**: No significant differences in p62 protein levels are observed. A non-significant decrease in p62 protein levels with ketone body treatment is observed, (n=3). **b**: No significant differences in LC3-II protein are observed. A non-significant increase in LC3-II levels are observed with bafilomycin and ketone body treatment and KB-Baf groups, (n=3).
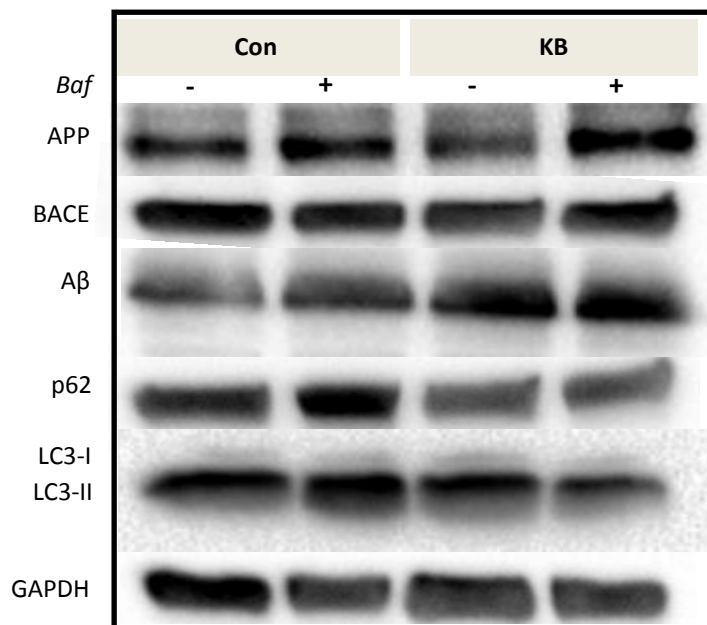
Figure 3.1.4c: Western blot data summarising results of amyloid processing and autophagy-related proteins. Representative blots are displayed.

3.1.5 The effect of basal autophagy and ketone body treatment on APP, BACE and Aβ distribution

Fluorescence microscopy of APP, BACE and Aβ allowed intracellular visualization of their localization and distribution under control conditions and following treatment. The micrographs indicating APP (Figure 3.1.5a), BACE (Figure 3.1.5) and Aβ (Figure 3.1.5c) revealed similar trends in their localization and distribution. Under control conditions it was observed that the proteins were primarily cytoplasmic and formed small spherical aggregates that are homogenously distributed throughout the cytoplasm. Nuclear signal was observed but no cellular membrane-derived signal. Cells also displayed nuclear signal upon treatment with bafilomycin. Ketone body treatment caused a loss of nuclear signal, while treatment with both ketone bodies and bafilomycin result in increased nuclear localization of APP and BACE (Figure 3.1.5a and b, KB-Baf).

Bafilomycin treatment caused an increase in aggregated APP as evidenced by the appearance of larger, brighter structures (Figure 3.1.5a, Con-Baf). The same was observed in cells treated with both ketone bodies and bafilomycin (Figure 3.1.5a, KB-Baf). A concomitant decrease in the diffuse levels of APP was observed in both bafilomycin treated groups compared to the control and ketone body treated groups. Ketone body treatment had no apparent effect on APP (Figure 3.1.5a, KB). The same was the case for BACE in cells; however ketone body treatment does seem to increase aggregation of Aβ in cells treated with ketone bodies and with both ketone bodies and bafilomycin. Bafilomycin treatment did not increase nuclear signal of Aβ as observed for APP and BACE (Figure 3.1.5a and b, Con-Baf).

Thus these results indicate that autophagy inhibition causes aggregation of APP, BACE and Aβ and that this aggregation extends to the nucleus in the case of APP and BACE. This suggests that autophagy is instrumental in controlling the local availability and, in part, distribution of these proteins present in cells. Our results suggest that APP processing occurs through autophagy and that inhibition of autophagy causes protein aggregation.
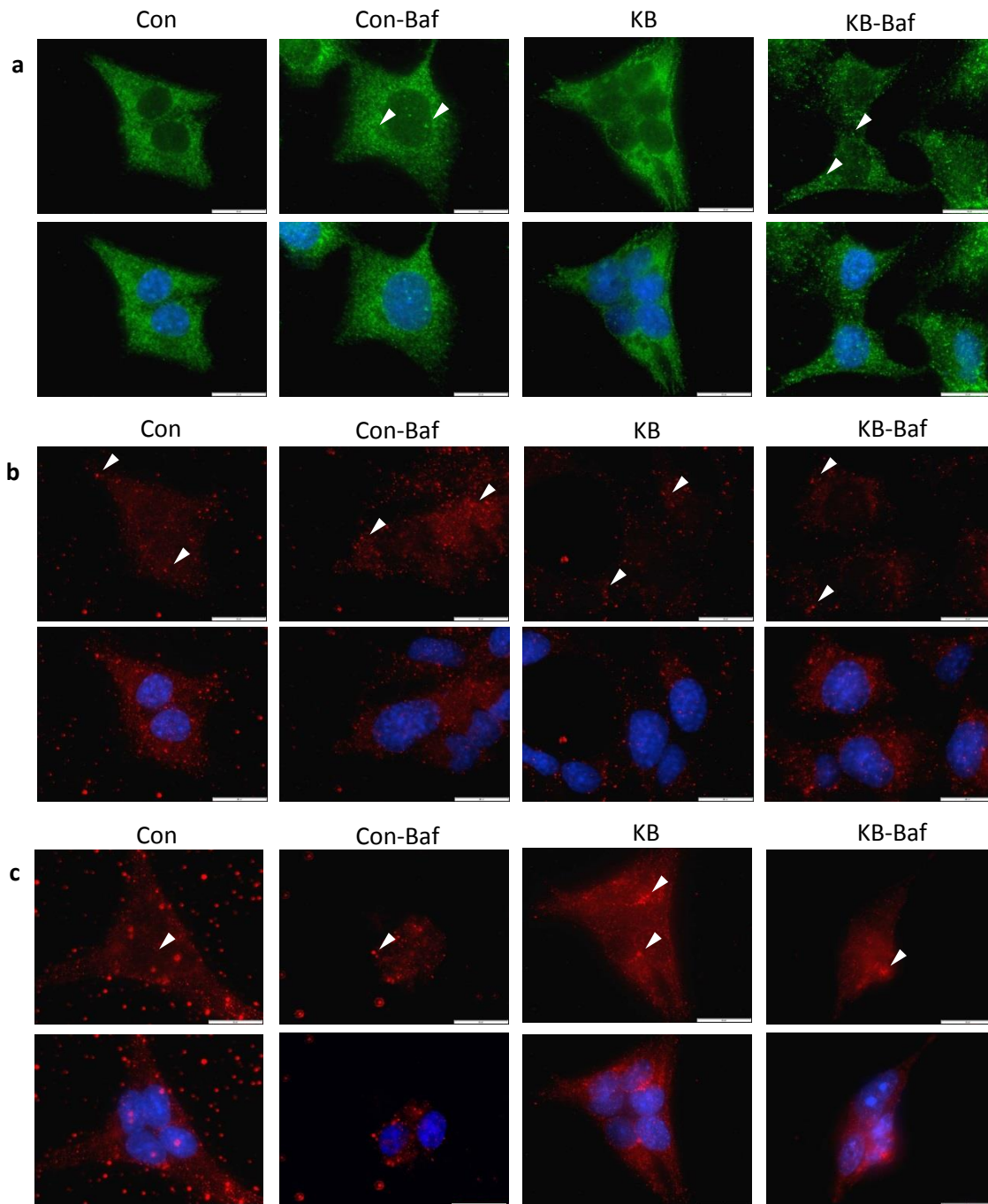
Figure 3.1.5: Representative micrographs of stained GT1-7 cells exposed to the following conditions: Control (Con), bafilomycin (Con-Baf: 4 hrs 400 nM), ketone bodies (KB: 24 hrs 6 mM) or bafilomycin and ketone bodies (KB-Baf: 24 hrs 6 mM + 4 hrs 400 nM). **a**: Green = APP, blue = Hoechst 33342. **b**: Red = BACE, blue = Hoechst 33342. **c**: Red = Aβ, blue = Hoechst 33342. 100X magnification. Scale bar = 20 μm. Arrowheads indicate aggregated protein.

SECTION 2: The role of ketone body supplementation under neurotoxic conditions

In the following section we report results that assess the effect of ketone body supplementation in paraquat-induced neurotoxicity. Since our data in section 1 indicated a role for ketone bodies in ATP localization as well as autophagy and protein clearance, we hypothesized that they would influence ATP levels, mitochondrial dynamics, and autophagy in a neurotoxicity model. We further hypothesized that ketone bodies would confer neuroprotection due to their role in upregulating autophagy.

3.2.1 Reductive capacity

A WST-1 assay was performed to assess GT1-7 cells' reductive capacity following treatment (Figure 3.2.1). Paraquat caused a significant reduction in the reductive capacity compared to the control condition [56.9 ± 2.1% ($p < 0.05$)] while treatment with ketone bodies alone had no effect on cell viability [95.9 ± 3%]. Co-treatment with both paraquat and ketone bodies, however, caused a significant increase in the reductive capacity compared to paraquat treated cells [66.5 ± 2 % ($p < 0.05$)]. Hence, we observe a rescue effect brought about by ketone body exposure, decreasing paraquat induced neurotoxicity.
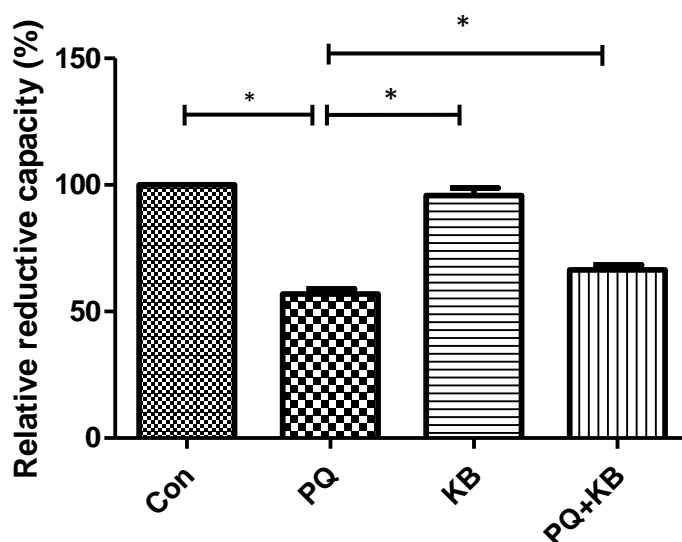
Figure 3.2.1: Relative reductive capacity compared to control (Con) following treatment with paraquat (PQ: 24 hrs 600 μM), ketone bodies (KB: 24 hrs 6 mM) or paraquat in the presence of ketone bodies (PQ + KB: 24 hrs 600 μM + 6 mM). (n=3). *p <0.05.

3.2.2 The effect of paraquat and ketone body treatment on autophagy and apoptosis

LC3-II is used as an indicator of autophagy, as previously mentioned. It is associated with the autophagosomal membrane and in this way provides an indication of autophagosomal number (Mizushima *et al.,* 2010). PARP is cleaved during apoptosis execution, to form an 85 kDa protein (Tewari *et al.,* 1995). No significant differences in the expression levels of LC3-II or cleaved PARP was observed in the treatment groups (Figure 3.2.2). A strong trend was observed, however, for decreased LC3-II expression upon paraquat treatment [35.8 ± 18.3%] and in the co-treatment group [32.6 ± 15.9%].
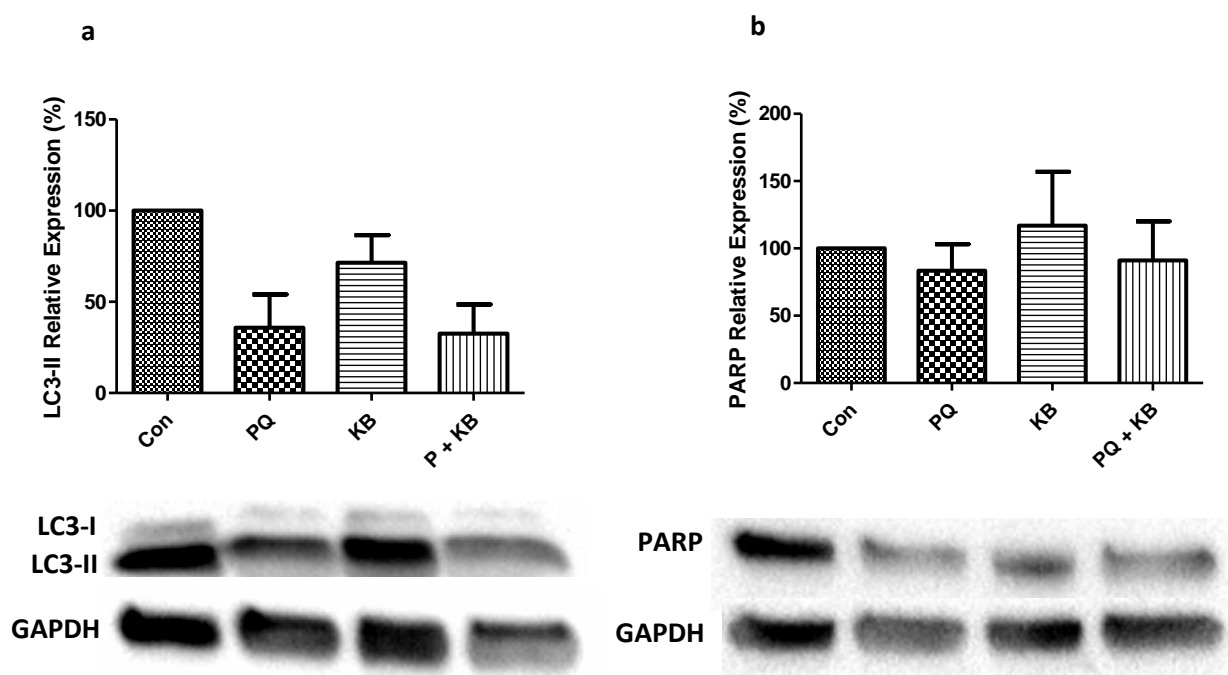
Figure 3.2.2: Relative expression levels of LC3-II and cleaved PARP proteins according to the following groups: Control (Con), paraquat (PQ: 24 hrs 600 µM), ketone bodies (KB: 24 hrs 6 mM) or paraquat in the presence of ketone bodies (PQ + KB: 24 hrs 600 µM + 6 mM). **a**: No significant differences in LC3-II protein levels are observed. A non-significant trend for decreased LC3-II with paraquat treatment is observed, (n=3). **b**: No significant differences in cleaved PARP are observed, (n=3). Representative blots are displayed.

3.2.3 Mitochondrial morphology following paraquat and ketone body treatment

Mitochondrial network morphology is an indicator of the functionality of cells. Fragmented mitochondria often indicate cellular stress, while a predominantly fused network is associated with viable cells (Chan, 2006). TMRE staining revealed that control cells displayed elongated mitochondria that form a highly interconnected network (Figure 3.2.3). Treating cells with paraquat resulted in the complete loss of network connectivity, characterized by numerous individual (fragmented) mitochondria. Fragmented mitochondria with very bright fluorescent signal were apparent in cells treated with paraquat, and with both paraquat and ketone bodies. Cells treated with ketone bodies displayed elongated mitochondria with a high degree of network connectivity, similar to control cells. Co-treated cells displayed both fused and fragmented mitochondria; however a greater degree of mitochondrial connectivity was visible compared to cells treated with paraquat only.

Figure 3.2.3: Representative micrographs of mitochondria stained with TMRE, under control conditions (Con) and following treatment with paraquat (PQ: 24 hrs 600 µM), keton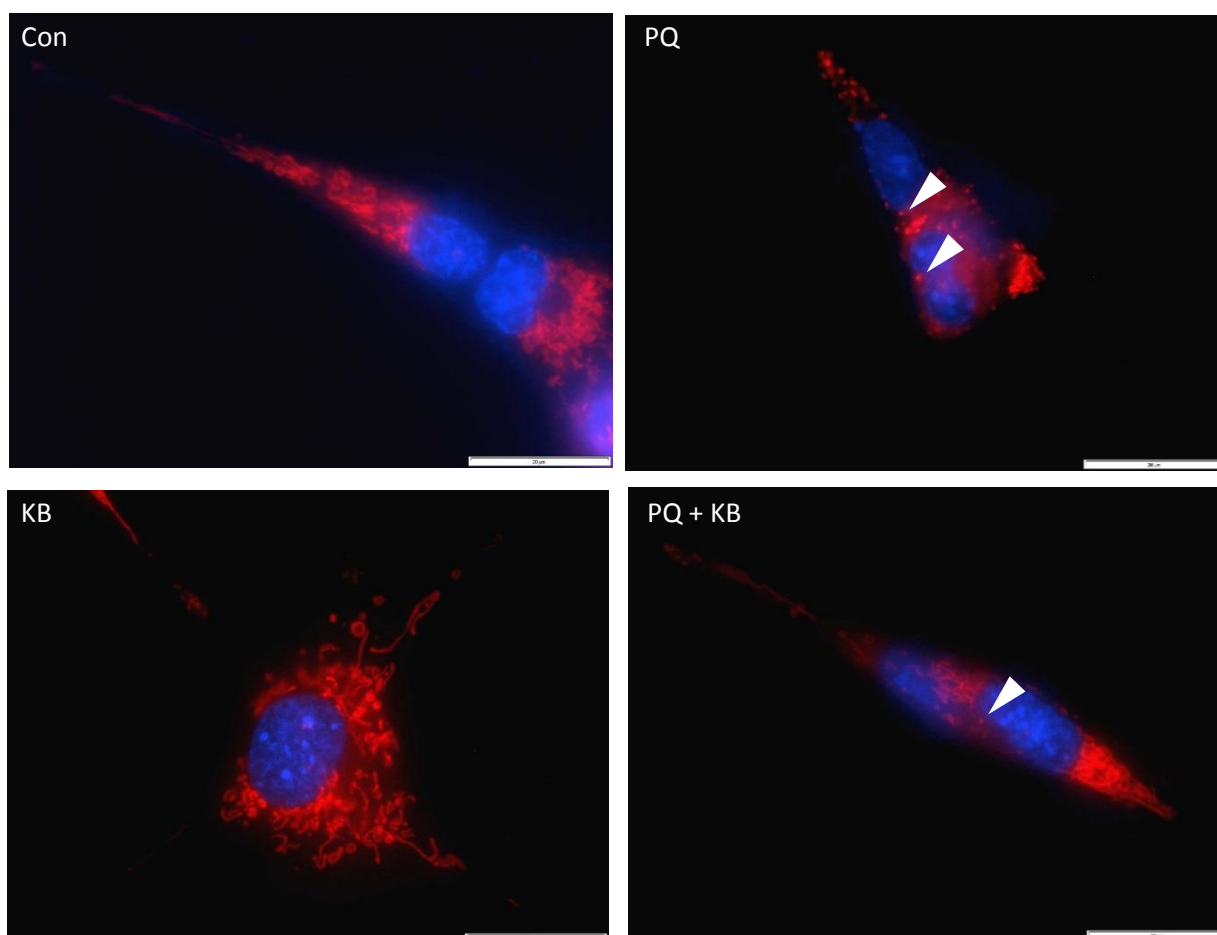e bodies (KB: 24 hrs 6 mM) or paraquat in the presence of ketone bodies (PQ + KB: 24 hrs 600 µM + 6 mM). Red = TMRE, blue = Hoechst 33342. 100X magnification. Scale bar = 20 µm. Arrowheads indicate fragmented mitochondria.

3.2.4 Mitochondrial network morphology indicated by form factor and aspect ratio

Micrographs, in this case indicating mitochondria through TMRE staining, were processed using ImageJ software to generate skeletonized images of the mitochondrial network (Figure 3.2.4a). These images were then used to calculate the average form factor (degree of branching) and aspect ratio (length) (Mortiboys *et al.,* 2008) of mitochondria in cells treated with paraquat, ketone bodies and both paraquat and ketone bodies. A form factor close to one indicates a completely fragmented network, while a decrease in aspect ratio indicates spherical mitochondria.

No significant differences in form factor were observed between groups, however, the control condition displayed the lowest form factor value (Figure 3.2.4c), indicating the most connected mitochondrial network of all groups. Cells treated with paraquat were characterized by the most fragmented mitochondrial network, as indicated by the high form factor. No significant differences in the aspect ratio were observed between groups(Figure 3.2.4d). Control cells, however, had the highest value, indicating elongated mitochondria, and paraquat treatment resulted in the lowest aspect ratio, indicating rounded mitochondria.

A particle count of the edited images (Figure 3.2.4b) displays surprising results with ketone body treatment resulting in the highest count, while paraquat had the lowest count. These differences can be explained, however by the observation that paraquat treatment caused severe cell shrinkage, while this effect was not seen in the control and ketone body groups. Thus the effect of mitochondrial networking would be masked by the greater overall number of mitochondria in these groups.

Although no statistically significant differences were observed, robust changes in morphology and corresponding changes in both aspect ratio and form factor were observed, supporting the detrimental impact of paraquat treatment as well as the beneficial effect of ketone body supplementation.

Figure 3.2.4a: Processed micrographs of mitochondria stained with TMRE, under control conditions (Con) and following treatment with paraquat (PQ: 24 hrs 600 µM), ketone bodies (KB: 24 hrs 6 mM) or paraquat in the presence of ketone bodies (PQ + KB: 24 hrs 600 µM + 6 mM).100X magnification. These images were used to generate the form factor and aspect ratio.
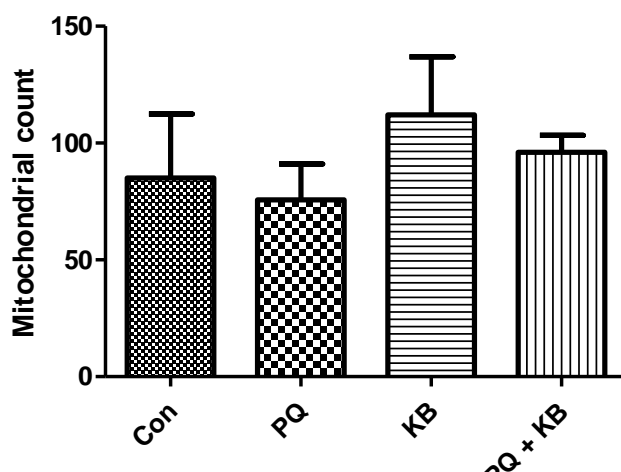
Figure 3.2.4b: Mitochondrial count as indicated by TMRE-stained particles according to the following groups: Control (Con), paraquat (PQ: 24 hrs 600 µM), ketone bodies (KB: 24 hrs 6 mM) or paraquat in the presence of ketone bodies (PQ + KB: 24 hrs 600 µM + 6 mM).Graph indicates mean value of counted mitochondria ± SEM, (n=3).
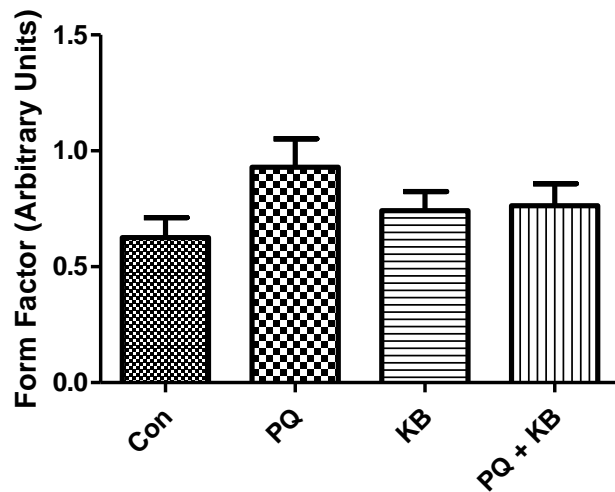
Figure 3.2.4c: Degree of branching indicated by form factor analysis of mitochondria stained with TMRE, under control conditions (Con), or following treatment with paraquat (PQ: 24 hrs 600 µM), ketone bodies (KB: 24 hrs 6 mM) or paraquat in the presence of ketone bodies (PQ + KB: 24 hrs 600 µM + 6 mM). Graph indicates mean values ± SEM, (n=3).

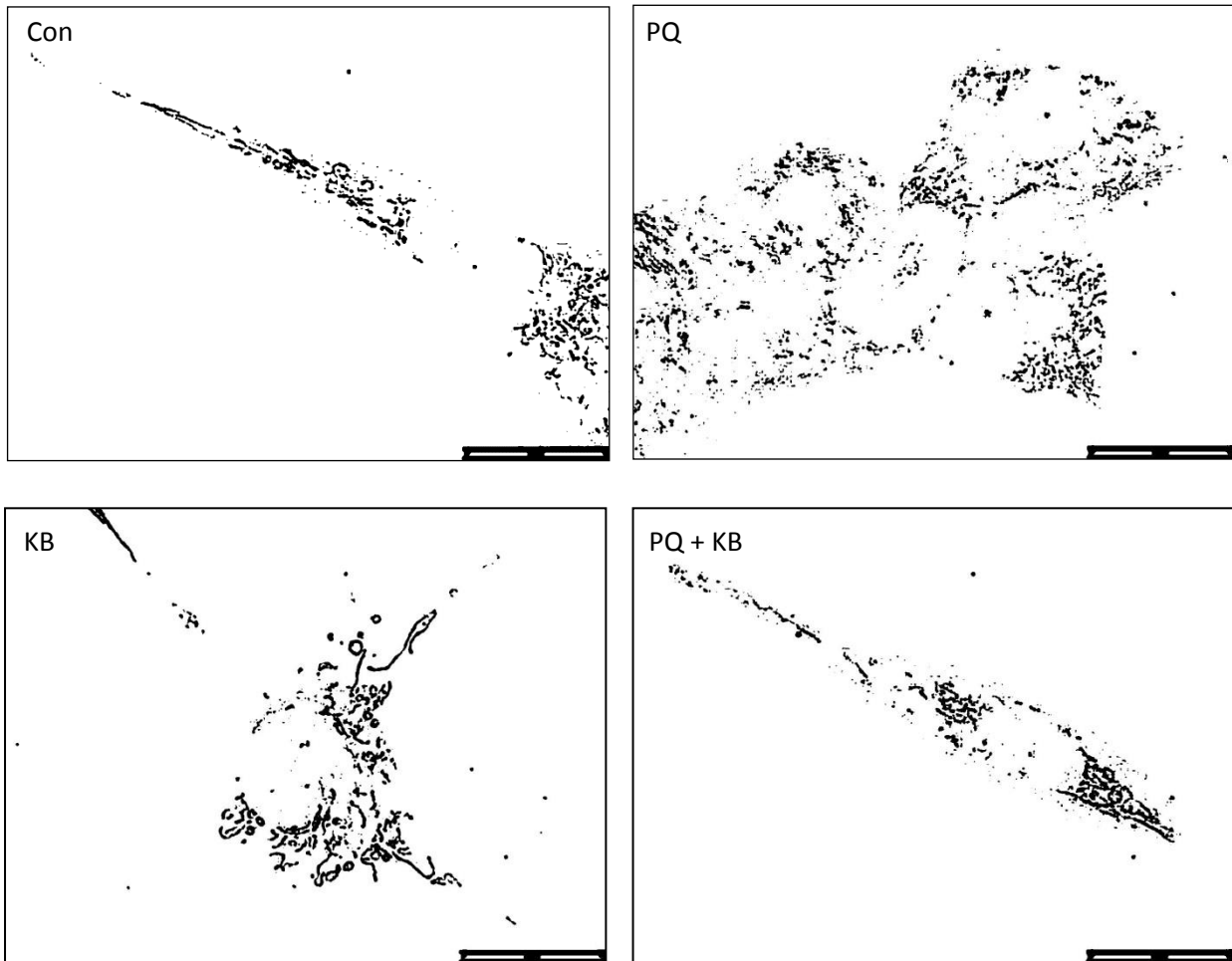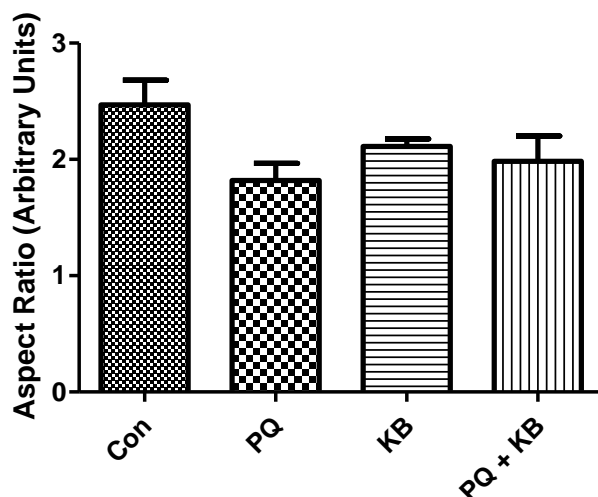Figure 3.2.4d: Length indicated by aspect ratio analysis of mitochondria stained with TMRE, under control conditions (Con), or following treatment with paraquat (PQ: 24 hrs 600 µM), ketone bodies (KB: 24 hrs 6 mM) or paraquat in the presence of ketone bodies (PQ + KB: 24 hrs 600 µM + 6 mM). Graph indicates mean values ± SEM, (n=3).

3.2.5 Oxidative capacity following paraquat and ketone body treatment

3.2.5.1 TMRE mean intensity

Flow cytometry was performed with cells stained with TMRE to assess the mitochondrial polarization state of a whole cell population (Figure 3.2.5.1b). The mean intensity increased relative to that of control cells following treatment with paraquat, although this change was not statistically significant [168.2 ± 25.4%]. Intensity remained similar to that of control cells in the presence of ketone bodies [83.7 ± 7.1%], however, a statistically significant increase was revealed when cells were treated with paraquat in the presence of ketone bodies [180.8 ± 19.4% (p<0.05)]. A statistically significant decrease was observed between the paraquat and ketone bodies groups. This decrease was lost in the co-treatment group (Figure 3.2.5.1a).

Figure 3.2.5.1a: Mean fluorescence intensity of a population of GT1-7 cells stained with TMRE, presented as a percentage of control. Cells were untreated (Con), or treated with paraquat (PQ: 24 hrs 600 µM), ketone bodies (KB: 24 hrs 6 mM) or paraquat in the presence of ketone bodies (PQ + KB: 24 hrs 600 µM + 6 mM, (n= 3). Mean ± SEM. *p<0.05
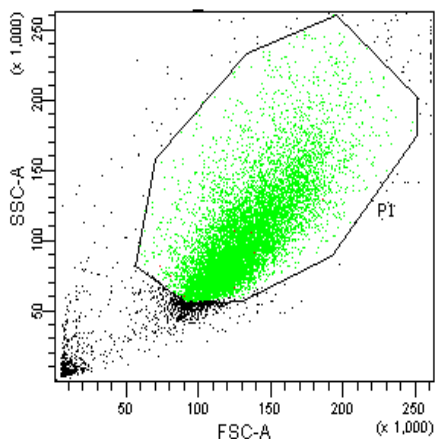
Figure 3.2.5.1b: Representative graph of control GT1-7 neuronal cells stained with TMRE.
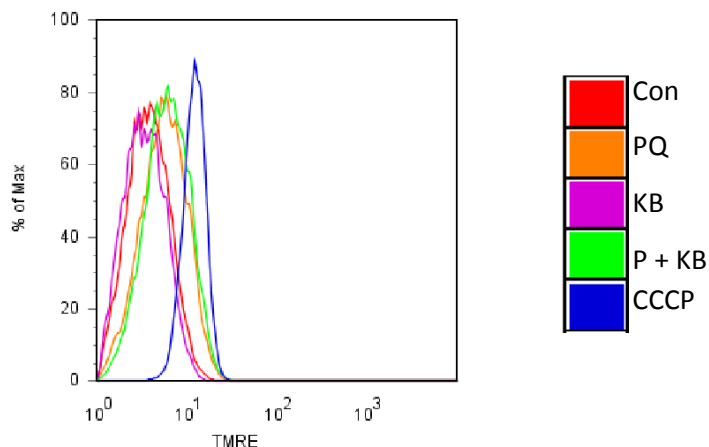
Figure 3.2.5.1c: Representative graph of fluorescence intensity of GT1-7 cells stained with TMRE, presented as intensity histograms. Cells were untreated (Con), or treated with paraquat (PQ: 24 hrs 600 µM), ketone bodies (KB: 24 hrs 6 mM) or paraquat in the presence of ketone bodies (PQ + KB: 24 hrs 600 µM + 6 mM). Cells treated with carbonyl cyanide chlorophenylhydrazone (CCCP) represent a positive control.

3.2.5.2 Dichlorofluorescein mean intensity

In order to assess generic ROS levels, mean intensity analysis was performed as well as micrographs captured following staining with dichlorofluorescein (DCF). DCF staining is visible as green punctae. Cells treated with paraquat displayed the strongest DCF signal (Figure 3.2.5.2a). Few small DCF-positive areas were visible in control, ketone bodies and co-treatment groups. Flow cytometry analysis revealed no significant differences in the mean fluorescence intensity between groups (Figure 3.2.5.2b); however the co-treatment group (PQ + KB) had a much higher value compared to control, ketone body and paraquat only treated groups.
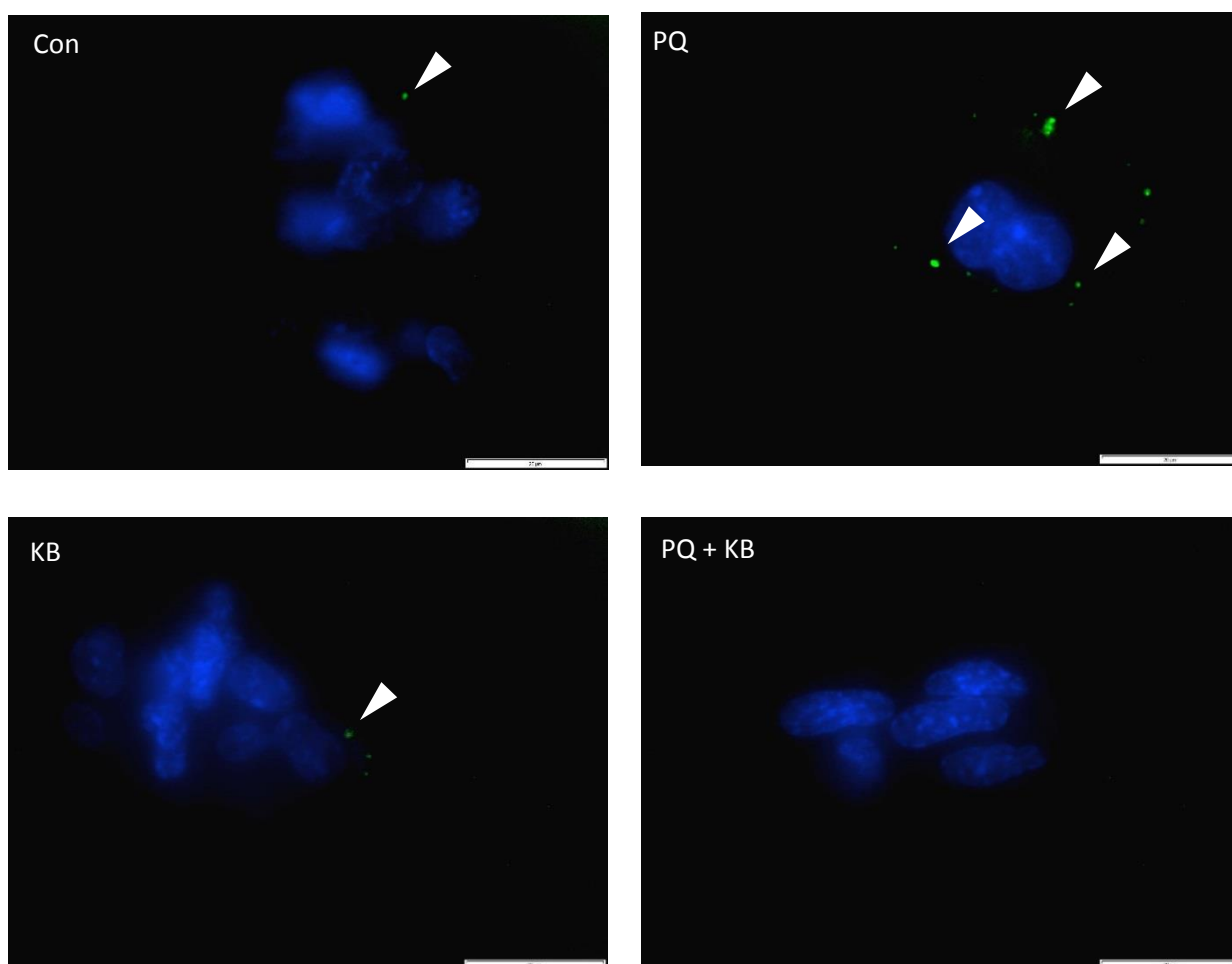
Figure 3.2.5.2a: Representative micrographs of cells stained with dichlorofluorescein (DCF). Cells were untreated (Con), or treated with paraquat (PQ: 24 hrs 600 µM), ketone bodies (KB: 24 hrs 6 mM) or paraquat in the presence of ketone bodies (PQ + KB: 24 hrs 600 µM + 6 mM. Green = DCF, blue = Hoechst 33342. 100X magnification. Scale bar = 20 µm. Arrowheads indicate DCF-stained areas.
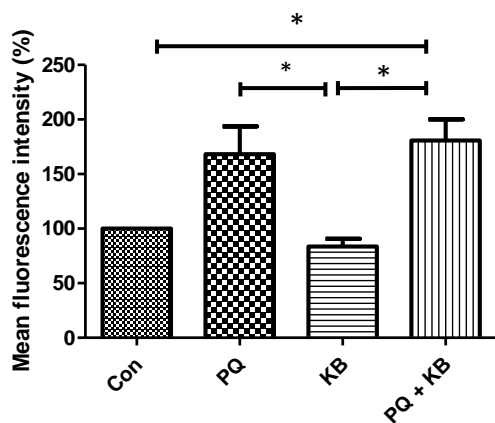
82
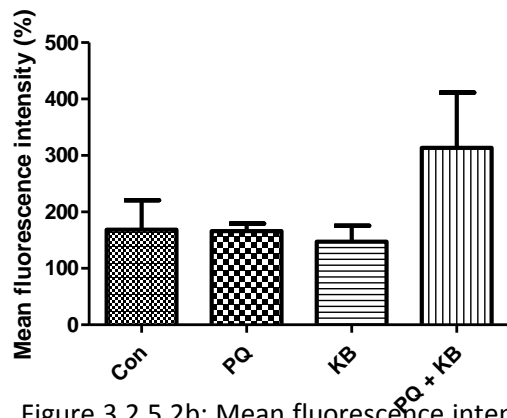
Figure 3.2.5.2b: Mean fluorescence intensity values of a population of GT1-7 cells stained with DCF, presented as a percentage of control. Cells were untreated (Con), or treated with paraquat (PQ: 24 hrs 600 µM), ketone bodies (KB: 24 hrs 6 mM) or paraquat in the presence of ketone bodies (PQ + KB: 24 hrs 600 µM + 6 mM, (n=3).
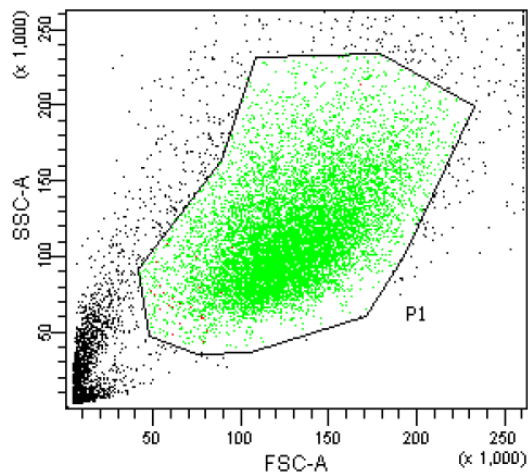
Figure 3.2.5.2c: Representative graph of control GT1-7 neuronal cells stained with DCF.
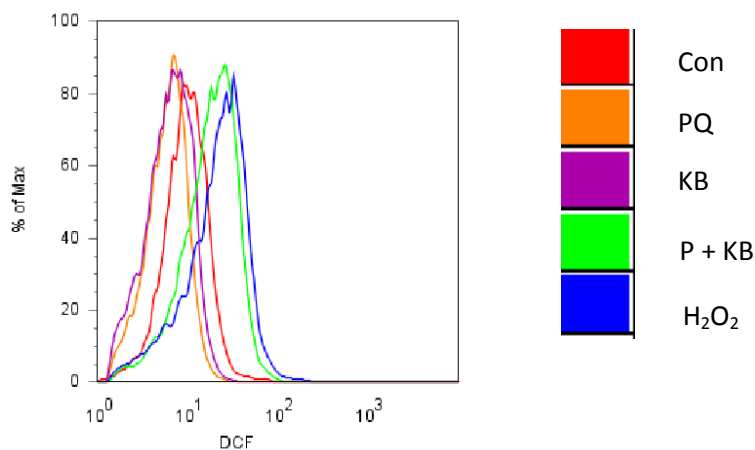
Figure 3.2.5.2d: Representative graph of fluorescence intensity of GT1-7 cells stained with DCF, presented as intensity histograms. Cells were untreated (Con), or treated with paraquat (PQ: 24 hrs 600 µM), ketone bodies (KB: 24 hrs 6 mM) or paraquat in the presence of ketone bodies (PQ + KB: 24 hrs 600 µM + 6 mM. Cells treated with hydrogen peroxide (H_2O_2) represent a positive control.

3.2.6 The effect of paraquat and ketone body treatment on ATP concentration

A luciferase-based ATP assay was used to measure total ATP levels following treatment with paraquat, ketone bodies and paraquat in the presence of ketone bodies (Figure 3.2.6). Paraquat treatment caused a statistically significant reduction in ATP concentration compared to the control condition with values of 2.86 ± 0.1 and 2.41 ± 0.1 pM (p<0.05) detected, respectively. Cells treated with ketone bodies displayed a similar concentration as controls [2.84 ± 0.08 pM]. Co-treatment did not cause an increase in ATP concentration compared to paraquat treatment [2.26 ± 0.08 pM].
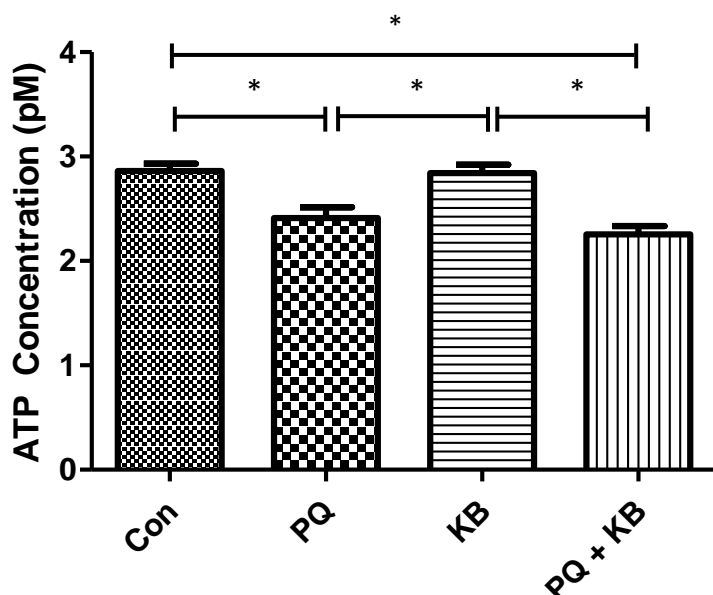
Figure 3.2.6: Total ATP concentration in an injury model. ATP concentration (pM) according to the following treatment groups: Control (Con), paraquat (PQ: 24 hrs 600 µM), ketone bodies (KB: 24 hrs 6 mM) or paraquat in the presence of ketone bodies (PQ + KB: 24 hrs 600 µM + 6 mM), (n=4). Graph represents mean ± SEM.*p<0.05

3.2.7 The effect of paraquat and ketone body treatment on ATP distribution

ATP, as previously mentioned, is indicated by the ATeam construct (Figure 3.2.7a). Localization was dispersed in control cells as was seen in section 1, with the presence of multiple small 'hotspots' visible (Figure 3.2.7b). Paraquat treatment resulted in a robust decrease of detected signal, which reflects the decreased ATP concentration seen in Figure 3.2.6. Ketone bodies caused ATP to accumulate in a number of single hotpots and the overall distribution was less diffuse than in the control condition. In the co-treatment group less overall signal was observed than in control and ketone bodies groups; however more signal compared to the paraquat treatment. A small number of hotspots were observed which supports the ATP concentration data which suggests that ketone bodies can rescue from ATP depletion induced by paraquat exposure, by changing ATP localization and distribution. ATP localization changes are apparent in mitochondrial ATP (as we assessed) but this could also be true of ATP in the cytosol.

	CFP-Don	YFP-Acc	FRET	Don/FRET LUT
Con				
PQ				
KB				
PQ + KB				
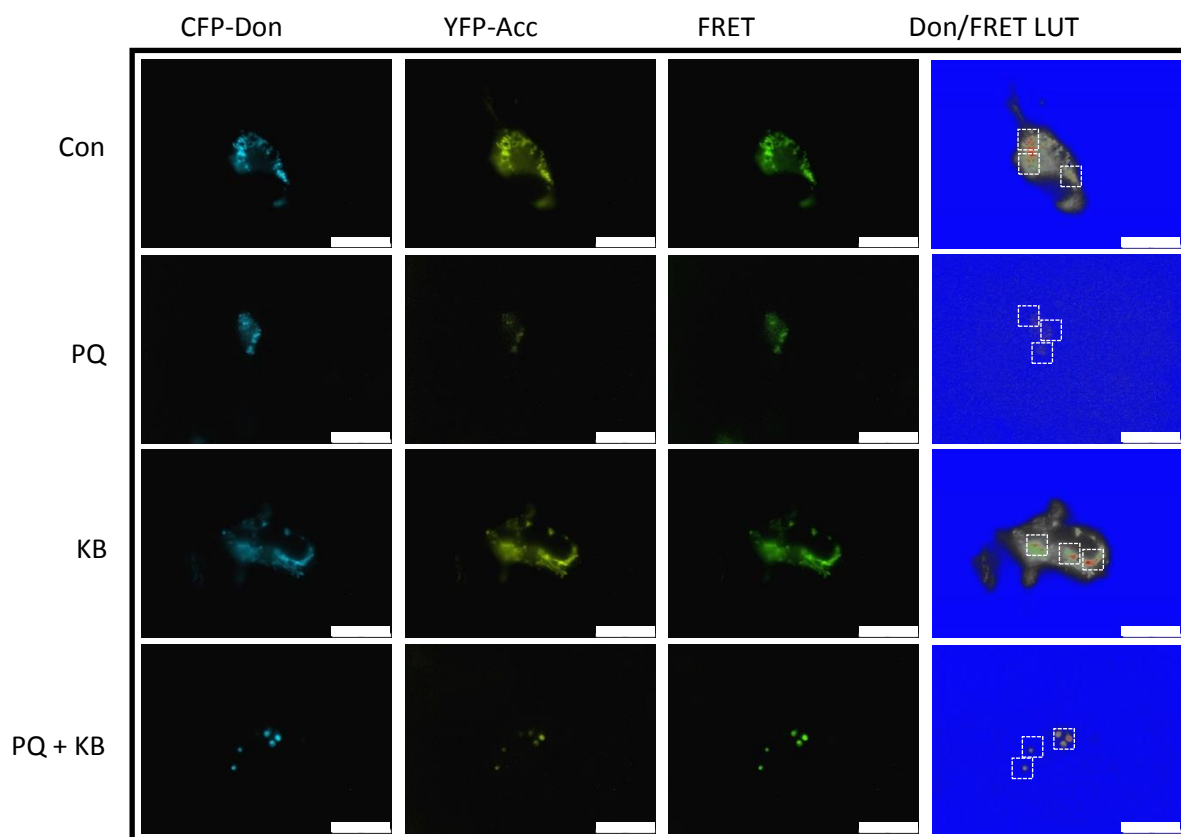
Figure 3.2.7a: Representative fluorescent micrographs of cells transfected with the ATeam ATP indicator in an injury model. Micrographs display control (Con), paraquat (PQ: 24 hrs 600 μM), ketone bodies (KB: 24 hrs 6 mM) or paraquat in the presence of ketone bodies (PQ + KB: 24 hrs 600 μM + 6 mMtreatment groups. Panel A shows images of the FDonor channel, panel B shows FAcceptor channel, panel C shows the FRET channel and panel D shows a lookup table of images generated by the ratio of FFret and FDon. Scale bar = 20 μm. 100X magnification.
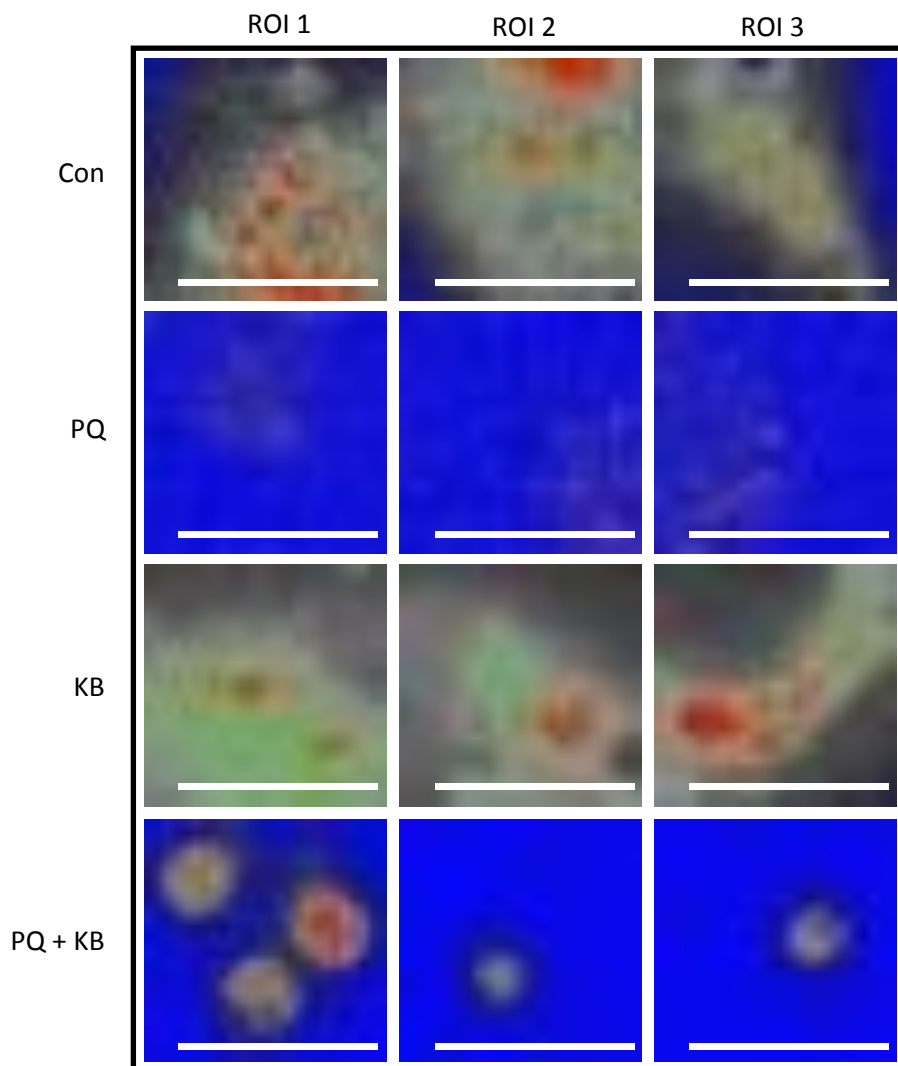
Figure 3.2.7b: Selected regions of micrographs displayed in 3.2.7a indicating ATP distribution and distinct 'hotspots' generated by the ratio of FFret and FDon and processed using a lookup table. Scale bars = 4 μm.

3.2.8 The effect of paraquat and ketone body treatment on neuronal ultrastructure

Transmission electron microscopy (TEM) was performed to determine the effect of paraquat and ketone body treatment, as well as co-treatment, on the neuronal ultrastructure of cells, with a particular focus on mitochondria and vacuolar structures.

Micrographs reveal that under control conditions, mitochondria are characterized by a predominantly elongated morphology (Figure 3.2.8b). Cristae structure ares well demarcated. In addition, well-defined vacuolar structures are visible (Figure 3.2.8c). Cells treated with paraquat display decreased mitochondrial integrity, indicated by swollen and disrupted mitochondrial morphology (Figure 3.2.8e). Less defined vacuolar structures are present (Figure 3.2.8f). In the ketone body treated group mitochondria that are similar to the control group can be observed (Figure 3.2.8h) as well as an increased number of vacuolar structures (Figure 3.2.8i). Co-treatment resulted in fewer vacuolar structures being observed (Figure 3.2.8l).

Control and ketone body treated cells display intact nuclei (Figure 3.2.8a and g). Paraquat treatment resulted in distinct nuclear morphology, as indicated by large white areas within nuclei with disrupted chromatin (Figure 3.2.8d). Co-treatment resulted in nuclear morphology with some euchromatin integrity (Figure 3.2.8j).

.

Structure Overview	Mitochondria	Vacuolar Structures
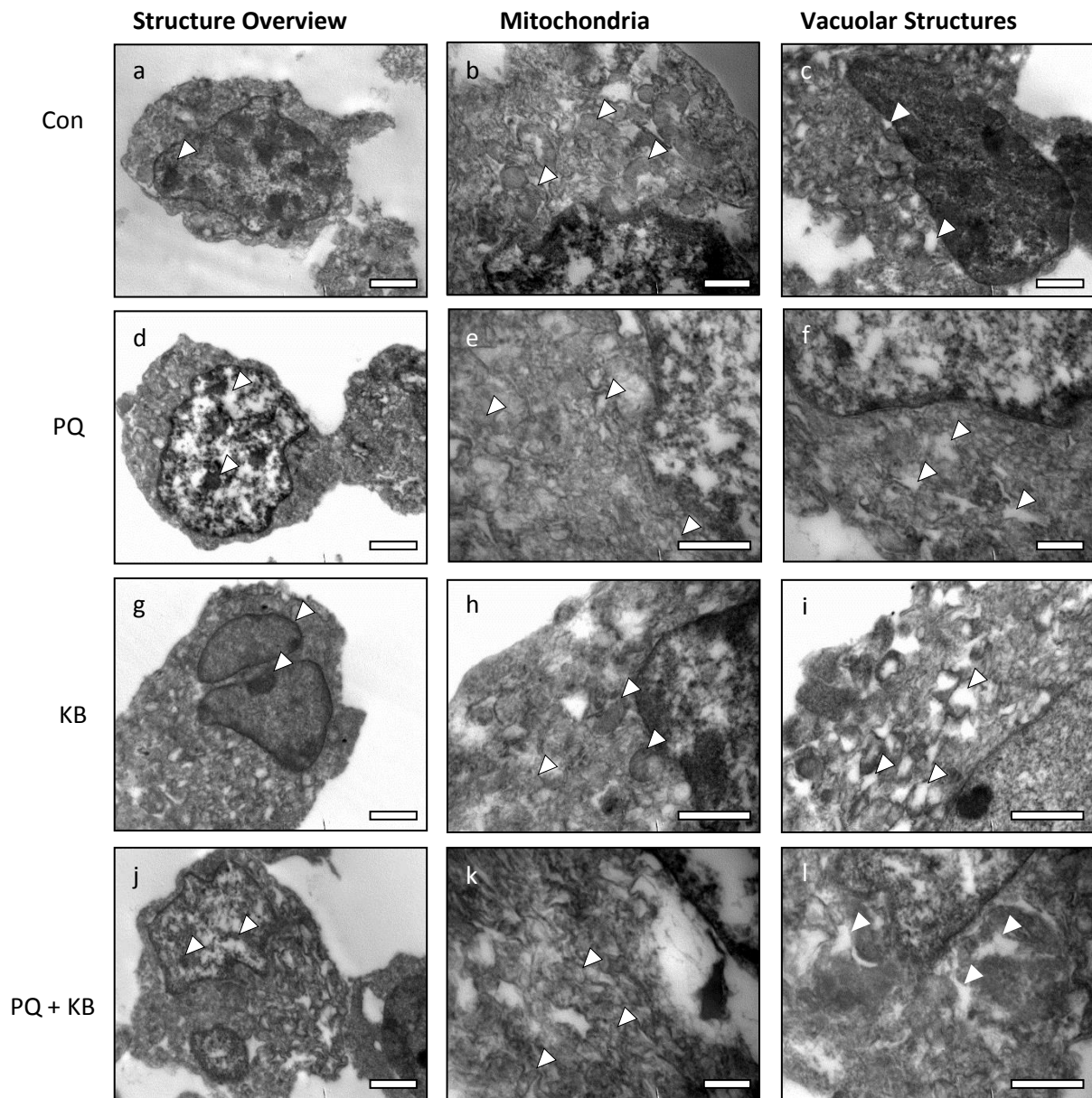
Figure 3.2.8a-l: Representative transmission electron micrographs of GT1-7 cells arranged according to treatment condition: control (Con), paraquat (PQ: 24 hrs 600 µM), ketone bodies (KB: 24 hrs 6 mM) or paraquat in the presence of ketone bodies (PQ + KB: 24 hrs 600 µM + 6 mM). Lower magnification images (first panel) indicate general cellular ultrastructure; higher magnification images reveal the presence of mitochondria (second panel) and vacuolar structures indicative of autophagic processes (third panel). Arrowheads indicate structures of interest. Scale bar for a and j = 2000 nm; b, e, h, I, k, l = 1000 nm; c, d, f, g = 5000 nm.

Chapter 4: DISCUSSION AND CONCLUSION

Ketone bodies have been demonstrated to confer a host of beneficial effects in the context of neurodegenerative diseases (Paoli *et al.,* 2013). These benefits include preventing cell death after exposure to an ischemic insult (Samoilova *et al.,* 2010), decreasing Aβ deposition (Van der Auwera *et al.,* 2005) and ameliorating cognitive deficits (Zhang *et al.,* 2013). Importantly, these benefits extend to human subjects; significant improvement in cognitive performance was found in AD patients (Henderson *et al.,* 2009) and undiagnosed individuals suspected of suffering from AD (Benge *et al.,* 2009). This is supported by the comprehensive benefits of caloric restriction in primates demonstrated by Colman *et al.* (2014). Although it is known that ketone bodies improve the energetic state of cells, evidenced by increasing ATP levels in the absence of glucose (Arakawa *et al.,* 1991), it remains unclear how this change in ATP is brought about and how it connects to protein aggregation. This is important because the cell's energetic state is a deciding factor in the survival and activation of cell death pathways (Loos and Engelbrecht, 2009).

Evidence suggests that ketone bodies favour protein degradation (Finn and Dice, 2005) and impact on aggregate prone species involved in AD pathology (Van der Auwera *et al.,* 2005; Zhang *et al.,* 2013). Indeed, inducing autophagy through starvation improves AD symptoms in its own right. Autophagy is disrupted in AD, and AD brains are characterized by the accumulation of undigested autophagic vacuoles (Boland *et al.,* 2008). This is attributed to lysosomal dysfunction, resulting in decreased degradative capacity of neurons (Nixon and Yang, 2011). It has been demonstrated that inhibited autophagy can lead to Aβ deposition through its modulation of the APP processing pathway (Pickford *et al.,* 2008). Conversely, inducing autophagy slows AD disease progression in mice (Yang *et al.,* 2011; Spilman *et al.,* 2010). How ketone body availability affects neuronal autophagy and neuronal viability in the context of neurodegeneration remains however largely unclear (Figure 4a).

Thus we aimed to assess the role of ketone bodies in the context of AD using two distinct approaches. First, we aimed to investigate the molecular link between ketone body exposure and amyloid processing by performing Western blot analysis, fluorescence microscopy as well as quantitative and qualitative assessment of neuronal ATP concentration and distribution in a suitable *in vitro* model. The latter was motivated by the

major role of ATP in neuronal cell survival. In this context we also aimed to assess to what extent ketone body exposure is able to impact on autophagic flux, i.e. the protein degradation rate through autophagy. Secondly, we used an injury model using paraquat exposure and assessed the effect of ketone body treatment by performing Western blot analysis, a reductive capacity assay, mitochondrial morphology assessment, transmission electron microscopy, ATP quantification and qualitative assessment as well as flow cytometry. We hypothesized that ketone body supplementation would upregulate autophagy and increase intracellular ATP concentration. In addition, we predicted that ketone bodies would play a protective role in the context of neurotoxicity, specifically by maintaining ATP levels, mitochondrial morphological characteristics and cellular viability.

4.1.1 Ketone body treatment and basal autophagy relocalizes intracellular ATP without affecting its total concentration

To our surprise, neither the inhibition of autophagosomal/lysosomal fusion nor the exposure to ketone bodies impacted on total ATP availability (Figure 3.1.1). This may suggest that, in these conditions and cells, basal protein degradation through autophagy is not a major contributor to metabolite substrate provision and ATP synthesis. It also suggests that ketone bodies do not increase the ATP generation profile under control conditions.

Others have demonstrated a similar lack of change in ATP levels when silencing a PFKFB3, an enzyme responsible for a rate-limiting step in the glycolytic pathway (De Bock *et al.,* 2013). ATP levels remained unchanged despite other important changes that were triggered by silencing, such as impairing endothelial cell motility and a decrease in ATP hotspots. Luciferase-based assays such as the one utilized here are not always the most reliable method to detect ATP (Kennedy *et al.,* 1999). ATP concentration can be misleading if it is considered in isolation, and using an ATP sensor as an additional assessment grants a clearer understanding of the energetic milieu within cells. However, some have observed a decrease in ATP levels upon autophagy inhibition by 3-methyladenine (Hernández–Gea *et al.*, 2012). Arakawa *et al.* (1991) described elevated ATP levels after two hour treatment with 20 mM β-OHB. We did not find observe this effect; however we used a much lower concentration of ketone bodies. Nevertheless, both ketone body and bafilomycin treatment affected ATP localization in our experiments.

Treatment with ketone bodies and bafilomycin both caused the accumulation of ATP derived emission within cells (Figure 3.1.2a and b). In the control condition ATP distribution appeared diffuse, with many small hotspots visible. This distribution changed upon bafilomycin and ketone body treatment where large localized areas of signal could be seen. The observed increase in signal may represent an adaptive mechanism of cells to the alternative energetic pathways activated upon ketone body treatment, as ketone bodies are able to enter the TCA cycle (Prins, 2008). This is a likely scenario as it has been demonstrated that ketone bodies contribute a substantial amount of TCA cycle flux in rat neurons, and can support most, if not all of neuronal oxidative metabolism (Chowdhury *et*

al., 2014). Autophagy inhibition may cause a stress response in cells as they are forced to rely on other metabolic pathways apart from the catabolism of amino acids.

Our findings are to our knowledge the first to indicate ATP relocalization changes upon ketone body treatment and autophagy inhibition. This deserves further attention in future research.

4.1.2 Autophagy targets APP and BACE for degradation

Bafilomycin treatment increased the levels of APP and BACE in the presence and absence of ketone bodies (Figure 3.1.3a and b) suggesting that autophagy is involved in targeting APP and BACE. However statistical significance was not obtained. We believe that the basal turnover rates of these specific proteins are too low to lead to more robust changes in the intervention time investigated. The autophagy machinery was only inhibited for two hrs, which may be too short to provide a large enough time window to observe protein accumulation. In addition, it is possible that bafilomycin is not the ideal autophagy inhibitor in this particular cell line and it may be beneficial to use an inhibitor of lysosomal function such as E64d or pepstatin A instead (Mizushima *et al.,* 2010).

The opposite pattern was observed with regards to Aβ expression levels (Figure 3.1.3c). A significant decrease was seen with bafilomycin treatment, in the presence and absence of ketone bodies. These data are somewhat surprising as we anticipated increased aggregation of the Aβ peptide when autophagy was inhibited. We speculate that the aggregate prone behaviour of Aβ has been affected by the equilibrium between soluble oligomeric amyloid species, a known phenomenon which complicates AD research when assessing particular protein species (Benilova *et al.,* 2012). It could also be the case that the antibody used for Western blot analysis showed non-specific binding effects.

Pickford *et al.* (2008) described no significant change in APP levels in AD transgenic mice with a beclin deficiency, while Tian *et al.* (2011) successfully demonstrated that autophagy deficient mice had a non-significant increase of 25% in full-length APP compared to wild-type mice, supporting our findings. APP C-terminal fragment (APP-CTF) levels showed the same pattern with the inhibition of autophagy leading to a greater accumulation significantly different from controls (Tian *et al.,* 2011). These data strengthen the notion

that it is important which protein fragment of APP is considered, and our data support the literature with regards to APP expression.

BACE1 activity is intimately linked to Aβ levels – pharmacological inhibition decreases Aβ levels in the brain (Fukomoto *et al.,* 2010) and BACE$^{-/-}$ mice do not present with any cerebral Aβ deposition (Vassar *et al.,* 2009). Chen *et al.* (2015) demonstrated that autophagy inhibition through 3-methyladenine increased the levels of BACE1 in a model of glucose-oxygen deprivation. These data support the trend of BACE protein expression levels increasing upon bafilomycin treatment (Figure 3.1.3b).

The decrease in Aβ that we describe (Figure 3.1.3c) is in contrast with current literature, and suggests that autophagy is involved in producing Aβ. Others have found that inhibiting autophagy leads to Aβ accumulation (Tian *et al.,* 2011, Pickford *et al.,* 2008) and that increasing autophagy via a small molecule enhancer can decrease the levels of APP-CTF. Atg5, Beclin-1 and ULK-1, essential components of the autophagy pathway, are involved in this degradation (Tian *et al.,* 2011). This finding suggests that autophagy is not only involved in the clearance of amyloid, but also in its generation (Yu *et al.,* 2004, Yu *et al.,* 2005) which further contributes to the complexity of protein clearance and warrants further investigation.

4.1.3 Ketone body treatment may enhance autophagic flux

Although no significant effect of ketone bodies on autophagy was observed (Figure 3.1.4), ketone body exposure decreased p62 and increased LC3-II protein levels, suggesting upregulation of autophagy. This is supported by the change in APP and BACE protein levels, which both decreased upon ketone body exposure. However, concomitant inhibition of autophagosomal/lysosomal fusion in the presence of ketone bodies did not consistently increase LC3-II and p62 levels. Additional means to assess autophagic flux are here recommended, such as the detection of p62 and LC3 punctae through immunofluorescence, or the use of autophagy specific tandem proteins, that allow discerning between the autophagosomal and lysosomal pool size (Mizushima *et al.,* 2010). It is also possible that autophagy inhibition was not complete, although we chose the concentration and duration of bafilomycin treatment based on dose response experiments by others in our research group. This deserves further attention in the future.

The lack of a robust increase in LC3-II or p62 protein levels in the concomitant treatment with ketone bodies and bafilomycin may be due to the fact that we did not deprive cells of glucose during the course of ketone body treatment. However, others have found that ketone bodies increase autophagy with glucose deprivation,(Camberos-Luna *et al.,* 2015). Such a scenario is less aligned with the physiological response to ketosis induced by starvation. Grey *et al.* (1975) demonstrated that glucose levels remained unchanged despite increased levels of free fatty acids and β-OHB.   Further research that dissects the relationship between substrate availability, such as predominantly glucose *versus* amino acids or fatty acids is required to enhance our understanding of this research question.

4.1.4 Basal autophagy targets and degrades APP, BACE and Aβ

Fluorescence microscopy of APP, BACE and Aβ revealed their intracellular localization pattern and allowed assessment of possible localization and distribution changes when exposed to bafilomycin and ketone body treatment. Autophagy inhibition had an effect on the aggregation of all three proteins, with the most robust changes observed in APP (Figure 3.1.5a). These results support the results observed in the APP and BACE Western blot data, that autophagy is involved in the clearance of these two proteins. The fluorescence microscopy data for Aβ showing aggregation upon autophagy inhibition contradicts Western blotting data which suggests that autophagy increases its levels. Findings in the literature support the clearance role of autophagy here (Tian *et al.,* 2011; Chen *et al.,* 2015) and supports the notion that autophagy is involved in the clearance of these proteins.

APP is found in various membrane-rich subcellular compartments including the nucleus, mitochondria and microsomes (Selkoe *et al.,* 1988). Our results support this finding since spherical localization, which could be indicative of the latter two structures, was observed, and could also explain the nuclear signal. BACE is a transmembrane aspartic protease that occurs primarily within acidic intracellular compartments such as endosomes and the trans-Golgi, with its active site localized at the luminal interface (Vassar *et al.,* 2009). This could explain the spherical aggregations observed – these may indicate endosomes or the like, containing BACE. In future studies this question may be confirmed by co-staining cells for BACE and endosome or Golgi specific proteins. Aβ is associated with tubulovesicular compartments such as the ER, Golgi and endosomes as well as AV within cells (Yu *et al.,*

2005). The spherical aggregates shown in our micrographs (Figure 3.1.5c) support this and suggest the involvement of autophagy in Aβ breakdown.

We observed nuclear signal of APP, BACE and Aβ which was lost upon ketone body treatment but not upon autophagy inhibition (Figure 3.1.5). The nuclear localization of APP has been documented by Kimberly *et al*. (2001). They constructed a plasmid that encodes the APP protein intracellular domain (AICD) and reported that the majority of the synthesized protein localized to the nucleus, suggesting that it signals through the nucleus. Nuclear localization of APP, BACE and Aβ could suggest a possible role in regulating signalling or transcription, a compelling notion that warrants further investigation.

4.2.1 Ketone body exposure rescues paraquat-induced neurotoxicity

Paraquat is toxic to cells and exposure leads to oxidative stress-induced neuronal cell death (McCormack *et al*., 2005). Our results indicate that paraquat reduces the reductive capacity of cells compared to controls (Figure 3.2.1). However, this study has shown that ketone bodies ameliorate this effect, conferring neuronal protection in the presence of paraquat, and improving cell viability. This demonstrates the protective effects of ketone bodies.

Others have found that ketone bodies have an anti-oxidant effect by acting as inhibitors of mitochondrial permeability, thereby decreasing production of mitochondrial ROS (Kim *et al*., 2007). A similar protective effect was observed in mouse kidney (Shimazu *et al*., 2013). These researchers present evidence that β-OHB acts as an endogenous histone deacetylase inhibitor which confers protection against oxidative damage. This may explain the mechanism of action of the rescue effect we observed and deserves further study, especially in light of the regulatory role of acetylation status on autophagy (Mariño *et al.,* 2014).

4.2.2 Ketone body supplementation and paraquat affect autophagy

Our data indicate that paraquat itself enhances autophagy as both ketone body and paraquat treatment show decreased LC3-II protein levels (Figure 3.2.2), which may indicate enhanced clearance and fusion with lysosomes. This supports findings by González-Polo *et al.* (2007) who have demonstrated that paraquat induces several autophagy characteristics

96

in neuroblastoma cells. However, fusion inhibition is recommended for future research to assess autophagic flux (Rubinsztein *et al.,* 2009).

A trend for decreased cleaved PARP with paraquat treatment was observed (Figure 3.2.2b) suggesting its cleavage upon paraquat exposure. However, our data do not indicate robust changes in PARP activation. It has been demonstrated that paraquat induces apoptosis (Fei *et al.,* 2008) and that caspase-3, -8 and -9 are increased upon paraquat exposure (Hong *et al.,* 2013). It is likely that our experimental conditions did not allow the relatively far downstream effects of PARP activation to manifest.

4.2.3 Ketone body exposure preserves mitochondrial morphology without affecting mitochondrial polarization

The important role of mitochondrial network dynamics in cellular viability is becoming increasingly clear (Okamoto and Kondo-Okamoto, 2012) and mitochondrial morphology analysis revealed definite patterns. Our analysis of the mitochondrial network using TMRE reveals that paraquat-induced mitochondrial fragmentation (Figure 3.2.3), a common sign of cellular stress also induced by other stimuli, often as an intermediate step before cell death programs are activated (Ashktorab *et al.,* 2004; Cho *et al.,* 2009). Co-treatment conferred some degree of protection from unbalanced fission, as more fused mitochondria can be observed, however the network is still less fused than what was observed in the control and ketone body-exposed groups. Thus our data supports the findings in the literature that a steady balance between mitochondrial fission and fusion favouring fusion is found in viable cells (Okamoto and Kondo-Okamoto, 2012) and that it is protective (Chen *et al.,* 2007).

Morphological analysis was completed by calculating the form factor and aspect ratio of mitochondria as well as obtaining the mitochondrial count (Figure 3.2.4). Results reveal a strong trend towards branched, elongated, networked mitochondria in the control group and with ketone body treatment and fragmented, spherical mitochondria with paraquat treatment in the presence and absence of ketone bodies. However, the presence of ketone bodies seems to improve paraquat-induced mitochondrial fragmentation. Our results are in agreement with the literature, where mitochondrial damage and fragmentation have been reported following paraquat treatment (Narendra *et al.,* 2008) and there is evidence that oxidative stress causes mitochondrial damage and disrupts morphology (Jendrach *et al.,*

97

2008). Mishra *et al.* (2014) reported that supplementing cells with ketone bodies resulted in increased mitochondrial respiration within 30 min of administration, which could be a result of the increased fusion state seen in the paraquat and ketone body co-treatment group compared to cells exposed to paraquat (Figure 3.2.3).

Flow cytometry was performed to indicate ROS in two compartments. First, TMRE, a mitochondrial membrane potential dependent dye which associates with the inner mitochondrial membrane was used to indicate mitochondrial specific oxidative stress, and secondly DCF was employed to indicate general intracellular ROS. The TMRE analysis (Figure 3.2.5.1) revealed that paraquat treatment caused brighter signal emission compared to controls, and ketone body supplementation in the presence of paraquat further increased the fluorescence intensity to the highest levels. This was an unexpected result, considering that ketone body treatment did not change emission levels. Others have reported that paraquat treatment decreases detected TMRE signal over time (Huang *et al.,* 2012; He *et al.,* 2012b). We believe that the increased signal is a result of the paraquat-induced mitochondrial damage which, at the point of assessment, manifested in fragmented but highly polarized mitochondria. These mitochondria would increase mean intensity signal and somewhat mask the overall mitochondrial polarization state.

No significant difference in DCF mean intensity was observed (Figure 3.2.5.2); however the trend for the highest detected signal in the co-treatment group supports the findings of the TMRE analysis. Others have found increases in the DCF signal with paraquat exposure which we did not observe (Lee *et al.,* 2015; Kim *et al.,* 2011).

4.2.4 Ketone body exposure improves localized ATP availability without affecting total ATP concentration

We assessed intracellular ATP levels and found that paraquat treatment, both in the presence and absence of ketone bodies, caused a decrease in ATP concentration (Figure 3.2.6). Ketone bodies did not ameliorate the decrease in ATP induced by paraquat. Yang *et al.* (2007) demonstrated decreased ATP in Parkinson's disease transgenic mice treated with paraquat and Yang and Tiffany-Castiglioni (2007) reported a similar effect in neuroblastoma cells.

There are shortcomings to using the luciferase-based ATP assays, and as such visual methods employing ATP indicators are recommended. ATeam transfection allows for the detection of intracellular ATP (Imamura *et al.,* 2009). Paraquat caused a severe decrease in the overall ATP signal and a complete loss in signal was detected. Ketone body exposure caused the formation of larger hotspots, indicating ATP accumulation. Co-treatment increased the detected signal, with the presence of hotspots visible. Our results are supported by Veech *et al.* (2001) who reported that ketone body supplementation increases the free energy of cytosolic ATP hydrolysis, ΔG_{ATP}.

These results reflect the findings in the ATP concentration data (Figure 3.1.1 and 3.2.1) as well as the literature (Arakawa *et al.* 1991; Chowdhury *et al*., 2014). Increased signal suggests not only ATP availability but also ATP consumption. Hence, ketone bodies in the presence of paraquat may preserve ATP consumption to an extent.

4.2.5 Ketone body supplementation preserves neuronal ultrastructure and increases vacuolar structures

Transmission electron microscopy analysis reveals the ultrastructure of cells, and provides the opportunity to qualitatively assess subcellular compartments such as the nucleus, mitochondria as well as vacuolar structures. We observed that exposure to paraquat caused an increase in chromatin disruptions (Figure 3.2.8d), while ketone body co-treatment decreased the severity of the nuclear disruption observed (Figure 3.2.8j). Chromatin condensation is commonly associated with apoptotis (Yao *et al.,* 2001), however it can also occur during mitosis (Hendzel *et al.,* 1998) and what appears to be morphologically identical processes, are actually distinct events: mitosis-related condensed chromatin results from aggregated heterochromatin while euchromatin degradation is the inducing factor in the chromatin condensation with later collapse and aggregation of heterochromatin observed during apoptosis (Hendzel *et al.,* 1998). Our results suggest apoptosis-related chromatin condensation, which supports the results of paraquat decreasing cell viability (Figure 3.2.1) and the fact that paraquat induces apoptosis (Fei *et al.,* 2008).

Intact mitochondria observed in the control and ketone body groups support the mitochondrial morphology data (Figure 3.2.3). Cells exposed to paraquat displayed disrupted mitochondria, an effect also reported by others (Peixoto *et al.,* 2004; Fei *et al.,*

2008), who assessed mitochondrial function, which is intimately linked to mitochondrial morphology (Hoppins, 2014). In the co-treatment group a number of intact mitochondria are visible (Figure 3.2.8k), however they show mixed morphological characteristics, indicating that the paraquat-induced damage is decreased upon ketone body supplementation.

Vacuolar structures are visible in all of the groups; however ketone body supplementation caused an apparent increase in their number, while paraquat exposure resulted in less well defined, more disrupted vacuoles. The vacuolar structures observed may be considered representative of AV (Boland *et al.,* 2008). Our observation of increased AV with ketone body treatment is aligned with recent findings and link it to autophagy induction (McCarty *et al.,* 2015; Camberos-Luna *et al.,* 2015), further supporting our LC3 Western blotting data (Figure 3.1.4).

4.3 Summary and conclusion

Our investigation into the benefits of ketone bodies in the context of neurotoxicity revealed a number of findings. We demonstrated that the intracellular ATP distribution is controlled by autophagy and ketone body treatment, indicating a change in ATP demand during these conditions. Examples of ATP-consuming processes include transport mechanisms along the microtubule network (Mallik and Gross, 2004) and protein synthesis (Buttgereit and Brand, 1995). Enzymes involved in ATP generating processes are likely more active in the hotspots observed, such as components of the TCA cycle. In addition, ketone body supplementation improved localized ATP supply during neurotoxin exposure. However, the ATP relocalization effect did not reflect a change intracellular in ATP concentration. More sensitive methods to assess ATP levels may need to be employed, such as measuring mitochondrial respiration by means of an oxygraph (Skemiene *et al.,* 2013; Phielix *et al.,* 2008).

In addition we observed that APP and BACE, and likely Aβ, are targeted for degradation by the autophagic pathway. These proteins are associated with amyloid deposition, and thus our results suggest a beneficial role of autophagy in clearing toxic amyloid aggregates present in AD. Furthermore, we have shown that ketone body treatment may enhance the autophagic flux and in this way confer its beneficial effects. This could explain the beneficial

effect of ketone bodies on a host of neurodegenerative diseases, many associated with protein aggregation as integral to their etiology.

We also observed that ketone body supplementation serves a protective role in neurons exposed to a toxic environment; ketone body administration prevented oxidant-induced neuronal cell death. Mitochondrial morphology analysis, an important indicator of cell viability and thus the energetic capacity of neurons, revealed that cells treated with paraquat in the presence of ketone bodies presented with a morphological state more similar to control conditions, while mitochondria were completely fragmented in the injury-induced model. However, the beneficial effect on morphology did not reflect measurable changes in mitochondrial polarization. This may be due to the fact that changes in mitochondrial morphology occur early after changes in, for example, energetic substrate supply (Hoppins, 2014) while depolarization is a late event preceding cell death (Kroemer *et al.,* 2007).

Our hypothesis was not fully verified as no change in ATP concentration was observed and results of autophagy upregulation did not always reach statistical significance. However the changes observed upon ketone body administration cannot be ignored.Ketone body supplementation preserved neuronal ultrastructure and increased the presence of autophagic vacuoles, verifying our findings that ketone bodies stimulate autophagic flux.

Thus to conclude, based on our results, ketone bodies display great therapeutic value to improve dysfunctional autophagy and energetic supply, two major etiological factors in AD. In addition, they confer neuroprotection, at least in part by improving mitochondrial parameters (Figure 4b). This is an exciting prospect that requires further investigation.
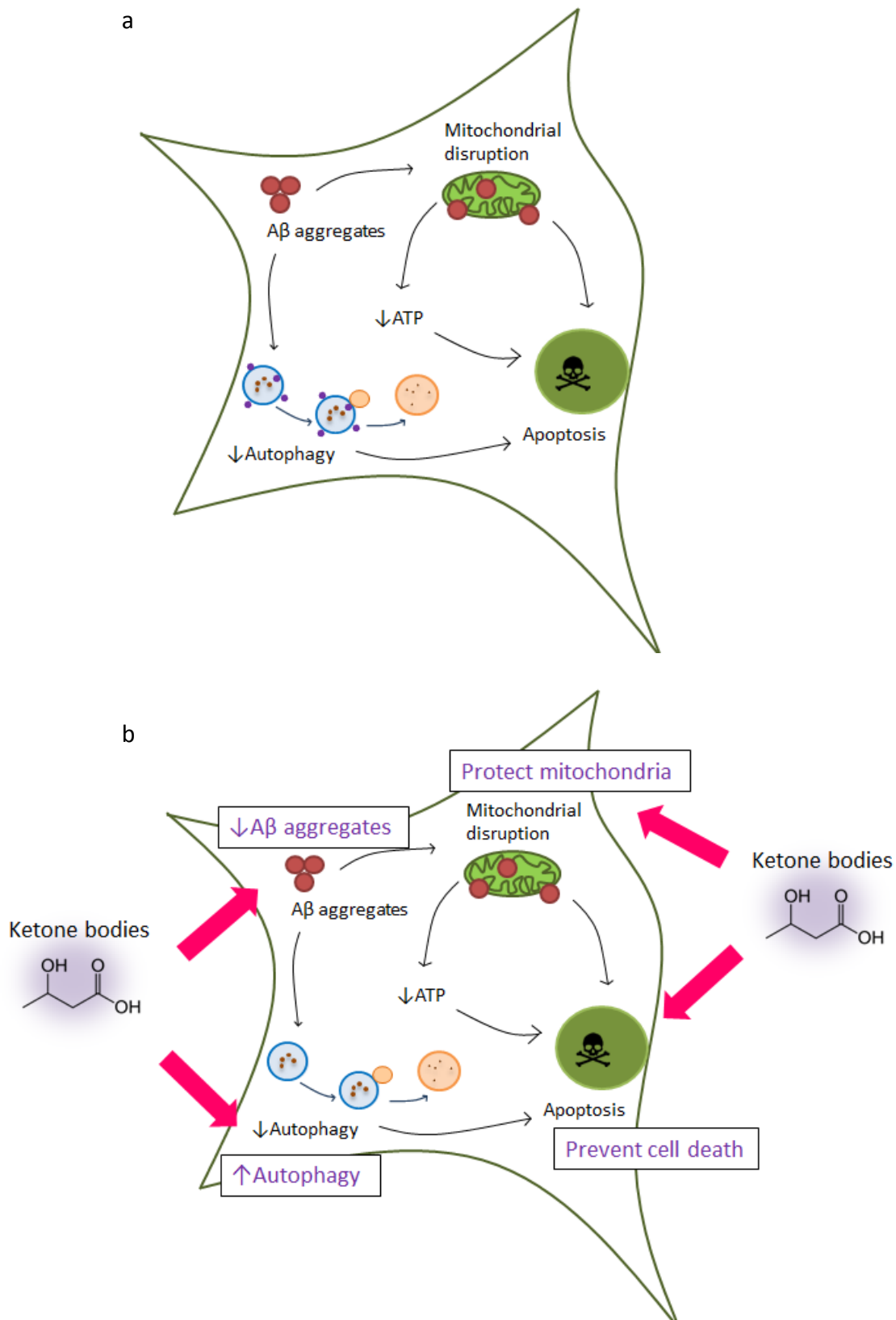
Figure 4a and b: Aβ aggregation disrupts autophagy, mitochondrial function and ATP production, activating apoptosis (a) while ketone bodies ameliorate these defects and confer neuroprotection (b).

4.4 Future recommendations

Future studies assessing additional parameters are recommended, and suggestions regarding the experimental model and methods employed will be offered and summarized below.

Firstly, the use of a murine hypothalamic neuronal cell line, GT1-7 cells, as an experimental model for simulating AD, could be improved by using primary isolated neurons from GFP-LC3 mice, which would simplify measuring the autophagic flux (Mizushima *et al.*, 2004). In addition transgenic APP knock-in mice harbouring Swedish and Beyreuther/Iberian mutations (Saito *et al.,* 2014) would provide a more physiologically relevant model of AD. Moreover, autophagic flux could be measured more accurately by employing a host of additional methods, including the assessment of tagged autophagic vacuoles, and/or lysosomes. In addition, using not only an acidification inhibitor such as bafilomycin, but also lysosomal-specific inhibitors such as pepstatin or E64d instead is recommended. Inhibiting autophagy for a longer time period, or using a higher concentration, in order to ensure complete inhibition could be beneficial.

The ATP concentration could be assessed more sensitively by assessing mitochondrial respiration, which would also better identify the biochemical pathways employed by ketone bodies to enhance local ATP supply. In addition, cells could be treated with inhibitors such as deoxyglucose to inhibit glycolysis or potassium cyanide to inhibit oxidative phosphorylation, and then assessed to determine how ATP supply recovers over time. The use of other ATeam constructs in addition to the mitochondrially targeted one employed here, i.e. targeted to cytoplasmic and nuclear ATP, would enhance our knowledge of whole-cell ATP supply.

Finally, this work has uncovered potential research avenues that warrant future research. It would be important to identify how ketone bodies increase autophagic flux. A possible meeting point between ketone body metabolism and the process of autophagy could be the role of intracellular transport mechanisms. One way in which to assess this is to measure the activity of cellular transporters such as dynein, which require ATP to transport cargo such as autophagic vacuoles (Iwata *et al.,* 2005), in response to ketone body treatment. Another research question to investigate is how ketone bodies influence protein synthesis, a key ATP

consumer within cells (Buttgereit and Brand, 1995). Expression of mTOR, a key regulator of protein synthesis (Green *et al.,* 2014), could be assessed here. Such research avenues will enhance our understanding and may provide new insights on how to use ketone bodies effectively as an adjuvant therapy in the context of neurodegeneration.

APPENDIX

A.1   Supplementary results

A.1.1   Neuronal reductive capacity following ketone body treatment

Guided by literature, a dose response was established in order to confirm that there is no toxicity using the desirable ketone body concentration. Treating cells with ketone bodies (β-OHB) yielded no significant differences in the cells' reductive capacity compared to the control condition. This result was seen at both 24 (Figure A.1.1a) and 48 hrs (Figure A.1.1b) after treatment with concentrations of 1.5 mM, 3 mM, 6 mM, and 12 mM of ketone bodies. 6 mM was selected as the treatment concentration for all subsequent experiments as it is physiologically relevant (Owen *et al.,* 1967) and found to be non-toxic.

a

b
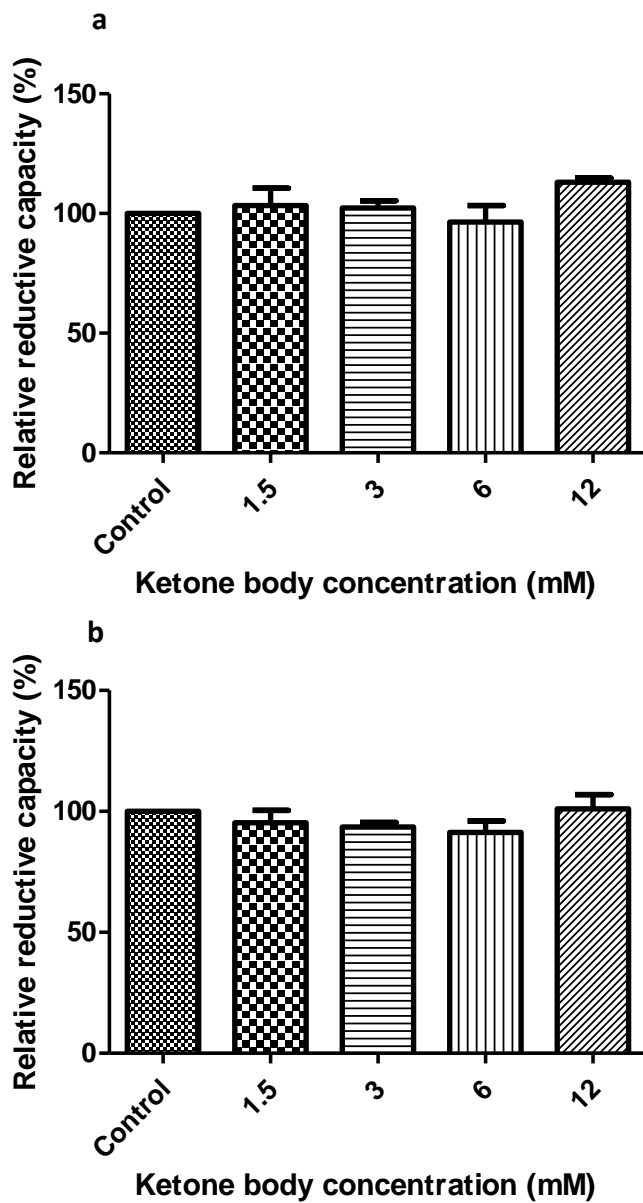
Figure A.1.1: Relative reductive capacity of GT1-7 cells following 24 h treatment (a) with different concentrations of beta-hydroxy butyrate (1.5 mM - 12 mM) and 48 h treatment (b), (n=2).

A.1.2 Amyloid beta-induced toxicity

Initial experiments were performed using an amyloid-induced toxicity model. However, a great degree of variability was observed, which made this model in this particular scenario less suitable. Amyloid beta was found to be toxic at a concentration of both 2 and 5 µM. Treating cells with 2 µM for 24 hrs caused a reduction in the relative reductive capacity compared to the control [86.9% ± 2.4% ($p < 0.05$)] while treating cells with 5 µM for 24 hrs caused an even greater reduction [61.8% ± 2.5% ($p < 0.05$)] as displayed in Figure A.1.2. It is important to note that it was necessary to break up larger peptide formations that the synthetic amyloid product used formed naturally, through water-bath sonication in order to see the toxic effect demonstrated in Figure A.1.2. The protocol describing this process, derived from a protocol by Ryan *et al.* (2010) can be found in section A.2. It was decided against using the amyloid peptide as a model for Alzheimer's disease due to difficulty in gaining consistent cell death data. In addition, challenges with timely delivery of the amyloid peptide (we experienced a waiting period of more than four months) further favoured utilization of the paraquat induced toxicity model.
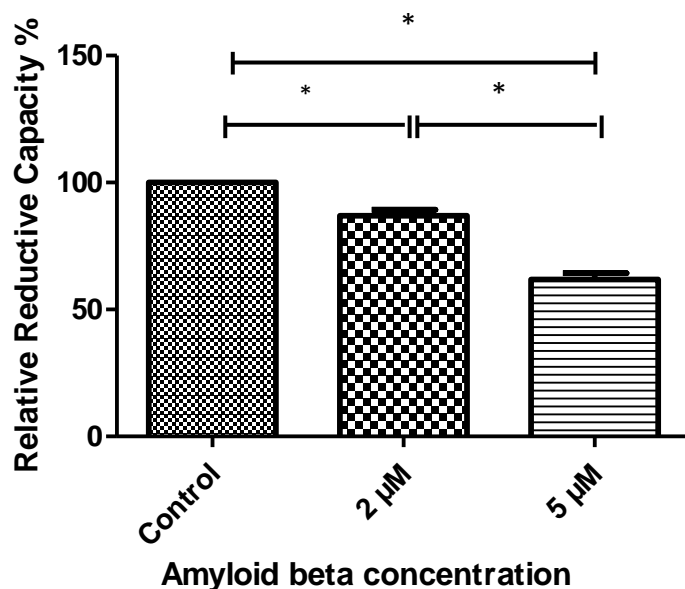
Figure A.1.2: Relative reductive capacity of GT1-7 cells following 24 h treatment with 2 µM and 5 µM amyloid beta peptide.*$p < 0.05$, (n=2).

A.1.3 Propidium iodide exclusion assay and Hoechst counterstain to assess membrane integrity and nuclear condensation

Hoechst 33342 is a DNA-intercalating dye that stains nuclei. It can also indicate regions of DNA condensation, or pyknosis, which is visible as small, bright areas within the nucleus. Pyknosis is often used as an indicator for apoptosis. Propidium iodide (PI) is a DNA intercalating fluorochrome which can only cross permeabilized membranes, and thus is used as a marker for necrosis-type cell death which is characterized by a loss of membrane integrity. Cells were stained with both Hoechst and PI to determine the mode of cell death present upon amyloid-beta treatment (Figure A.1.3). Control cells show a very low presence of PI-positive nuclei and also less pyknotic nuclei. Amyloid beta treatment caused an increase in PI-positive nuclei, as well as pyknotic nuclei. Nuclei that were both PI-positive and pyknotic were also observed, and were in fact more common than cells stained with PI alone. The double signal is indicative of late apoptosis, where the membrane becomes permeable. The presence of late apoptotic cells suggests that apoptosis is the main mechanism of amyloid beta-induced cell death, which has also been found by others (Loo *et al.,* 1993; Di Carlo, 2010).
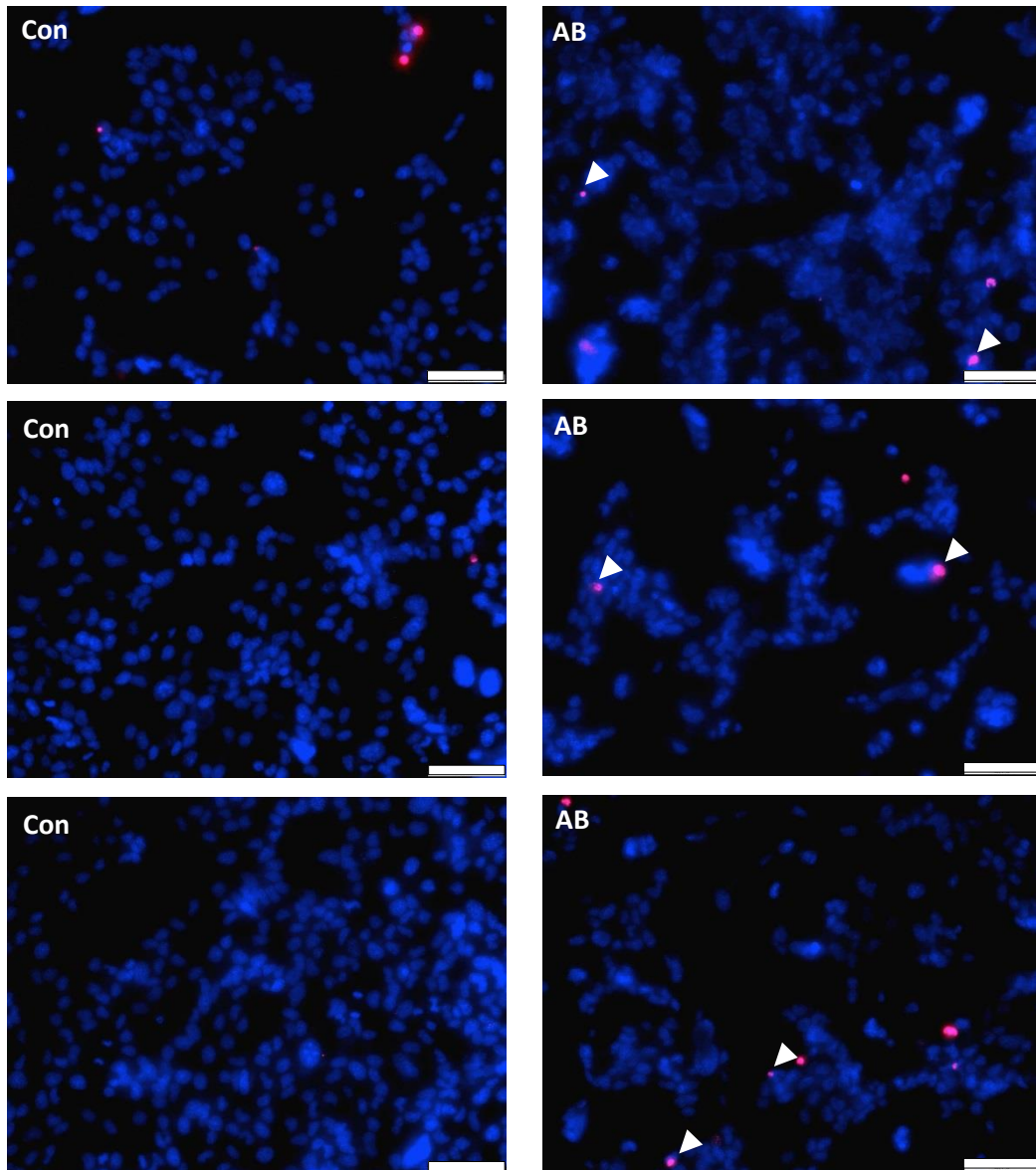
Figure A.1.3: Representative fluorescent micrographs of nuclei stained with Hoechst 33342 and propidium iodide. Cells were treated as control cells (Con) or with 5 µM amyloid beta peptide (AB). Arrowheads indicate prodidium iodide positive cells with pyknotic features.10X magnificationScale bar = 100 µm.

A.2   Protocols

A.2.1   WST-1 assay

- Warm WST-1 to 37 °C

- Add WST-1 to pre-warmed complete medium so that it makes up 5% of the well volume

- Aspirate treatment medium from experimental and control wells of 48-well plates

- Place 200 µl of pre-warmed medium containing WST-1 in each well using a sterile P200 pipette tip

- Wrap the plate in foil

- Incubate for 2 hrs at 37 °C (5% CO_2)

- Place the foil-wrapped plate on a shaker for 1 min to mix well contents

- Read the absorbance at a wavelength of 450 nm using a microplate reader

A.2.2   Transfection with ATeam indicator

- Seed cells at a density of 30 000 cells per well in NUNC 8-well chamber dishes

- Allow to adhere overnight

- Refresh the medium

- Make up **Mix 1** and **Mix 2** in two separate 0.5 ml eppies

- **Mix 1:** Add 10 µL lipofectamine and 100 µL serum-free medium to eppie (cold reagents)

- **Mix 2:** Add 1.46 µL DNA (to obtain a concentration of 400 ng DNA), 100 µL serum-free medium, and 16 µL P3000 reagent to Eppendorf tube

- Briefly vortex both eppies

- Add **Mix 1** to **Mix 2** and vortex

- Incubate for 5 min at room temperature

- Add 10 µL of the transfection medium to each well

- Incubate for 48 hrs at 37 °C, 5% CO_2, refreshing medium 1 h after addition of the transfection medium to minimize exposure to the toxic transfection reagent

- Image cells 48 - 72 hrs after transfection

A.2.3   ATP extraction

- Seed cells at 1 X 10^6 cells per petri (35 mm diameter)

- Grow until 80-90% confluent

- Trypsinize cells and place the cell suspension into 2 ml Eppendorf tubes

- Centrifuge at 4 °C (8000 rpm, 4 min) and wash (resuspend) with cold PBS

- Centrifuge again at 4 °C

- Resuspend in 50 µL ice cold lysis buffer (100 mM Tris-HCl and 4 mM EDTA, pH 7.75)

- Add 150 µL boiling lysis buffer

- Incubate samples for 2 min at 99 °C

- Centrifuge lysates at 10 000 rpm at 4 °C for 1 min

- Collect supernatants for ATP detection and store at -20 °C until ATP detection

A.2.4   ATP detection

- Thaw extracted ATP samples on ice

- Make up the ATP standard provided in the ATP kit by adding 15 µl of the standard solution after vortexing to a labelled sterile 500 µl Eppendorf tube together with 135 µl ATP-free water to make 150 µl of solution containing 10^{-8} M ATP

- Vortex this solution, and repeat the process by adding 15 µl of this solution and 135 µl ATP-free water to a fresh, labelled Eppendorf tube

- Repeat this sequence seven more times until you have a total of eight Eppendorf tubes, thus a range of ATP solutions ranging from 10^{-8} M ATP to 10^{-16} M ATP

- Pipette 50 µl of the ATP-free water and each of the standards in duplicate into a white 96-well plate, vortexing Eppendorf tubes before each addition

- Pipette 50 µl of samples in duplicate into the plate

- Label where each sample is in the plate on a paper template

- Make up the provided luciferase reagent according to the manufacturer's instructions in light protected conditions

- Flush the luminometer twice using the following substances: dH$_2$O, 70% ethanol and air

- Prime the luminometer with the luciferase reagent

111

- Set the luminometer's injector volume to 50 µl, the integration time to 10 sec and the delay before starting to 5 sec

- Select the wells to be measured and start the program

- Use the generated relative light unit measurements of the standard curve to calculate the sample ATP concentrations

A.2.5   Western blot analysis

A.2.5.1 Protein extraction

- Aliquote 1 ml RIPA buffer (recipe in section) into a 2 ml Eppendorf tube and add protease and phosphatase inhibitors in the following concentrations an hour or less before extraction:

  - Aprotinin (1 µg/ml)

  - Leupeptin (1 µg/ml)

  - PMSF (1 mM)

  - Na_3VO_4 (1 mM)

  - NaF (1 mM)

  - Benzamidine (1 µg/ml)

  - Pepstatin A (10 µg/ml)

- Vortex the solution and place Eppendorf tube on ice

- Remove treatment medium from flasks

- Rinse three times with cold PBS, removing as much as possible residual PBS after the last wash with a 1 ml pipette

- Add 50 µl of modified RIPA buffer to each flask and scrape the flask surface thoroughly using vertical motions

- Transfer the scraped contents to labelled 1 ml Eppendorf tubes

- Sonicate Eppendorf tubes 4 X 2 sec at an amplitude of six with a sec pause between each bout of sonication

- Place Eppendorf tubes on ice at 4 °C for approximately 2.5 hrs or until most of the bubble have disappeared

- Centrifuge for 10 min at 8000 rpm

- Carefully decant the supernatant into labelled Eppendorf tubes, place on ice and proceed with the Bradford protein determination assay immediately

A.2.5.2 Bradford assay

- Thaw BSA solution (0.2 mg/ml in dH$_2$O)

- Collect protein samples and keep on ice at all times

- Mark 2 ml Eppendorf tubes in duplicate for each concentration of BSA and each sample

- Prepare the standard curve by adding the correct amount of BSA and dH$_2$O to the relevant Eppendorf tubes according to the following table, making sure vortex the stock solution of BSA before each addition:

Concentration (µg/ml)	Volume of BSA (µl)	Volume of dH$_2$O
0 (Blank)	0	100
2	10	90
4	20	80
8	40	60
12	60	40
16	80	20
20	100	0

- For the samples add 95 µl dH$_2$O and 5 µl of protein to the relevant Eppendorf tubes

- Vortex all tubes briefly

- Add 900 µl Bradford working solution to each Eppendorf tubes and vortex again

- Incubate Eppendorf tubes at room temperature for at least 5 min

- Zero spectrophotometer by using one of the 'blank' Eppendorf tubes containing no BSA

- Read the absorbance values by using a spectrophotometer set to 595 nm, by adding the contents of each Eppendorf tube to 2 ml cuvettes

- Generate the standard curve by using the average of the read absorbance values against the concentration of BSA

- Aliquote samples into fresh Eppendorf tubes according to the volumes calculated from the standard curve and freeze at -80 °C until use

A.2.5.3 Making gels using Fast-Cast kit

- Assemble the gel casting stand using spacer and short plates
- Fill the gap between plates to the top with dH_2O using a disposable pipette
- Wait 5 min to check for leaks and readjust if necessary until watertight
- Remove the dH_2O by tipping the rig and use paper towel if necessary
- Make up the resolving and stacking gel according to the manufacturer's instructions
- <u>Resolving gel (for one gel):</u>
  - Add 3 ml of both Buffer A and Buffer B into a small glass beaker
  - 30 µl APS
  - 3 µl TEMED
- <u>Stacking gel (for one gel):</u>
  - Add 1 ml of Buffer A and Buffer B into a separate small glass beaker
  - 10 µl APS
  - 2 µl TEMED
- Mix the contents of both beakers thoroughly by swirling their contents
- Pour Resolver into the gel rig using a disposable pipette to approximately 1 cm from the top
- Pour the Stacker to the top using a new disposable pipette
- Insert the appropriate comb(s) gently, avoiding air bubbles
- Allow the gel(s) to set (30 min – 1 h)
- Use within three weeks
- Store at 4 °C and keep moist until use

A.2.5.4 Sample preparation for Western blotting

- Make a working solution of Laemmli's sample buffer by adding 850µl Laemmli's stock buffer solution + 150 µl β-mercaptoethanol
- Vortex thoroughly
- Thaw the appropriate number of samples needed on ice

114

- Add the appropriate amount of working solution of Laemmli's and RIPA buffer, as calculated, to each appropriate tube

- Close tubes and punch small hole in lid with tweezers or syringe needle

- Heat samples on heating block (95 °C) for 5 min

- Vortex each tube, spin down contents briefly (±10 sec) and place on ice immediately

A.2.5.5 Separating proteins on Western blot gels

- Carefully remove comb from gel and place in the U-shaped adaptor with short plate facing inward

- Insert assembly into the loading system and close the latches by pushing them inward while pushing down gently on the plates (the centre will form the buffer dam)

- Place the assembly in a gel tank and fill the buffer dam with cold 1X running buffer until it spills into the tank, then top up the tank until the buffer is level with the buffer at the top of the dam

- Wash the wells with running buffer, using an insulin syringe

- Add 7.5 µl of protein marker to the first lane on the far left of each gel

- Add the appropriate amount (calculated from Bradford protein quantification) of sample slowly into the appropriate lane, using the gel-loading tips

- Place the green lid with appropriate leads (black to black: red to red) on top of the tank and connect to the powerpack

- Run at 120 V (constant), for approximately 1 h until the sample dye front and smallest standard of the protein marker reaches the bottom of the gel

- Switch off power and disconnect electrodes. Remove gel plates from the tank and proceed to electrotransfer step immediately

A.2.5.6 Transferring proteins to membranes using Transfer Turbo and Chemi-Doc

- Open the "transfer pack" and place one of the stacks of blotting paper on the Biorad Transfer Blot cassette with the PVDF membrane on top

- Gently roll out any air bubbles

- Place the gel on top of the membrane with the low molecular weight protein side facing towards the centre of the cassette and again gently roll out any trapped air bubbles

- Place the remaining stack of blotting paper on the gel and roll out air bubbles, making sure to align the blotting paper, membrane and gel

- Place lid on top and lock in place

- Place the cassette in the Biorad Transfer Blot and set to transfer for 7-12 min, depending on protein

- Check that protein has transferred and then place in methanol for ±30 sec, then leave to dry completely.

- Pour Ponceau stain on top and swirl until red bands appear strongly

- Pour off the stain and rinse with dH_2O until membrane is clear.

- Rinse membrane 3 X 5 min with TBS-T

- Block for 2 hrs in 5% milk (5 ml fat-free Parmalat long-life milk in 100 ml TBS-T)

- Wash 3 X 5 min in TBS-T

- Place membrane in a 50ml tube containing 5 ml of primary antibody made up in TBS-T (1:1000)

- Place on rotator in 4 ^{0}C walk-in fridge overnight

A.2.5.7 Imaging membranes

- Remove the membrane from the primary antibody and wash 3 X 5 min in TBS-T

- Place membrane in a 50 ml tube containing 5ml of the appropriate secondary made up in TBS-T (1:10 000)

- Prepare ECL substrate in a 1:1 ratio of solution A:B in a foil covered tube

- Pour off the TBS-T from membrane and add ECL, spreading evenly over surface of membrane by gentle tilting

- Swirl gently for 2 min

- Place membrane on tray of Biorad Chemidoc, taking care to remove bubbles

- Image the membrane by using ImageLab software, using the 'Custom' slider to select the optimum exposure time

A.2.5.8 Stripping and reprobing membranes

- Wash membrane 2 X 5 min with dH_2O

- Strip with 0.2 M NaOH at room temperature for 5 min on shaker

- Wash membrane 2 X 5 min with dH_2O

- Block with 3% milk in TBS-T for 1 h at room temperature

- Wash 3 X 5 min in TBS-T

- Proceed as per normal Western blot technique with primary[0] antibody overnight and then secondary antibody

A.2.6 Staining with amyloid antibodies

- Seed cells in NUNC 8-well chamber dishes at a density of 10 000 cells per well

- Treat with the appropriate agents

- Aspirate treatment medium and rinse with pre-warmed sterile PBS

- Add 200 µl ice cold methanol/acetone (1:1) fixative per well

- Keep on ice and incubate for 10 min at 4°C

- Aspirate fixative, leave to airdry for 20 min at room temperature

- Rinse each well with 400 µl S-PBS

- Add 100 µL FBS per well and incubate for 20 min at room temperature

- Drain the FBS without washing

- Add 50 µL primary antibody at the correct concentration

- Incubate for 90 min at room temperature in a humidifying chamber

- Rinse wells carefully with 200 µl S-PBS

- Add 50 µl secondary antibody (1:200) to wells and incubate for 30 min at room temperature in a light-protected humidifying chamber

- Add 50 µl Hoechst without removing secondary antibody to counterstain nuclei and incubate another 10 min in a light-protected humidifying chamber

- Wash three times with 400 µl S-PBS and mount using a small amount of fluorescent mounting medium

NOTE: All antibodies and Hoechst are made up in S-PBS. Secondary antibodies were briefly centrifuged and the supernatant used to prevent aspirating crystals.

A.2.7 Imaging cells stained for APP, Aβ and BACE

- After staining, transport the NUNC chamber dish to the fluorescent microscope, protected from light

- Set the magnification to 100X and apply a small drop of lens oil to the objective

- Search for cells using the Dapi filter at a low intensity (10-30%) to visualize nuclei

- Optimize the focus using the appropriate filters for the stained markers: Dapi for nuclei, FITC for APP, and TxRed for both Aβ and BACE

- Obtain a minimum of five random regions per treatment group for each different marker

A.2.8 Flow cytometry

- Seed cells at 2 X 10^6 cells per T25 flask and treat as usual, seeding an extra flask treated for the control condition

- After treatment trypsinize cells, centrifuge (1500 rpm for 3 min) and resuspend in 2 ml warm S-PBS

- Divide the cell suspension of each treatment group between two 15 ml tubes; 1 ml for DCF staining and 1 ml for TMRE

- Add the correct concentration of DCF (50 µM) and TMRE (1 µM) to the relevant tubes with the lights off

- Add CCCP (to serve as a positive control) to one of the extra control tubes at a concentration of 5 µM, and add 1 µM TMRE

- Leave the final tube unstained for an unstained control

- Keep the tubes at 37 °C and in the dark while not using them for flow cytometry

- Perform flow cytometry on DCF-stained cells, acquiring a minimum of 10 000 cells and using a 488 nm laser and 610LP, 616/23BP emission filters

- Add 100 µl hydrogen peroxide to the control DCF tube to serve as a positive control, incubate for 1 min and perform flow cytometry

- Perform flow cytometry on TMRE cells, acquiring a minimum of 10 000 cells using a 488 nm laser and 502LP, 530/30BP emission filters

A.2.9 Staining and imaging mitochondria

- Seed cells at a density of 15 000 cells per well in a NUNC 8-chamber dish and treat

- After treatment, refresh the medium with 300 µl pre-warmed complete medium per well and keep the dish in an incubated chamber

- Aspirate the medium from the first well to be imaged and replace with 200 µl of medium containing 100 nM (2 µl) TMRE and 10 µl Hoechst

- Wait five min for the fluorochromes to infiltrate cells

- Set the magnification to 100X and apply a small drop of lens oil to the objective

- Search for cells using the Dapi filter at a low intensity (10-30%) to visualize nuclei

- Optimize the focus using the appropriate filters for the stained markers: Dapi for Hoechst-stained nuclei and Texas Red or TMRE which binds to polarized mitochondria

- Obtain a minimum of five cells per treatment group

A.2.10 Morphological assessment of mitochondria

- After imaging mitochondria as described above, raw images were analysed using ImageJ software according to the following sequence:
    - Binarize images, apply the 'Concolve' and then the 'Gaussian blur' filters and adjust the threshold to distinguish mitochondria from background signal
    - Quantify mitochondrial morphological characteristics and use them to calculate mitochondrial length (aspect ratio) and the degree of branching (form factor)
    - Aspect ratio: ratio between the major and minor axes of the ellipse equivalent to the mitochondrion
    - Form factor: $(Pm^2)/4\pi Am$. Pm is the length of the mitochondrial outline and Am is the area of the mitochondrion
    - A minimum of three cells on three separate micrographs were analysed in this manner and the obtained aspect ratio and form factor values averaged

A.2.11 Imaging cells stained with dichlorofluorescein (DCF)

- Seed cells at a density of 30 000 cells per well in a NUNC 8-chamber dish and treat

- After treatment, refresh the medium with 300 µl pre-warmed complete medium containing 50 µM DCF dye and Hoechst (1:200)

- Allow the dye to develop for 20 min, keeping the dish incubated and protected from light

- Set the magnification to 100X and apply a small drop of lens oil to the objective

- Search for cells using the Dapi filter at a low intensity (10-30%) to visualize nuclei

- Optimize the focus using the appropriate filters for the stained markers: Dapi for Hoechst-stained nuclei and FITC for DCF

- Capture a minimum of five images per treatment group

A.3 Buffers and solutions

A.3.1 RIPA buffer

Prepare 100 ml modified RIPA buffer as follows:

- Add 790 mg Tris base to 75 ml dH_2O

- Add 900 mg NaCl and stir the solution until all solids are dissolved

- Using HCl, adjust the pH to 7.4

- Add 10 ml of 10% NP-40 to the solution

- Add 2.5 ml of 10% Na-deoxycholate and stir until the solution is clear

- Add 1 ml of 100 mM EDTA to the solution

- Adjust the volume to 100 ml using a graduated cylinder

- Store RIPA buffer at 2-8 °C until ready to use

A.3.2 Phosphate buffered saline (PBS)

- Dissolve the following reagents in 1 l dH_2O:
    - 8 g NaCl
    - 0.2 KCl
    - 1.44 g Na_2HPO_4
    - 0.24 g KH_2PO_4

120

A.3.3 Bradford stock solution

- Dilute 500 mg Coomassie Brilliant blue G250 in 250 ml 95% ethanol

- Add 500 ml phosphoric acid, mix thoroughly using a stirrer bar

- Adjust the volume to 1 l with dH_2O

- Filter the solution and store at 4 °C

   Working solution:

- Dilute the stock solution in a 1:5 ratio with dH_2O

- Filter with two filter papers to obtain a solution with a light brown colour (light sensitive)

A.3.4 Laemmli's loading buffer

- Mix the following ingredients to make up stock solution:

   o 3.8 ml dH_2O

   o 1 ml 0.5 M Tris-HCl, pH 6.8

   o 0.8 ml glycerol

   o 1.6 ml 10% (w/v) SDS

   o 0.4 ml 0.05% (w/v) Bromophenol blue

A.3.5 Running buffer (10X)

- Dissolve 60.6 g Tris and 288g glycine in 1.5 l dH_2O

- Add 20 g SDS

- pH to 8.6 with concentrated HCl and then make up the volume to 2 l with dH_2O

A.3.6 Tris-buffered saline (TBS)

- Dissolve 48.4 g Tris and 160 g NaCl in 1200 ml dH_2O

- Mix the solution using a magnetic stirrer

- Adjust the pH to 7.6 with concentrated HCl

- Make up to 2 l with d dH_2O

- Store at room temperature

- To make 1 l of TBS-T working solution dilute 100 ml stock in 900 ml dH_2O and add 1 ml Tween-20

- Mix the solution until clear

A.3.7 Amyloid beta preparation

- Add 22.15 µL DMSO to the amyloid salt in the vial to make up an undiluted stock solution of 10 mM

- Add 443 µL of sterile PBS to the 10 mM solution to make up a stock solution of 500 µM

- Make aliquots at appropriate volumes and store at -20 °C until use

- When needed, thaw the appropriate number of Eppendorf tubes and add medium to gain the required concentration

- Sonicate the solution for 10 min in a water-bath sonicator to break up existing peptides

- Keep at 4 °C overnight to allow oligomers to form

REFERENCES

Ahmed M, Davis J, Aucoin D, Sato T, Ahuja S, Aimoto S e*t al*. Structural conversion of neurotoxic amyloid-[beta] 1-42 oligomers to fibrils. Nat Struct Mol Biol. 2010; 17, 5: 561-567.

Aiello LC and Wheeler P. The expensive-tissue hypothesis: the brain and the digestive system in human and primate evolution. Curr Anthropol. 1995: 199-221.

Alzheimer A. Über eigenartige Krankheitsfälle des späteren Alters. Zbl Ges Neurol Psych. 1911; 4: 356–385. (Translated and with an introduction by H Förstl and R Levy, 1991)

Apostolova LG, Green AE, Babakchanian S, Hwang KS, Chou YY, Toga AW *et al*. Hippocampal atrophy and ventricular enlargement in normal aging, mild cognitive impairment (MCI) and Alzheimer disease. Alzheimer Dis Assoc Disord. 2012; 26, 1: 17-27.

Arakawa T, Goto T and Okada Y. Effect of ketone body (D-3-hydroxybutyrate) on neural activity and energy metabolism in hippocampal slices of the adult guinea pig. Neuroscience Letters. 1991; 130, 1: 53-56.

Arrasate M, Mitra S, Schweitzer ES, Segal MR and Finkbeiner S. Inclusion body formation reduces levels of mutant huntingtin and the risk of neuronal death. Nature. 2004; 431: 805-810.

Ashktorab H, Frank S, Khaled AR, Durum SK, Kifle B and Smoot DT. Bax translocation and mitochondrial fragmentation induced by Helicobacter pylori. Gut. 2004; 53, 6: 805-813.

Ballatore C, Lee VMY and Trojanowski JQ. Tau-mediated neurodegeneration in Alzheimer's disease and related disorders. Nat Rev Neurosci. 2007; 8, 9: 663-672.

Barth S, Glick D and Macleod KF. Autophagy: assays and artifacts. J Pathol. 2010; 221, 2: 117-124.

Bayod S, Del Valle J, Canudas AM, Lalanza JF, Sanchez-Roigé S, Camins A *et al*. Long-term treadmill exercise induces neuroprotective molecular changes in rat brain. J Appl Phys. 2011; 111, 5: 1380-1390.

Beckett TL, Studzinski CM, Keller JN, Murphy MP and Niedowicz DM. A ketogenic diet improves motor performance but does not affect β-amyloid levels in a mouse model of Alzheimer's Disease. Brain Res. 2013; 1505: 61-67.

Bélanger M, Allaman I and Magistretti PJ. Brain energy metabolism: focus on astrocyte-neuron metabolic cooperation. Cell Metab. 2011; 14: 724-738.

Benge JF, Balsis S, Geraci L, Massman PJ and Doody RS. How well do the ADAS-cog and its subscales measure cognitive dysfunction in Alzheimer's disease? Dement Geriatr Cogn Disord. 2009; 28, 1: 63-69.

Benilova I, Karran E and De Strooper B. The toxic A [beta] oligomer and Alzheimer's disease: an emperor in need of clothes. Nature Neurosci. 2012; 15, 3: 349-357.

Berridge MV, Tan AS, McCoy KD and Wang R. The biochemical and cellular basis of cell proliferation assays that use tetrazolium salts. Biochemica. 1996; 4, 1: 15-19.

Bjørkøy G, Lamark T, Brech A, Outzen H, Perander M, Øvervatn A *et al.* p62/SQSTM1 forms protein aggregates degraded by autophagy and has a protective effect on huntingtin-induced cell death. The J Cell Biol. 2005; 171, 4: 603-614.

Boland B, Kumar A, Lee S, Platt FM, Wegiel J, Yu WH *et al*. Autophagy induction and autophagosome clearance in neurons: relationship to autophagic pathology in Alzheimer's disease. J Neurosci. 2008; 28, 27: 6926-6937.

Bosco D, Fava A, Plastino M, Montalcini T and Pujia A. Possible implications of insulin resistance and glucose metabolism in Alzheimer's disease pathogenesis. J Cell Mol Med. 2011; 15, 9:1807-1821.

Bové J, Martínez-Vicente M and Vila M. Fighting neurodegeneration with rapamycin: mechanistic insights. Nat Rev Neurosci. 2011; 12: 437-452.

Braak H and Del Tredici K. Alzheimer's disease: Pathogenesis and prevention. Alzheimers Dement. 2012; 8: 227-233.

Bradford MM. A rapid and sensitive method for the quantitation of microgram quantities of protein utilizing the principle of protein-dye binding. Anal Biochem. 1976; 72: 248-254.

Brookmeyer R, Johnson E, Ziegler-Graham K and Arrighi HM. Forecasting the global burden of Alzheimer's disease. Alzheimers Dement. 2007; 3: 186-191.

Bus JS and Gibson JE. Paraquat: Model for oxidant-initiated toxicity. Environ Health Persp. 1984; 55: 37-46.

Bushong EA, Martone ME, Jones YZ and Ellisman MH. Protoplasmic astrocytes in CA1 stratum radiatum occupy separate anatomical domains. J Neurosci. 2002; 22, 1: 183-192.

Businaro R, Ippoliti F, Ricci S, Canitano N, Fuso A. Alzheimer's Disease Promotion by Obesity: Induced Mechanisms—Molecular Links and Perspectives. Curr Gerontol Geriatr Res. 2012; 2012: 1-13.

Buttgereit F and Brand MD. A hierarchy of ATP-consuming processes in mammalian cells. Biochem J. 1995; 312: 163-167.

Caccamo A, Majumder S, Richardson A, Strong R and Oddo S. Molecular interplay between mammalian target of rapamycin (mTOR), amyloid-β, and Tau: effects on cognitive impairments. J Biol Chem. 2010; 285: 13107–13120.

Cahill GF. Fuel metabolism in starvation. Annu Rev Nutr. 2006; 26: 1-22.

Calkins MJ and Reddy PH. Amyloid beta impairs mitochondrial anterograde transport and degenerates synapses in Alzheimer's disease neurons. Biochim Biophys Acta. 2011; 1812: 507-513.

Calkins MJ, Manczak M, Mao P, Shirendeb U and Reddy PH. Impaired mitochondrial biogenesis, defective axonal transport of mitochondria, abnormal mitochondrial dynamics and synaptic degeneration in a mouse model of Alzheimer's disease. Hum Mol Gen. 2011; 20, 23: 4515-4529.

Camberos-Luna L, Gerónimo-Olvera C, Montiel T, Rincon-Heredia R and Massieu L. The Ketone Body, β-Hydroxybutyrate Stimulates the Autophagic Flux and Prevents Neuronal Death Induced by Glucose Deprivation in Cortical Cultured Neurons. Neurochem Res. 2015; 1-10.

Capetillo-Zarate E, Staufenbiel, Abramowski D, Haass C, Escher A, Stadelmann C *et al*. Selective vulnerability of different types of commissural neurons for amyloid β-protein-induced neurodegeneration in APP23 mice correlates with dendritic tree morphology. Brain. 2006; 129, 11: 2992-3005.

Carulla N, Caddy GL, Hall DR, Zurdo J, Gairí M, Feliz M *et al.* Molecular recycling within amyloid fibrils. Nature. 2005; 436: 554–558.

Cataldo AM, Barnett JL, Berman SA, Li J, Quarless S, Bursztajn S, Lippa C *et al*. Gene expression and cellular content of cathepsin D in Alzheimer's disease brain: evidence for early up-regulation of the endosomal-lysosomal system. Neuron. 1995; 14: 671-680.

Cha M, Han S, Son SM, Hong H, Choi Y, Byun J *et al.* Mitochondria-specific accumulation of amyloid β induces mitochondrial dysfunction leading to apoptotic cell death. PLoS One. 2012; 7, 4: e34929.

Chan DC. Mitochondrial fusion and fission in mammals. Annu Rev Cell Dev Biol. 2006; 22: 79-99.

Chen H, McCaffery JM and Chan DC. Mitochondrial fusion protects against neurodegeneration in the cerebellum. Cell. 2007; 130, 3: 548-562.

Chen R, Zhang T, Sun Y, Sun Y, Chen W, Shi N *et al*. Oxygen-glucose deprivation regulates BACE1 expression through induction of autophagy in Neuro-2a/APP695 cells. Neural Regener Res. 2015; 10, 9: 1433-1440.

Cheng B, Yang X, An L, Gao B, Liu X, Liu S. Ketogenic diet protects dopaminergic neurons against 6-OHDA neurotoxicity via up-regulating glutathione in a rat model of Parkinson's disease. Brain Res. 2009; 1286: 25-31.

Chertkow H. Diagnosis and treatment of dementia: introduction. Introducing a series based on the Third Canadian Consensus Conference on the Diagnosis and Treatment of Dementia. Can Med Assoc J. 2008; 178, 3: 316-321.

Cho DH, Nakamura T, Fang J, Cieplak P, Godzik A, Gu Z *et al*. S-nitrosylation of Drp1 mediates β-amyloid-related mitochondrial fission and neuronal injury. Science. 2009; 324, 5923: 102-105.

Chong MS and Sahadevan S. Preclinical Alzheimer's disease: diagnosis and prediction of progression. Lancet Neurol. 2005; 4: 576-579.

Chopra M, Galbraith S and Darnton-Hill I. A global response to a global problem: the epidemic of overnutrition. Bull World Health Organ. 2002; 80, 12: 952-958.

Chopra M, Lawn JE, Sanders D, Barron P, Abdool Karim SS, Bradshaw D *et al.* Achieving the health millennium development goals for South Africa: challenges and priorities. Lancet. 2009; 374: 1023-1031.

Chou E. Alzheimer's disease: background, current and future treatments. Int J Med Students. 2014; 2, 2: 56-63.

Chowdhury GM, Jiang L, Rothman DL and Behar KL. The contribution of ketone bodies to basal and activity-dependent neuronal oxidation in vivo. J Cereb Blood Flow Metab. 2014; 34, 7: 1233-1242.

Chung WS, Allen NJ and Eroglu C. Astrocytes control synapse formation, function, and elimination. Cold Spring Harb Perspect Biol. 2015; 7, 9: a020370.

Cleveland DW, Hwo SY and Kirschner MW. Physical and chemical properties of purified tau factor and the role of tau in microtubule assembly. J Mol Biol. 1977; 116, 2: 227-247.

Colman RJ, Beasley TM, Kemnitz JW, Johnson SC, Weindruch R and Anderson RM. Caloric restriction reduces age-related and all-cause mortality in rhesus monkeys. Nat Commun. 2014; 5: 1-5.

Cook DG, Leverenz JB, McMillan PJ, Kulstad JJ, Ericksen S, Roth RA *et al*. Reduced hippocampal insulin-degrading enzyme in late-onset Alzheimer's disease is associated with the apolipoprotein E-epsilon4 allele. Am J Pathol. 2003; 162: 313-319.

DaRocha-Souto B, Scotton TC, Coma M, Serrano-Pozo A, Hashimoto T, Sereno L *et al.* Brain oligomeric β-amyloid but not total amyloid plaque burden correlates with neuronal loss and astrocyte inflammatory response in amyloid precursor protein/tau transgenic mice. J Neuropathol Exp Neurol. 2011; 70, 5: 360-376.

De Barreda EG, Pérez M, Ramos PG, de Cristobal J, Martín-Maestro P, Morán A *et al.* Tau-knockout mice show reduced GSK3-induced hippocampal degeneration and learning deficits. Neurobol Dis. 2010; 37, 3:622-629.

De Bock K, Georgiadou M, Schoors S, Kuchnio A, Wong BW, Cantelmo AR *et al*. Role of PFKFB3-driven glycolysis in vessel sprouting. Cell. 2013; 154: 651-663.

De Felice F, Wu D, Lambert MP, Fernandez SJ, Velasco PT, Lacor PN, *et al.* Alzheimer's disease-type neuronal tau hyperphosphorylation induced by Aβ oligomers. Neurobiol Aging. 2008; 29: 1334-1347.

Degenhardt K, Mathew R, Beaudoin B, Bray K, Anderson D, Chen G *et al.* Autophagy promotes tumor cell survival and restricts necrosis, inflammation and tumorigenesis. Cancer Cell. 2006; 10, 1: 51-64.

Di Carlo M. Beta amyloid peptide: from different aggregation forms to the activation of different biochemical pathways. Eur Biophys J. 2010; 39: 877-888.

Dietrich MO, Liu Z-W, Horvath TL. Mitochondrial dynamics controlled by mitofusins regulate Agrp neuronal activity and diet-induced obesity. Cell. 2013; 155: 188-199.

Ding F, Yao J, Rettberg JR, Chen S and Brinton RD. Early decline in glucose transport and metabolism precedes shift to ketogenic system in female aging and Alzheimer's mouse brain: implication for bioenergetics intervention. PLoS One. 2013; 8, 11: e79977.

Dzeja PP and Terzic A. Phosphotransfer networks and cellular energetics. J Exp Biol. 2003; 206: 2039-2047.

Elmore S. Apoptosis: a review of programmed cell death. Toxicol Pathol. 2007; 35, 4: 495-516.

Escott-Price V, Bellenguez C, Wang L-S, Choi S-H, Harold D, Jones L *et al*. Gene-wide analysis detects two new susceptibility genes for Alzheimer's disease. PLoS One. 2014; 9, 6: e94661.

Essmann F, Bantel H, Totzke G, Engels IH, Sinha B, Schulze-Osthoff K *et al*. Staphylococcus aureus alpha-toxin-induced cell death: predominant necrosis despite apoptotic caspase activation. Cell Death Differ. 2003; 10: 1260-1272.

Fehm HL, Kern W and Peters A. The selfish brain: competition for energy resources. Prog Brain Res. 2006; 153: 129-140.

Fei Q, McCormack AL, Di Monte DA,and Ethell DW. Paraquat neurotoxicity is mediated by a Bak-dependent mechanism. J Biol Chem. 2008;, 283, 6: 3357-3364.
Finn PF and Dice JF. Ketone bodies stimulate chaperone-mediated autophagy. J Biol Chem. 2005; 280, 27: 25864-25870.

Fontana L, Partridge L and Longo VD. Extending healthy life span - from yeast to humans. Science. 2010; 328, 5976: 321-326.

Forsberg A, Engler H, Almkvist O, Blomquist G, Hagman G, Wall A *et al.* PET imaging of amyloid deposition in patients with mild cognitive impairment. Neurobiol Aging. 2008; 29, 10: 1456-1465.

Frisoni GB, Fox NC, Jack CR, Scheltens P and Thompson PM. The clinical use of structural MRI in Alzheimer disease. Nat Rev Neurol. 2010; 6: 67-77.

Fukumoto H, Takahashi H, Tarui N, Matsui J, Tomita T, Hirode M *et al.* A noncompetitive BACE1 inhibitor TAK-070 ameliorates Abeta pathology and behavioral deficits in a mouse model of Alzheimer's disease. J Neurosci. 2010; 30, 33: 11157–11166.

Galluzzi L, Bravo-San Pedro JM, Vitale I, Aaronson SA, Abrams JM, Adam D, Alnemri ES *et al*. Essential versus accessory aspects of cell death: Recommendations of the NCCD 2015. Cell Death Differ. 2015; 22, 1: 58-73.

Galluzzi L, Vitale I, Abrams JM, Alnemri ES, Baehrecke EH, Blagosklonny MW *et al.* Molecular definitions of cell death subroutines: recommendations of the Nomenclature Committee on Cell Death 2012. Cell Death Differ. 2012; 19, 1: 107-120.

García-Mesa Y, López-Ramos JC, Giménez-Llort L, Revilla S, Guerra R, Gruart A *et al*. Physical exercise protects against Alzheimer's disease in 3xTg-AD mice. J Alz Dis. 2011; 24: 421-454.

Gillardon F, Rist W, Kussmaul L, Vogel J, Berg M, Danzer K *et al.* Proteomic and functional alterations in brain mitochondria from Tg2576 mice occur before amyloid plaque deposition. Proteomics. 2007; 7, 4: 605-616.

Ginsberg S, Alldred MJ, Counts SE, Cataldo AM, Neve RL, Jiang Y *et al.* Microarray analysis of hippocampal CA1 neurons implicates early endosomal dysfunction during Alzheimer's disease progression. Biol Psychiatry. 2010; 68: 885-893.

González-Polo RA, Niso-Santano M, Ortíz-Ortíz MA, Gómez-Martín A, Morán JM, García-Rubio *et al*. Relationship between autophagy and apoptotic cell death in human neuroblastoma cells treated with paraquat: could autophagy be a "brake" in paraquat-induced apoptotic death? Autophagy. 2007; 3, 4: 366-367.

Götz J, Eckert A, Matamales M, Ittner LM and Liu X. Modes of Ab toxicity in Alzheimer's disease. Cell Mol Life Sci. 2011; 68: 3359-3375.

Gouras GK, Tampellini D, Takahashi RH and Capetillo-Zarate E. Intraneuronal b-amyloid accumulation and synapse pathology in Alzheimer's disease. Acta Neuropathol. 2010; 119: 523-541.

Grant WB: Dietary links to Alzheimer's disease. J Alzheimers Dis. 1999. 1999 update; 1: 197-201.

Grey NJ, Karl I and Kipnis DM. Physiologic mechanisms in the development of starvation ketosis in man. Diabetes. 1975; 24, 1: 10-16.

Green DR, Galluzzi L and Kroemer G. Metabolic control of cell death. Science. 2014; 345, 6203: 1250256.

Grumati P, Coletto L, Schiavinato A, Castagnaro S, Bertaggia E, Sandri M *et al*. Physical exercise stimulates autophagy in normal skeletal muscles but is detrimental for collagen VI-deficient muscles. Autophagy. 2011; 7, 12: 1415-1423.

Grundke-Iqbal I, Iqbal K, Tung YC, Quinlan M, Wisniewski HM and Binder LI. Abnormal phosphorylation of the microtubule-associated protein τ (tau) in Alzheimer cytoskeletal pathology. Proc Natl Acad Sci USA. 1985; 83: 4913-4917.

Halassa MM, Fellin T, Takano H, Dong JH and Haydon PG. Synaptic islands defined by the territory of a single astrocyte. J Neurosci. 2007; 27, 24: 6473-6477.

Hanley PJ, Mickel M, Löffler M, Brandt U and Daut J. KATP channel-independent targets of diazoxide and 5-hydroxydecanoate in the heart. J Physiol. 2002; 542: 735-741.

Hara T, Nakamura K, Matsui M, Yamamoto A, Nakahara Y, Suzuki-Migishima R *et al.* Suppression of basal autophagy in neural cells causes neurodegenerative disease in mice. Nature. 2006; 441, 7095: 885-889.

Harman D. Aging: a theory based on free radical and radiation chemistry. J Gerontol. 1956; 11: 298-300.

Harris JJ, Jolivet R and Attwell D. Synaptic energy use and supply. Neuron. 2012; 75, 5: 762-777.

Hartl FU and Hayer-Hartl M. Converging concepts of protein folding in vitro and in vivo. Nat Struct Mol Biol. 2009; 16, 6: 574-581.

He C, Sumpter R and Levine B. Exercise induces autophagy in peripheral tissues and in the brain. Autophagy. 2012; 8, 10: 1548–1551. (a)

He X, Wang L, Szklarz G, Bi Y and Ma Q. Resveratrol inhibits paraquat-induced oxidative stress and fibrogenic response by activating the nuclear factor erythroid 2-related factor 2 pathway. J Pharmacol Exp Ther. 2012; 342, 1: 81-90. (b)

Henderson ST, Vogel JL, Barr LJ, Garvin F, Jones JJ and Costantini LC. Study of the ketogenic agent AC-1202 in mild to moderate Alzheimer's disease: a randomized, double-blind, placebo-controlled, multicenter trial. Nutr Metab (Lond). 2009; 6, 1: 31-55.

Hendzel MJ, Nishioka WK, Raymond Y, Allis CD, Bazett-Jones DP *et al.* Chromatin condensation is not associated with apoptosis. J Biol Chem. 1998; 273, 38: 24470-24478.

Hernández–Gea V, Ghiassi–Nejad Z, Rozenfeld R, Gordon R, Fiel MI, Yue Z *et al*. Autophagy releases lipid that promotes fibrogenesis by activated hepatic stellate cells in mice and in human tissues.Gastroenterology. 2012; 142, 4: 938-946.

Herrero-Mendez A, Almeida A, Fernández E, Maestre C, Moncada S and Bolaños JP. The bioenergetic and antioxidant status of neurons is controlled by continuous degradation of a key glycolytic enzyme by APC/C–Cdh1. Nat Cell Biol. 2009; 11, 6: 747-752.

Hofman A, Grobbee DE, De Jong PT and Van den Ouweland FA. Determinants of disease and disability in the elderly: the Rotterdam Elderly study. Eur J Epidemiol. 1991; 7: 403-422.

Hong GL, Liu JM, Zhao GJ, Wang L, Liang G, Wu B *et al*. The reversal of paraquat-induced mitochondria-mediated apoptosis by cycloartenyl ferulate, the important role of Nrf2 pathway. Exp Cell Res. 2013; 319, 18:, 2845-2855.

Hong M and Lee VM. Insulin and insulin-like growth factor-1 regulate Tau phosphorylation in cultured human neurons. J Biol Chem. 1997; 272: 19547-19553.

Honig LS and Boyd CD. Treatment of Alzheimer's disease: current management and experimental therapeutics. Curr Transl Geriatr and Exp Gerontol Rep. 2013; 2: 174-181.

Hoppins S. The regulation of mitochondrial dynamics. Curr Opin Cell Biol. 2014; 29, 46-52.

Hoyer S. Brain glucose and energy metabolism abnormalities in sporadic Alzheimer disease. Causes and consequences: an update. Exp Gerontol. 2000; 35, 9: 1363-1372.

Huang CL, Lee YC, Yang YC, Kuo TY and Huang NK. Minocycline prevents paraquat-induced cell death through attenuating endoplasmic reticulum stress and mitochondrial dysfunction. Toxicol Lett. 2012; 209, 3: 203-210.

Imamura H, Nhat KP, Togawa H, Saito K, Iino R, Kato-Yamada Y *et al*. Visualization of ATP levels inside single living cells with fluorescence resonance energy transfer-based genetically encoded indicators. PNAS. 2009; 106, 37: 15651-15656.

Iwata A, Riley BE, Johnston JA and Kopito RR. HDAC6 and microtubules are required for autophagic degradation of aggregated huntingtin. J Biol Chem. 2005; 280, 48: 40282-40292.

Jaber N, Dou Z, Chen JS, Catanzaro J, Jiang YP, Ballou LM *et al*. Class III PI3K Vps34 plays an essential role in autophagy and in heart and liver function. PNAS. 2012; 109, 6: 2003-2008.

Jack CR, Knopman DS, Jagust WJ, Shaw LM, Aisen PS, Weiner MW *et al.* Hypothetical model of dynamic biomarkers of the Alzheimer's pathological cascade. Lancet Neurol. 2010; 9: 119-128.

Janson J, Laedtke T, Parisi JE, O'Brien P, Petersen RC and Butler PC. Increased risk of type 2 diabetes in Alzheimer disease. Diabetes. 2004; 53 2:474-481.

Jendrach M, Mai S, Pohl S, Vöth M and Bereiter-Hahn J. Short-and long-term alterations of mitochondrial morphology, dynamics and mtDNA after transient oxidative stress. Mitochondrion. 2008; 8, 4: 293-304.

Jin M, Shepardson N, Yang T, Chen G, Walsh D and Selkoe DJ. Soluble amyloid β-protein dimers isolated from Alzheimer cortex directly induce Tau hyperphosphorylation and neuritic degeneration. PNAS. 2011; 108, 14: 5819-5824.

Johnstone M, Gearing AJ, Miller KM. A central role for astrocytes in the inflammatory response to β-amyloid; chemokines, cytokines and reactive oxygen species are produced. J Neuroimmunol. 1999; 93, 1: 182-193.

Kabeya Y, Mizushima N, Ueno T, Yamamoto A, Kirisako T, Noda T *et al.* LC3, a mammalian homologue of yeast Apg8p, is localized in autophagosome membranes after processing. EBMO J. 2000; 19, 21: 5720-5728.

Kalaria RN, Maestre GE, Arizaga R, Friedland RP, Galasko D, Hall K *et al*. Alzheimer's disease and vascular dementia in developing countries: prevalence, management, and risk factors. Lancet Neurol. 2008; 7: 812-826.

Kalmijn S, Launer LJ, Ott A, Witteman JC, Hofman A and Breteler MM. Dietary fat intake and the risk of incident dementia in the Rotterdam Study. Ann Neurol. 1007; 42: 776-782.

Kapogiannis D and Mattson MP. Disrupted energy metabolism and neuronal circuit dysfunction in cognitive impairment and Alzheimer's disease. Lancet Neurol. 2011; 10: 187-198.

Kaushik S, Rodriguez-Navarro JA, Arias E, Kiffin R, Sahu S, Schwartz GJ *et al.* Autophagy in hypothalamic AgRP Neurons regulates food intake and energy balance. Cell Metab. 2011; 14: 173-183.

Kennedy HJ, Pouli AE, Ainscow EK, Jouaville LS, Rizzuto R and Rutter GA. Glucose Generates Sub-plasma Membrane ATP Microdomains in Single Islet β-Cells. POTENTIAL ROLE FOR STRATEGICALLY LOCATED MITOCHONDRIA. J Biol Chem. 1999; 274,19: 13281-13291.

Kim DY, Davis LM, Sullivan PG, Maalouf M, Simeone TA, Brederode JV *et al*. Ketone bodies are protective against oxidative stress in neocortical neurons. J Neurochem. 2007; 101, 5: 1316-1326.

Kim H, Lee SW, Baek KM, Park JS and Min JH. Continuous hypoxia attenuates paraquat-induced cytotoxicity in the human A549 lung carcinoma cell line. Exp Mol Med. 2011; 43, 9: 494-500.

Kimberly WT, Zheng JB, Guénette SY and Selkoe DJ. The intracellular domain of the β-amyloid precursor protein is stabilized by Fe65 and translocates to the nucleus in a notch-like manner. J Biol Chem. 2001; 276, 43: 40288-40292.

Kimelberg HK. Functions of mature mammalian astrocytes: a current view. Neuroscientist. 2010; 16, 1:79-106.

Klionsky DJ. The molecular machinery of autophagy: unanswered questions. J Cell Sci. 2005; 118(Pt 1): 7–18.

Klionsky DJ, Abdalla FC, Abeliovich H, Abraham RT, Acevedo-Arozena A, Adeli K *et al*. Guidelines for the use and interpretation of assays for monitoring autophagy. Autophagy. 2012; 8, 4: 445-544.

Klionsky DJ, Elazar Z, Seglen PO and Rubinsztein DC. Does bafilomycin A1 block the fusion of autophagosomes with lysosomes? Autophagy. 2008; 4, 7: 849-850.

Knopp RH, Magee MS, Raisys V, Benedetti T and Bonet B. Hypocaloric diets and ketogenesis in the management of obese gestational diabetic women. J Am Coll Nutr. 1991; 10, 6: 649-667.

Komatsu M, Waguri S, Koike M, Sou YS, Ueno T, Hara T *et al*. Homeostatic levels of p62 control cytoplasmic inclusion body formation in autophagy-deficient mice. Cell. 2007; 131: 1149–1163.

Komatsu M, Waguri S, Ueno T, Iwata J, Murata S, Tanida I *et al.* Impairment of starvation-induced and constitutive autophagy in Atg7-deficient mice. J Cell Biol. 2005; 169, 3: 425-434.

Kossoff E. The fat is in the fire: ketogenic diet for refractory status epilepticus. Epilepsy Curr. 2011; 11: 88-89.

Kroemer G, Dallaporta B and Resche-Rigon M. The mitochondrial death/life regulator in apoptosis and necrosis. Annu Rev Physiol. 1998; 60, 1: 619-642.

Kroemer G, Galluzzi L and Brenner C. Mitochondrial membrane permeabilization in cell death. Physiol Rev. 2007; 87, 1: 99-163.

Kuma A, Hatano M, Matsui M, Yamamoto A, Nakaya H, Yoshimori T *et al*. The role of autophagy during the early neonatal starvation period. Nature. 2004; 432: 1032-1036.

Laeger T, Pöhland R, Metges CC, Kuhla B. The ketone body b-hydroxybutyric acid influences agouti-related peptide expression via AMP-activated protein kinase in hypothalamic GT1-7 cells. J Endocrinol. 2012; 213: 193-203.

Lee HJ, Han J, Jang Y, Kim SJ, Park JH, Seo KS *et al*. Docosahexaenoic acid prevents paraquat-induced reactive oxygen species production in dopaminergic neurons via enhancement of glutathione homeostasis. Biochem Biophys Res Commun. 2015; 457, 1: 95-100.

Lee HK, Kumar P, Fu Q, Rosen KM and Querfurth HW. The insulin/Akt signaling pathway is targeted by intracellular β-amyloid. Mol Biol Cell. 2009; 20: 15331544.

Lee JA. Autophagy in neurodegeneration: two sides of the same coin. BMB Rep. 2009; 42, 6: 324-330.

Lee JH, Yu WH, Kumar A, Lee S, Mohan PS, Peterhoff CM *et al*. Lysosomal proteolysis and autophagy require presenilin 1 and are disrupted by Alzheimer-related PS1 mutations. Cell. 2010; 141, 7: 1146-1158.

Lee YJ, Jeong SY, Karbowski M, Smith CL and Youle RJ. Roles of the mammalian mitochondrial fission and fusion mediators Fis1, Drp1, and Opa1 in apoptosis. Mol Biol Cell. 2004; 15, 11: 5001-5011.

Leibbrandt M, Finn A and Woolard I. Describing and decomposing post-apartheid income inequality in South Africa. Development Southern Africa. 2012; 29, 1: 19-34.

Lipinski MM, Zheng B, Lu T, Yan Z, Py BF, Ng A *et al*. Genome-wide analysis reveals mechanisms modulating autophagy in normal brain aging and in Alzheimer's disease. PNAS. 2010; 107, 32: 14164-14169.

Lipton SA. Failures and successes of NMDA receptor antagonists: molecular basis for the use of open-channel blockers like memantine in the treatment of acute and chronic neurologic insults. NeuroRx. 2004; 1, 1: 101-110.

Liu Y, Liu F, Grundke-Iqbal I, Iqbal K and Gong CX. Deficient brain insulin signalling pathway in Alzheimer's disease and diabetes. J Pathol. 2011; 225, 1: 54-62.

Lockshin RA and Zakeri Z. Apoptosis, autophagy, and more. Int J Biochem. 2004; 36: 2405-2419.

Logothetis NK. What we can do and what we cannot do with fMRI. Nature. 2008; 453, 7197: 869-878.

Loo DT, Copani A, Pike CJ, Whittemore ER, Walencewicz AJ and Cotman CW. Apoptosis is induced by beta-amyloid in cultured central nervous system neurons. Proc Natl Acad Sci. 1993; 90, 17: 7951-7955.

Loos B, Du Toit AD and Hofmeyr JH. Defining and measuring autophagosome flux—concept and reality. Autophagy. 2014; 10, 11: 2087-2096.

Loos B and Engelbrecht AM. Cell death. Autophagy. 2009; 5, 5: 590-603.

Loos B, Engelbrecht AM, Lockshin RA, Klionsky DJ and Zakeri Z. The variability of autophagy and cell death susceptibility. Autophagy. 2013; 9, 9: 1270-1285.

Magistretti PJ and Pellerin L. Cellular mechanisms of brain energy metabolism and their relevance to functional brain imaging. Phil Trans R Soc Lond. 1999; 354: 1155-1163.

Magistretti PJ. Neuron-glia metabolic coupling and plasticity. J Exp Biol. 2006; 209, 12: 2304-2311.

Majumder S, Richardson A, Strong R and Oddo S. Inducing autophagy by rapamycin before, but not after, the formation of plaques and tangles ameliorates cognitive deficits. PloS One. 2011; 6, 9: e25416.

Mallik R and Gross SP. Molecular motors: strategies to get along. Curr Biol. 2004; 14, 2: R971-R982.

Mariño G, Pietrocola F, Eisenberg T, Kong Y, Malik SA, Andryushkova, A *et al*. Regulation of autophagy by cytosolic acetyl-coenzyme A. Mol Cell. 2014; 53, 5:710-725.

Martinez-Vicente M, Sovak G, Cuervo AM. Protein degradation and aging. Exp Geront. 2005; 40: 622-633.

Martinez-Vicente M, Talloczy Z, Wong E, Tang G, Koga H, Kaushik S *et al.* Cargo recognition failure is responsible for inefficient autophagy in Huntington's disease. Nat Rev Neurosci. 2010; 13, 5: 567-576.

Marx SO, Reiken S, Hisamatsu Y, Jayaraman T, Burkhoff D, Rosemblit N *et al.* PKA phosphorylation dissociates FKBP12. 6 from the calcium release channel (ryanodine receptor): defective regulation in failing hearts. Cell, 2000; 101, 4: 365-376.

Matsue H, Yang C, Matsue K, Edelbaum D, Mummert M, Takashima. A Contrasting impacts of immunosuppressive agents (rapamycin, FK506, cyclosporin A, and dexamethasone on bidirectional dendritic cell-T cell interaction during antigen presentation. J Immunol. 2002; 169, 7: 3555-3564.

Mattson MP and Liu D. Energetics and oxidative stress in synaptic plasticity and neurodegenerative disorders. Neuromol Med. 2002; 2, 2: 215-231.

Maynard SD and Gelblum J. Retrospective case studies of the efficacy of caprylic triglyceride in mild-to-moderate Alzheimer's disease. Neuropsychiatr Dis Treat. 2013; 9: 1629-1635.

McCarthy S, Somayajulu M, Sikorsa M, Borowy-Borowski H and Pandey S. Paraquat induces oxidative stress and neuronal cell death: neuroprotection by water-soluble Coenzyme Q_{10}. Toxicol Appl Pharmacol. 2004; 201, 1: 21-31.

McCarty MF, DiNicolantonio JJ and O'Keefe JH. Ketosis may promote brain macroautophagy by activating Sirt1and hypoxia-inducible factor-1. Med Hypotheses. 2015; 85, 5: 631-639.

McCormack AL, Atienza G, Johnston LC, Andersen JK, Vu S and Di Monte DA. Role of oxidative stress in paraquat-induced dopaminergic cell degeneration. J Neurochem. 2005; 93; 4: 1030-1037.

McCormack AL, Thiruchelvam M, Manning-Bog AB, Thiffault C, Langston JW, Cory-Slechta DA *et al.* Environmental risk factors and Parkinson's Disease: selective neurodegeneration of nigral dopaminergic neurons caused by the herbicide paraquat. Neurobiol Dis. 2002; 10: 119-127.

McKhann GM, Knopman DS, Chertkow H, Hyman BT, Jack CR, Kawas CH *et al*. The diagnosis of dementia due to Alzheimer's disease: Recommendations from the National Institute on Aging-Alzheimer's Association workgroups on diagnostic guidelines for Alzheimer's disease. Alzheimers Dement. 2011; 7, 3: 263-269.

Mellon PL, Windle JJ, Goldsmith PC, Padula CA, Roberts JL and Weiner RI. Immortalization of hypothalamic GnRH neurons by genetically targeted tumorigenesis. Neuron. 1990; 5: 1-10.

Mishra P, Carelli V, Manfredi G and Chan DC. Proteolytic cleavage of Opa1 stimulates mitochondrial inner membrane fusion and couples fusion to oxidative phosphorylation. Cell Met., 2014 19, 4: 630-641.

Mizushima N and Yoshimori T. How to interpret LC3 immunoblotting. Autophagy. 2007; 3, 6: 542-545.

Mizushima N, Yamamoto A, Matsui M, Yoshimori T and Ohsumi Y. In vivo analysis of autophagy in response to nutrient starvation using transgenic mice expressing a fluorescent autophagosome marker. Mol Biol Cell. 2004; 15, 3: 1101-1111.

Mizushima N, Yoshimori T and Levine B. Methods in mammalian autophagy research. Cell. 2010; 140, 3: 313-326.

Moloney AM, Griffin RJ, Timmons S, O'Connor R, Ravid R and O'Neill C. Defects in IGF-1 receptor, insulin receptor and IRS-1/2 in Alzheimer's disease indicate possible resistance to IGF-1 and insulin signalling. Neurobiol Aging. 2010; 31, 2: 224-243.

Morris MC, Evans DA, Bienias JL, Tangney CC, Bennett DA, Aggarwal N *et al.* Dietary fats and the risk of incident Alzheimer disease. Arch Neurol. 2003; 60, 2: 194-200.

Morrissette DA, Parachikova A, Green KN and LaFerla FM. Relevance of transgenic mouse models to human Alzheimer's disease. J Biol Chem. 2009; 284, 10: 6033-6037.

Mortiboys H, Thomas KJ, Koopman WJ, Klaffke S, Abou-Sleiman P, Olpin S *et al*. Mitochondrial function and morphology are impaired in parkin-mutant fibroblasts. Ann Neurol. 2008; 64, 5: 555-565.

Mosconi L. Brain glucose metabolism in the early and specific diagnosis of Alzheimer's disease. Eur J Nucl Med. 2005; 32, 4: 486-510.

Narendra D, Tanaka A, Suen DF and Youle RJ. Parkin is recruited selectively to impaired mitochondria and promotes their autophagy. J Cell Biol. 2008;, 183, 5: 795-803.

Nedelsky NB, Todd PK and Taylor JP. Autophagy and the ubiquitin-proteasome system: Collaborators in neuroprotection. Biochim Biophys Acta. 2008; 1782, 12: 691-699.

Nixon RA. Autophagy, amyloidogenesis and Alzheimer disease. J Cell Sci. 2007; 120: 4081-4091.

Nixon RA and Yang DS. Autophagy failure in Alzheimer's disease – locating the primary defect. Neurobiol Dis. 2011; 43, 1: 38-45.

Nixon RA, Wegiel J, Kumar A, Yu WH, Peterhoff C, Cataldo A, *et al.* Extensive involvement of autophagy in Alzheimer disease: and immune-electron microscopy study. J Neuropathol Exp Neurol. 2005; 64, 2: 133-122.

O'Brien RJ and Wong PC. Amyloid precursor protein processing and Alzheimer's disease. Annu Rev Neurosci. 2011; 34: 185-204.

Okamoto K and Kondo-Okamoto N. Mitochondria and autophagy: critical interplay between the two homeostats. BBA-General Subjects. 2012; 1820, 5: 595-600.

Owen OE, Morgan AP, Kemp HG, Sullivan JM, Herrera MG and Cahill GF. Brain metabolism during fasting. J Clin Invest. 1967; 46, 10: 1589-1595.

Pagani L and Eckert A. Amyloid-beta interaction with mitochondria. J Alzheimers Dis. 2011: 1-12.

Palop JJ and Mucke L. Epilepsy and cognitive impairments in Alzheimer disease. Arch Neurol. 2009; 66, 4: 435-440.

Palop JJ and Mucke L. Amyloid-β-induced neuronal dysfunction in Alzheimer's disease: from synapses toward neural networks. Nature Neurosci. 2010; 13, 7: 812-818.

Pan T, Kondo S, Le W and Jankovic J. The role of autophagy-lysosome pathway in neurodegeneration associated with Parkinson's disease. Brain. 2008; 131, 8: 1969-1978.

Paoli A, Rubini A, Volek JS and Grimaldi KA. Beyond weight loss: a review of the therapeutic uses of very-low-carbohydrate (ketogenic) diets. Eur J Clin Nutr. 2013; 67, 8: 789-796.

Peila R, Rodriguez BL and Lauren LJ. Type-2 diabetes, diabetes, Apo E gene and the risk for dementia and related pathogenesis: the Honolulu-Asia Aging Study. Diabetes. 2002; 51, 4: 1256-1262.

Peixoto F, Vicente J and Madeir, VM. A comparative study of plant and animal mitochondria exposed to paraquat reveals that hydrogen peroxide is not related to the observed toxicity. Toxicol In Vitro. 2004; 18, 6: 733-739.

Perneczky R, Wagenpfeil S, Komossa K, Grimmer T, Diehl J and Kurz A. Mapping scores onto stages: mini-mental state examination and clinical dementia rating. Am J Geriatr Psychiatry. 2006; 14, 2: 139-144.

Petersen RC, Caracciolo B, Brayne C, Gauthier S, Jelic and Fratiglioni L. Mild cognitive impairment: a concept in evolution. J Intern Med. 2014; 275, 3: 214-228.

Petersen RC, Smith GE, Waring SC, Ivnik RJ, Tangalos EG, Kokmen E. Mild cognitive impairment: clinical characterization and outcome. Arch Neurol. 1999; 56: 303–308.

Phelps ME. Positron emission tomography provides molecular imaging of biological processes. PNAS. 2000; 97, 16: 9226-9233.

Phielix E, Schrauwen-Hinderling VB, Mensink M, Lenaers E, Meex R, Hoeks J *et al*. Lower intrinsic ADP-stimulated mitochondrial respiration underlies in vivo mitochondrial dysfunction in muscle of male type 2 diabetic patients. Diabetes. 2008; 57, 11: 2943-2949.

Pickford F, Masliah E, Britschgi M, Lucin K, Narasimhan R, Jaeger PA *et al.* The autophagy-related protein beclin 1 shows reduced expression in early Alzheimer disease and regulates amyloid β accumulation in mice. J Clin Invest. 2008; 118, 6: 2190-2199.

Prins ML. Cerebral metabolic adaptation and ketone metabolism after brain injury. J Cereb Blood Flow Metab. 2008; 28: 1-16.

Rangaraju V, Calloway N and Ryan TA. Activity-driven local ATP synthesis is required for synaptic function. Cell. 2014; 156: 825-835.

Ravikumar B, Sarkar S, Davies JE, Futter M, Garcia-Arencibia M, Green-Thompson ZW *et al.* Regulation of mammalian autophagy in physiology and pathophysiology. Physiol Rev. 2010; 90: 1383-1435.

Ravikumar B, Vacher C, Berger Z, Davies JE, Luo S, Oroz LG *et al*. Inhibition of mTOR induces autophagy and reduces toxicity of polyglutamine expansions in fly and mouse models of Huntington disease. Nat Genet. 2004; 36, 6: 585-595.

Reddy PH. Amyloid beta, mitochondrial structural and functional dynamics in Alzheimer's disease. Exp Neurol. 2009; 218: 286-292.

Reger MA, Henderson ST, Hale C, Cholerton B, Baker LD, Watson GS *et al.* Effects of β-hydroxybutyrate on cognition in memory-impaired adults. Neurobiol Aging. 2004; 25, 3: 311-314.

Resnick SM, Pham DL, Kraut MA, Zonderman AB and Davatzikos C. Longitudinal studies of older adults: a shrinking brain. J Neurosci. 2003; 23: 3295-3301.

Robinson A, Grösgen S, Mett J, Zimmer VC, Haupenthal VJ, Hundsdörfer B *et al.* Upregulation of PGC-1a expression by Alzheimer's disease-associated pathway: presenilin 1/amyloid precursor protein (APP)/intracellular domain of APP. Aging Cell. 2014; 13: 263-272.

Roher AE, Chaney MO, Kuo YM, Webster SD, Stine WB, Haverkamp LJ *et al.* Morphology and toxicity of Aβ-(1-42) dimer derived from neuritic and vascular amyloid deposits of Alzheimer's disease. J Biol Chem. 1996; 271: 20631-20635.

Rose C, Menzies FM, Renna M, Acevedo-Arozena A, Corrochano S, Sadiq O *et al.* Rilmenidine attenuates toxicity of polyglutamine expansions in a mouse model of Huntington's disease. Hum Mol Gen. 2010; 19, 11: 2144-2153.

Ross CA and Poirier MA. What is the role of protein aggregation in neurodegeneration? Nat Rev Mol Cell Biol. 2005; 6: 891-898.

Rubinsztein DC, Cuervo AM, Ravikumar B, Sarkar S, Korolchuk V, Kaushik S *et al*. In search of an "autophagomometer". Autophagy. 2009; 5, 5: 585-589.

Ruskin DN, Ross JL, Kawamura M, Ruiz TL, Geiger JD and Masino SA. A ketogenic diet delays weight loss and does not impair working memory or motor function in the R6/2 1J mouse model of Huntington's disease. Physiol Behav. 2011; 103, 5: 501-507.

Ryan DA, Narrow WC, Federoff HJ and Bowers WJ. An improved method for generating consistent soluble amyloid-beta oligomer preparations for in vitro neurotoxicity studies. J Neurosci Methods. 2010; 190, 2: 171-179.

Sadowski M, Pankiewicz J, Scholtzova H, Ji Y, Quartermain D, Jensen CH *et al.* Amyloid-β deposition is associated with decreased hippocampal glucose metabolism and spatial memory impairment in APP/PS1 mice. J Neuropathol Exp Neurol. 2004; 63, 5: 418-428.

Saido TC. Metabolism of amyloid β peptide and pathogenesis of Alzheimer's disease. Proc Jpn Acad , Ser B Phys Biol Sci. 2013; 89, 7: 321-339.

Saito T, Matsuba Y, Mihira N, Takano J, Nilsson P, Itohara S *et al*. Single App knock-in mouse models of Alzheimer's disease. Nat Neurosci. 2014; 17, 5: 661-663.

Sambamurti K, Refolo LM, Shioi J, Pappolla MA, Robakis NK. The Alzheimer's amyloid precursor is cleaved intracellularly in the trans-golgi network or in a post-golgi compartment. Ann N Y Acad Sci. 1992; 674: 118-128.

Samoilova M, Weisspapir M, Abdelmalik P, Velumian AA and Carlen PL. Chronic in vitro ketosis is neuroprotective but not anti-convulsant. J Neurochem. 2010; 113: 826-835.

Sarkar S. Regulation of autophagy by mTOR-dependent and mTOR-independent pathways: autophagy dysfunction in neurodegenerative diseases and therapeutic application of autophagy enhancers. Biochem Soc Trans. 2013; 41, 5: 1103-1130.

Scarmeas N, Luchsinger JA, Schupf N, Brickman AM, Cosentino S, Tang MX *et al*. Physical activity, diet, and risk of Alzheimer disease. JAMA. 2009; 302, 6: 627-637.

Schenk D, Barbour R, Dunn W, Gordon G, Grajeda H, Guido T *et al*. Immunization with amyloid-β attenuates Alzheimer-disease-like pathology in the PDAPP mouse. Nature. 1999; 400, 6740: 173-177.

Schröder BA, Wrocklage C, Hasilik A and Saftig P. The proteome of lysosomes. Proteomics. 2010; 10: 4053-4076.

Schworer CM, Shiffer KA and Mortimore GE. Quantitative relationship between autophagy and proteolysis during graded amino acid deprivation in perfused rat liver. J Biol Chem. 1981; 256, 14: 7652-7658.

Selkoe DJ, Podlisny MB, Joachim CL, Vickers EA, Lee G, Fritz LC *et al*. Beta-amyloid precursor protein of Alzheimer disease occurs as 110-to 135-kilodalton membrane-associated proteins in neural and nonneural tissues. PNAS. 1988; 85, 19: 7341-7345.

Settembre C, Fraldi A, Medina DL, Ballabio A. Signals from the lysosome: a control centre for cellular clearance and energy metabolism. Nat Rev Mol Cell Biol. 2013; 14, 5: 283-296.

Shen S, Kepp O and Kroemer G. The end of autophagic cell death? Autophagy. 2012; 8, 1: 1-3.

Shimazu T, Hirschey MD, Newman J, He W, Shirakawa K, Le Moan N *et al*. Suppression of oxidative stress by β-hydroxybutyrate, an endogenous histone deacetylase inhibitor. Science. 2013; 339, 6116: 211-214.

Singh R, Kaushik S, Wang Y, Xiang Y, Novak A, Komatsu M, *et al.* Autophagy regulates lipid metabolism. Nature. 2009; 458; 7242: 1131-1135.

Shoji M, Golde TE, Ghiso J, Cheung TT, Estus S, Shaffer LM *et al*. Production of the Alzheimer amyloid beta protein by normal proteolytic processing. Science. 1992; 258, 5079: 126-129.

Skemiene K, Rakauskaite G, Trumbeckaite S, Liobikas J, Brown GC and Borutaite V. Anthocyanins block ischemia-induced apoptosis in the perfused heart and support mitochondrial respiration potentially by reducing cytosolic cytochrome c. Int J Biochem Cell Biol. 2013; 45, 1: 23-29.

Smith D, Pernet A, Hallett WA, Bingham E, Marsden PK and Amiel SA. Lactate: a preferred fuel for human brain metabolism in vivo. J Cereb Blood Flow Metab. 2003; 23: 658-664.

Sou YS, Waguri S, Iwata JI, Ueno T, Fujimura T, Hara T *et al.* The Atg8 conjugation system is indispensable for proper development of autophagic isolation membranes in mice. Mol Biol Cell. 2008; 19, 11: 4762-4775.

Spilman P, Podlutskaya N, Hart MJ, Debnath J, Gorostiza O, Bredesen D *et al*. Inhibition of mTOR by rapamycin abolishes cognitive deficits and reduces amyloid-β levels in a mouse model of Alzheimer's disease. PLoS One. 2010; 5, 4: e9979.

Swart C, Haylett W, Kinnear C, Johnson G, Bardien S and Loos B. Neurodegenerative disorders: Dysregulation of a carefully maintained balance? Exp Geront. 2014; 58: 279-291.

Tanida I, Minematsu-Ikeguchi N, Ueno T and Kominami E. Lysosomal turnover, but not a cellular level, of endogenous LC3 is a marker for autophagy. Autophagy. 2005; 1, 2: 84-91.

Tewari M, Quan LT, O'Rourke K, Desnoyers S, Zeng Z, Beidler DR *et al*. Yama/CPP32β, a mammalian homolog of CED-3, is a CrmA-inhibitable protease that cleaves the death substrate poly (ADP-ribose) polymerase. Cell. 1995; 81, 5: 801-809.

Tian Y, Bustos V, Flajolet M and Greengard P. A small-molecule enhancer of autophagy decreases levels of Aβ and APP-CTF via Atg5-dependent autophagy pathway. FASEB J. 2011; 25, 6: 1934-1942.

Tian Y, Chang JC, Fan EY, Flajolet M and Greengard P. Adaptor complex AP2/PICALM, through interaction with LC3, targets Alzheimer's APP-CTF for terminal degradation via autophagy. PNAS. 2013; 110, 42: 17071-17076.

Townsend M, Mehta T and Selkoe DJ. Soluble Aβ inhibits specific signal transduction cascades common to the insulin receptor pathway. J Biol Chem. 2007; 282: 33305-33312

Trudeau K, Molina AJ, Guo W and Roy S. High glucose disrupts mitochondrial morphology in retinal endothelial cells implications for diabetic retinopathy. Am J Pathol. 2010; 177, 1: 447-455.

Trushina E, Dutta T, Persson XMT, Mielke MM and Petersen RC. Identification of altered metabolic pathways in plasma and CSF in mild cognitive impairment and Alzheimer's disease using metabolomics. PLoS One. 2013; 8, 5: e63644.

Truter I. Prescribing of drugs for Alzheimer's disease: a South African database analysis. Int Psychogeriatr. 2010; 22, 2: 264-269.

Vagelatos NT and Eslick GD. Type 2 diabetes as a risk factor for Alzheimer's disease: the confounders, interactions, and neuropathology associated with this relationship. Epidemiol Rev. 2013; 35: 152-160.

Van der Auwera I, Wera S, Van Leuven F and Henderson ST. A ketogenic diet reduces amyloid beta 40 and 42 in a mouse model of Alzheimer's disease. Nutr Metab. 2005; 2, 1: 28.

Van Leuven F. Single and multiple transgenic mice as models for Alzheimer's disease. Prog Neurobiol. 2000; 61: 305-312.

VanItallie TB, Nonas C, Di Rocco A, Boyar K, Hyams K and Heymsfield SB. Treatment of Parkinson disease with diet-induced hyperketonemia: a feasibility study. Neurology. 2005; 64, 4: 728-730.

Vassar R, Kovacs DM, Yan R and Wong PC. The beta-secretase enzyme BACE in health and Alzheimer's disease: regulation, cell biology, function, and therapeutic potential. J Neurosci. 2009; 29: 12787–12794.

Veech RL, Chance B, Kashiwaya Y, Lardy HA and Cahill GF. Ketone bodies, potential therapeutic uses. IUBMB Life. 2001; 51, 4: 241-247.

Vingtdeux V, Chandakkar P, Zhao H, d'Abramo C, Davies P and Marambaud P. Novel synthetic small-molecule activators of AMPK as enhancers of autophagy and amyloid-β peptide degradation. FASEB J. 2011; 25, 1: 219-231

Vishnu N, Khan MJ, Karsten F, Groscher LN, Waldeck-Weierman M, Rost R *et al.* ATP increases within the lumen of the endoplasmic reticulum upon intracellular Ca2+-release. Mol Biol Cell. 2014; 25, 3: 368-379.

Volterra A and Meldolesi J. Astrocytes, from brain glue to communication elements: the revolution continues. Nat Rev Neurosci. 2005; 6, 8: 626-640.

Wang X, Su BO, Lee HG, Li X, Perry G, Smith MA and Zhu X. Impaired balance of mitochondrial fission and fusion in Alzheimer's disease. Nat Rev Neurosci. 2009; 29, 28: 9090-9103.

Westermann B. Mitochondrial fusion and fission in cell life and death. Nat Rev Mol Cell Biol. 2012; 11, 12: 872-884.

Whitehouse PJ, Price DL, Struble RG, Clark AW, Coyle JT and Delon MR. Alzheimer's disease and senile dementia: loss of neurons in the basal forebrain. Science. 1982; 215, 4537: 1237-1239.

Wimo A, Winblad B and Jönsson L. The worldwide societal costs of dementia: Estimates for 2009. Alzheimers Dement. 2010; 6: 98-103.

Wortmann M. Dementia: a global health priority – highlights from an ADI and World Health Organization report. Alzheimer's Res Ther. 2012; 4, 5: 40.

Xie H, Hou S, Jiang J, Sekutowicz M, Kelly J and Bacskai BJ. Rapid cell death is preceded by amyloid plaque-mediated oxidative stress. PNAS. 2013; 110, 19: 7905-7909.

Yang W and Tiffany-Castiglioni E. The bipyridyl herbicide paraquat induces proteasome dysfunction in human neuroblastoma SH-SY5Y cells. J Toxicol Environ Health Part .A. 2007;,70, 21: 1849-1857.

Yang DS, Stavrides P, Mohan PS, Kaushik S, Kumar A, Ohno M *et al*. Reversal of autophagy dysfunction in the TgCRND8 mouse model of Alzheimer's disease ameliorates amyloid pathologies and memory deficits. Brain. 2011; 134: 258-277.

Yang W, Chen L, Ding Y, Zhuang X and Kang UJ. Paraquat induces dopaminergic dysfunction and proteasome impairment in DJ-1-deficient mice. Hum Mol Gen. 2007; 16, 23: 2900-2910.

Yang Z, Huang J, Geng J, Nair U and Klionsky DJ. Atg22 recycles amino acids to link the degradative and recycling functions of autophagy. Mol Biol Cell. 2006; 17, 12: 5094-5104.

Yao N, Tada Y, Park P, Nakayashiki H, Tosa Y and Mayama S. Novel evidence for apoptotic cell response and differential signals in chromatin condensation and DNA cleavage in victorin-treated oats. Plant J. 2001; 28, 1: 13-26.

Yu L, McPhee CK, Zheng L, Mardones GA, Rong Y, Peng J *et al.* Termination of autophagy and reformation of lysosomes regulated by mTOR. Nature. 2010; 465, 7300: 942-946.
Yu WH, Cuervo AM, Kumar A, Peterhoff CM, Schmidt SD, Lee JH *et al*. Macroautophagy – a novel amyloid-b (Ab) peptide-generating pathway activated in Alzheimer's disease. J Cell Biol. 2005; 171: 87-98.

Yu WH, Kumara A, Peterhoff C, Kulnane Shapiro L, Uchiyamad Y, Lamb BT *et al*. Autophagic vacuoles are enriched in amyloid precursor protein-secretase activities: implications for β-amyloid peptide over-production and localization in Alzheimer's disease. Int J Biochem Cell Biol. 2004; 36: 2531-2540.

Zhang J, Cao Q, Li S, Lu X, Zhao Y, Guan JS *et al*. 3-Hydroxybutyrate methyl ester as a potential drug against Alzheimer's disease via mitochondria protection mechanism. Biomaterials. 2013; 34, 30: 7552-7562.

Zhao L, Teter B, Morihara T, Lim GP, Ambegaokar SS, Ubeda OJ *et al*. Insulin-degrading enzyme as a downstream target of insulin receptor signaling cascade: implications for Alzheimer's disease intervention. J Neurosci. 2004; 24, 49: 11120-11126.

Zhao Z, Lange DJ, Voustianiouk A, MacGrogan D, Ho L, Suh J *et al*. A ketogenic diet as a potential novel therapeutic intervention in amyotrophic lateral sclerosis. BMC Neurosci. 2006; 7, 1: 29.

Zong WX, Ditsworth D, Bauer DE, Wang ZQ and Thompson CB. Alkylating DNA damage stimulates a regulated form of necrotic cell death. Genes Dev. 2004; 18, 11: 1272-1282.